FOSSIL ENERGY

DOE/BC/15101-1
(OSTI ID: 785909)

DISCRETE FEATURE APPROACH FOR HETEROGENEOUS RESERVOIR PRODUCTION ENHANCEMENT

Semi-Annual Report
January 1, 1999-June 30, 1999

By:
William S. Dershowitz
Trenton Cladouhos

Date Published: September 2001

Work Performed Under Contract No. DE-AC26-98BC15101

Golder Associates Inc.
Redmond, Washington

National Energy Technology Laboratory
National Petroleum Technology Office
U.S. DEPARTMENT OF ENERGY
Tulsa, Oklahoma

DISCLAIMER

This report was prepared as an account of work sponsored by an agency of the United States Government. Neither the United States Government nor any agency thereof, nor any of their employees, makes any warranty, expressed or implied, or assumes any legal liability or responsibility for the accuracy, completeness, or usefulness of any information, apparatus, product, or process disclosed, or represents that its use would not infringe privately owned rights. Reference herein to any specific commercial product, process, or service by trade name, trademark, manufacturer, or otherwise does not necessarily constitute or imply its endorsement, recommendation, or favoring by the United States Government or any agency thereof. The views and opinions of authors expressed herein do not necessarily state or reflect those of the United States Government.

This report has been reproduced directly from the best available copy.

DOE/BC/15101-1
Distribution Category UC-122

Discrete Feature Approach for Heterogeneous Reservoir Production Enhancement

By
William S. Dershowitz
Trenton Cladouhos

September 2001

Work Performed Under DE-AC26-98BC15101

Prepared for
U.S. Department of Energy
Assistant Secretary for Fossil Energy

Purna Halder, Project Manager
National Petroleum Technology Office
P.O. Box 3628
Tulsa, OK 74101

Prepared by
Golder Associates Inc.
4104 148th Avenue, NE
Redmond, WA 98052

TABLE OF CONTENTS

	Page No.
1. EXECUTIVE SUMMARY	1
2. PROGRESS OVERVIEW FOR REPORTING PERIOD	3
2.1 Overview of Progress	3
2.2 Project Deliverables	3
2.3 Issues and Resolutions	3
3. TASK PROGRESS	5
3.1 Active Tasks	5
3.2 Task Progress	5
3.2.1 Task 1.1.3 Application of Neural Nets to the Identification of Fracture Sets	5
3.2.1.1 Background	5
3.2.1.2 Kohonen Neural Network Algorithm	7
3.2.1.3 Implementation for Heterogeneous Reservoir Data	8
3.2.1.4 Algorithm Demonstration, Yates Field Tract 17	15
3.2.1.5 Applications for Heterogeneous Reservoir Data	21
3.2.2 Task 1.3.1 Hetereogeneous Reservoir Interdisciplinary Database	25
3.2.3 Tasks 2.X.2 Preliminary DFN Model Development, North Stoney Point	25
3.2.3.1 Task 2.2.2 Derivation of DFN Model Parameters	25
3.2.3.2 Task 2.3.2 DFN Model Implementation	31
1.1.4 Tasks 2.X.3 Preliminary DFN Model Development, South Oregon Basin (Phosphoria)	37
1.1.4.1 Task 2.2.3 Geological Background, North and South Oregon Basins	37
1.1.4.2 Task 2.2.3 Derivation of DFN Model Parameters	60
1.1.4.3 Task 2.3.3 DFN Model Implementation	68
1.1.4.4 Task 2.4.3 DFN Model Calibration	71
1.1.5 Tasks 2.X.4 Preliminary DFN Model Development, North Oregon Basin (Tensleep)	77
1.1.5.1 Task 2.2.4 Derivation of DFN Model Parameters	77
1.1.1.2 Task 2.3.4 DFN Model Implementation	91
1.1.1.3 Task 2.4.4 DFN Model Calibration	95
1.1.6 Task 3.2 Stoney Point Reservoir Improvement Strategy	95
1.1.6.1 Task 3.2.1 DFN Strategy for IOR	95
3.2.6.2 Task 3.2.2 DFN Analysis of Stoney Point	105
3.2.7 Task 3.3 South Oregon Basin Reservoir Improvement Strategy	115
3.2.7.1 Task 3.3.1 DFN Strategy for IOR	115
3.2.7.2 Task 3.2.2 DFN Analysis of South Oregon Basin	115
3.2.8 Task 3.4 North Oregon Basin Reservoir Improvement Strategy	123
3.2.8.1 Task 3.4.1 DFN Strategy for IOR	123
3.2.8.2 Task 3.4.2 DFN Analysis of North Oregon Basin	123
3.2.9 Task 5.1.2 Web Site Updates	131
3.2.10 Task 5.2.1 Reports	131
3.2.11 Task 5.2.3 Presentations	131
3.2.12 Task 6 Management	132
4. CONCLUSIONS	133
5. REFERENCES	135

LIST OF FIGURES

Figure 3-1 Self-Organizing (Kohonen) Network Model	9
Figure 3-2 Contour Plot of Test Data with Three Fracture Sets	13
Figure 3-3 Neural Net Performance Results for 3 Set Test Case	17
Figure 3-4 Contour Plot of Joint Orientations in Three Yates Wells	18
Figure 3-5 Contour Plot of Sets Identified by Structural Geologist	19

Figure 3-6 Contour Plots of Sets Identified by Neural Network 23
Figure 3-7 Example of Stratamodel Data from South Oregon Basin 27
Figure 3-8 Example of Stratamodel data from North Oregon Basin 28
Figure 3-9 Example Tracer Breakthrough Curves From North Oregon Basin 29
Figure 3-10 Core Photos from Orchard 14, North Oregon Basin 30
Figure 3-11 Location Map of Stoney Point Field 33
Figure 3-12 Faults Interpreted at Stoney Point Field 34
Figure 3-13 Stoney Point Conceptual Model 35
Figure 3-14 Conceptual DFN Model at Stoney Point: Top View 39
Figure 3-15 Conceptual DFN Model at Stoney Point: Side View 40
Figure 3-16 Fracture Orientations in Stoney Point Conceptual DFN Model 41
Figure 3-17 Map of Big Horn Basin Showing Location of Oregon Basin Fields 42
Figure 3-18 Surface Geologic Map of Oregon Basin Fields 43
Figure 3-19 Regional Structural Cross-Section of Oregon Basin 44
Figure 3-20 Phosphoria Reservoir Structure Map with Strike and Dip of FMS Fractures Shown at Wells 50
Figure 3-21 Phosphoria Structure Edge Enhancement of 3D Seismic 51
Figure 3-22 Gros Ventre Structure Edge Enhancement of 3D Seismic 52
Figure 3-23 Subseismic Lineaments Mapped from Average Peak Amplitude within Orchard Window of South Oregon Basin 55
Figure 3-24 Trends of Seismic Lineaments 56
Figure 3-25 Fracture Subsets on Subseismic Lineament Map 57
Figure 3-26 Example Porosity Fence Diagram 58
Figure 3-27 Zeisman Dome Outcrop Photos 61
Figure 3-28 Wind River Canyon Photos: Phosphoria Formation 62
Figure 3-29 Wind River Canyon Photos: Tensleep Formation 63
Figure 3-30 Fracture Intensities in Phosphoria (AKA Embar) from FMI Wells 65
Figure 3-31 Phosphoria Fracture Orientations 69
Figure 3-32 Forward Modeling for Fracture Size: SOB 70
Figure 3-33 Northeast View of DFN Model of Phosphoria at SOB 73
Figure 3-34 Trace Map Views of DFN Model of Phosphoria at SOB 74
Figure 3-35 Fracture Orientations in Phosphoria Model 75
Figure 3-36 South Dome Tracer Test Results 79
Figure 3-37 Stratigraphic Correlations in North Oregon Basin 83
Figure 3-38 Anisotropy Associated with Eolian Laminations in the Tensleep 84
Figure 3-39 Cross Bedding Orientation in Tensleep Formation 85
Figure 3-40 Fracture Intensities in Tensleep from FMI Wells 86
Figure 3-41 Bedding Orientations in Government Tract 3B #16 89
Figure 3-42 Fracture Orientations in the Tensleep from FMI Wells 93
Figure 3-43 Forward Modeling for Fracture Sizes: NOB 97
Figure 3-44 3D View of DFN Model of Tensleep at NOB 98
Figure 3-45 Block Diagram of DFN Model of Tensleep at NOB 99
Figure 3-46 Fracture Orientations in Tensleep DFN Model 100
Figure 3-47 North Dome Tracer Test Bromide 102
Figure 3-48 North Dome Tracer Test Boron 103
Figure 3-49 Tributary Drainage Volume Algorithms 107
Figure 3-50 Compartments in Stoney Point DFN 109
Figure 3-51 Projected Areas of Compartments 110
Figure 3-52 Volumes of Compartments in Stoney Point Model 111
Figure 3-53 Well Configuration for Tributary Volume Analysis of Stoney Point Model 112
Figure 3-54 Tributary Volumes of Stoney Point Model 113
Figure 3-55 Well Pattern and Tributary Volumes Intersected in Stoney Point Model 114
Figure 3-56 South Oregon Basin Compartmentalization Analysis 118
Figure 3-57 Tributary Volumes in South Oregon Basin Model for $P_{32} = 0.2$ Model 119
Figure 3-58 Tributary Volumes in South Oregon Basin Model for $P_{32} = 0.3$ Model 120
Figure 3-59 South Oregon Basin Tributary Volume Analysis 121
Figure 3-60 Compartments in North Oregon Basin Model with $P_{32}=0.2$ 125

Figure 3-61 North Oregon Basin Compartmentalization Analysis 126
Figure 3-62 North Oregon Basin Model with $P_{32} = 0.2$ 127
Figure 3-63 Side View of Tributary Volumes of Vertical and Horizontal Wells in North Oregon Basin Model with $P_{32} = 0.2$ 128
Figure 3-64 North Oregon Basin Tributary Volume Analysis 129

LIST OF TABLES

Table 2-1 Project Deliverables 3
Table 3-1 Example Dataset for Kohonen Network Demonstration 11
Table 3-2 Kohonen Network for Example Data Set 11
Table 3-3 Kohonen Network for Yates Tract 17 Data Set 15
Table 3-4 Heterogeneous Reservoir Interdisciplinary Database 25
Table 3-5 Stoney Point DFN Model Parameters, Trenton Formation 36
Table 3-6 North and South Oregon Basin Data sources 45
Table 3-7 Stratigraphy from Walton modified after Dunn 49
Table 3-8 Phosphoria wells 64
Table 3-9 Phosphoria Fracture Intensities 67
Table 3-10 DFN Model Parameters, South Oregon Basin 71
Table 3-11 Tracer Tests, South Oregon Basin 77
Table 3-12 Tensleep Formation in North and South Oregon Basins 81
Table 3-13 Summary of Tensleep Fracture Intensities 87
Table 3-14 Parameters for Tensleep Dolomite Layering 91
Table 3-15 Preliminary Tensleep DFN Model Parameters 101
Table 3-16 Relevant Tracer Tests, North Oregon Basin 101
Table 3-17 Compartment Area and Volume Analysis, Stoney Point 108
Table 3-18 Tributary Volume Analysis, Stoney Point 108
Table 3-19 IOR Engineering Issues, South Oregon Basin 115
Table 3-20 Compartment Area and Volume Analysis, South Oregon Basin 116
Table 3-21 Tributary Volume Analysis, South Oregon Basin 117
Table 3-22 Implications of Tributary Volume Analysis, South Oregon Basin 117
Table 3-23 IOR Engineering Issues at North Basin 123
Table 3-24 Compartment Area and Volume Analysis, North Oregon Basin 124
Table 3-25 Tributary Volume Analysis, North Oregon Basin 124
Table 3-26 Implications of Tributary Volume Analysis, North Oregon Basin 131

1. EXECUTIVE SUMMARY

This report summarizes research carried out during the period January 1, 1999 to June 30, 1999 as part of the project, "Discrete Feature Approach for Heterogeneous Reservoir Production Enhancement." The report presents summaries of technology development for discrete feature modeling in support of the improved oil recovery (IOR) for heterogeneous reservoirs. In addition, the report provides information on project status, publications submitted, data collection activities, and technology transfer through the World Wide Web (WWW).

Research is described for derivation of discrete feature orientation distributions, and development of discrete feature network (DFN) models for project study sites at Stoney Point, Michigan, and North and South Oregon Basin, Wyoming. These models were used for preliminary calculations in support of IOR strategies for these sites.

Fracture orientation data is commonly obtained from fracture image logs and core logging. Fracture orientation distributions can be the key to understanding fracture patterns, and identifying key conductive features. Previous research has focused on development of algorithms for fracture orientation distribution analysis based on probabilistic neural network. During this period, we developed fracture orientation distribution algorithms based on the use of the Kohonen neural network. This network is particularly powerful for initial identification of fracture clusters, without relying on fracture orientation distribution assumptions.

2. PROGRESS overview FOR REPORTING PERIOD

2.1 Overview of Progress

This progress report describes activities during the period January 1, 1999 to June 30, 1999. Work was carried out on 21 tasks. The major activity during the reporting period was the development and preliminary application of discrete fracture network (DFN) models for Stoney Point, South Oregon Basin, and North Oregon Basins project study sites. In addition, research was carried out on analysis algorithms for discrete future orientation.

2.2 Project Deliverables

The following project deliverables were scheduled or submitted during this reporting period.

Deliverable	Scheduled Date	Date Submitted
Progress Report, October 1-Decembr 31, 1998	January 30, 1999	February 19, 1999

Table 2-1 Project Deliverables

The following papers were submitted or presented during the reporting period:

Dershowitz, W., T. Cladouhos, P. LaPointe, and W. Wadleigh (1999) Discrete Feature Network Methods for IOR in Heterogeneous Reservoirs. 1999 DOE Oil and Gas Conference, Technology Options for Producer Survival. Dallas, June 28-30, 1999.

Dershowitz,W., E. Wadleigh, G. Lee, and T. Eiben (1998) Discrete Fracture Network Approach for Thermally Assisted Gravity Segregation Enhanced Oil Recovery. Submitted for ISRM '99, Paris.

La Pointe, P. (1999) Predicting Hydrology of Fractured Rock Masses from Geology: Techniques, Successes and Failures from Recent Case Histories. International Symposium on the Dynamics of Fluids in Fractured Rocks: Concepts and Recent Advances. 10-12 February, 1999. Berkeley, CA. (Invited Presentation).

2.3 Issues and Resolutions

MIT research on fracture data synthesis algorithms as part of this contract was initiated on June 1, 1999.

3. TASK PROGRESS

3.1 Active Tasks

The following tasks were active during the quarter:

- Task 1.1.3 Orientation Analysis
- Task 1.3.0 Heterogeneous Reservoir Interdisciplinary Database
- Task 2.2.2 Preliminary DFN Model, Stoney Point
- Task 2.2.3 Preliminary DFN Model, South Oregon Basins
- Task 2.2.4 Preliminary DFN Model, North Oregon Basin
- Task 2.3.2 DFN Model Implementation, Stoney Point
- Task 2.3.3 DFN Model Implementation, North Oregon Basin
- Task 2.3.4 DFN Model Implementation, North Oregon Basin
- Task 2.4.3 DFN Model Validation/Calibration, South Oregon Basin
- Task 2.4.4 DFN Model Validation/Calibration, North Oregon Basin
- Task 3.2.1 Preliminary Reservoir Improvement Strategy, Stoney Point
- Task 3.3.2 IOR DFN Model Implementation, Stoney Point
- Task 3.3.1 Preliminary Reservoir Improvement Strategy, South Oregon Basin
- Task 3.2.2 IOR DFN Model Implementation, South Oregon Basin
- Task 3.4.1 Preliminary Reservoir Improvement Strategy, North Oregon Basin
- Task 3.4.2 IOR DFN Model Implementation, North Oregon Basin
- Task 5.1.2 Web Site Updates
- Task 5.2.3 Presentations
- Task 6 Management

3.2 Task Progress

This section describes progress during the reporting period for each of the active tasks.

3.2.1 Task 1.1.3 Application of Neural Nets to the Identification of Fracture Sets

3.2.1.1 Background

The key first step in the analysis of data from heterogeneous systems is to identify natural groups of data. Without first grouping the data for separate analysis, the variability in data values inherent in heterogeneous reservoirs unnecessarily reduces the spatial and statistical resolution of the data.

Any heterogeneous reservoir feature, such as fractures, laminations or shale lenses, has parameters that define it. More often than not, there may have been several depositional or

tectonic events that have produced these features. Each event may produce features with different characteristics. This is often evident in fracture patterns where multiple fracture sets are developed, each with there own defining characteristics. Sometimes the differences are obvious, for example, when there are two sets formed at right angles to one another. Other times the differences are more subtle, for example, when orientations are highly overlapping, but other features like planarity, mineral infillings, surface roughness and size may be the parameters that distinguish one set from another. In this situation, it may be difficult for the geologist to easily evaluate the natural groupings in the data.

The identification of groupings or sets within heterogeneous data is often addressed by using a form of statistical cluster analysis. There are several different types of clusters:

- Disjoint clusters in which the populations of each cluster do not overlap at all;
- Overlapping clusters, in which feature properties overlap to a greater or lesser extent such that there is some ambiguity as to which cluster each feature belongs to; and
- Hierarchical clusters, in which members of one cluster simultaneously, include features of another cluster.

All three of these types of clusters can be expressed as "Fuzzy clusters" defined by a probability of membership in each cluster. This probabilistic concept of cluster membership was the foundation for the development of the NeurISIS 1.0 fracture set orientation algorithm (Dershowitz et al., 1996). The NeurISIS 1.0 algorithm used a "probabilistic neural network" to assign features to clusters based on their relative probability of membership, and then iteratively defined the clusters based on the statistics of their members. The weakness of the NeurISIS 1.0 algorithm is that it does not determine the initial fracture set definitions, relying on the user to provide the initial set definitions.

Other common clustering algorithms include: single-linkage methods (neighbor and dendritic), Ward's minimum variance, and Gower's medium method. These clustering methods were evaluated but failed to provide appropriate capabilities for fractured reservoir data. The appropriate clustering algorithm depends on a number of factors, including

- type of data,
- shape of the clusters,
- underlying probability distribution of the data,
- degree of heterogeneity, and
- degree of overlap.

Regarding data type, fracture data from heterogeneous reservoirs is generally a combination of four types of data:

- ordinal parameters, such as joint roughness classes,
- class parameters, such as type of fracture or mineralization,
- continuous parameters such as aperture and permeability, and

- vector parameters, such as orientation.

Very few common-clustering methods can effectively use ordinal and class data; they are typically designed for using continuous variables only. Many of the common-clustering methods make assumptions such as approximately equal covariance matrices and multinormality. Unfortunately, data typically associated with features in heterogeneous reservoirs is unlikely to satisfy these constraints. Probability distributions are frequently not normal, and covariance matrices are rarely approximately equal. It is not even clear what a covariance matrix of mineral fillings would be.

Thus, the clustering algorithm for heterogeneous reservoir fracture data must satisfy a number of requirements:

- ability to handle all four parameter types,
- freedom from restrictions of normality, and
- ability to function with varying covariance matrices.

One approach which satisfies these requirements is the family of neural networks termed "self-organizing" or "Kohonen" networks (Kohonen, 1988). During this reporting period, we have developed the Kohonen networks for application to clustering of fracture data.

3.2.1.2 Kohonen Neural Network Algorithm

The topology of Kohonen networks consists of two layers, an input layer and an output layer. Each node in the input layer is connected to each node in the output layer by a connection with an associated weight.

A *slab* is a group of nodes with similar attributes. These attributes include parameters like the activation function, learning coefficient and momentum factor, as discussed later. All nodes in a slab receive their input from the same sources, be they other slabs or the initial input values, and they transmit their information to a common output destination. Figure 3-1 illustrates the basic Kohonen network topology.

The first step in application of the Kohonen network is to initialize the network by assigning values to the weights. These are typically random values selected in one of several ways depending upon the network analyst's preference, since there still remains much discussion as to the best way to assign these weights.

The next step is to train the network. This is done by using quantitative clustering criteria to measure how well the network is working in defining clusters. These "distance metrics" depend on the data being considered. Distance metrics for fracture data include Euclidean and Normalized. Both were evaluated, and as expected, Euclidean distance metrics outperformed normalized metrics.

Once the network distance metrics have been defined, the weights assigned to the Kohonen network are iterated until stable groups appear. This iteration proceeds as follows:

1. An input pattern is presented to the network, which can consist of geological attributes of each fracture and its orientation represented by the direction cosines of its normal vector.

2. Input patters are assigned to output nodes to which it is found to be closest in terms of the selected distance metric.
3. Once this winning output node has been selected, the nodes within a neighborhood of the winning node are adjusted to have similar properties.
4. This process is repeated, continuously reducing the learning rate and the neighborhood site until the calculated clusters or sets have stabilized.

The neighborhood starts off relatively large (although less than the number of output nodes). As training progresses, the properties of the output nodes tend to stabilize, and the neighborhood decreases along with the learning rate. Eventually, the neighborhood goes to 0, and only the winning node has its weight changed. At this point, the learning rate is also much smaller, and the clusters are as well defined, as they are likely to be.

3.2.1.3 Implementation for Heterogeneous Reservoir Data

The application of Kohonen networks to heterogeneous reservoir data requires conversion of fracture data to formats, which can be used to provide input to the networks. This is achieved by converting ordinal data to ranks and class data to presence/absence. For example, roughness might have three classes: (1) smooth, (2) rough, or (3) very rough. A roughness-input variable would be assigned to the number 1, 2, or 3 depending on which class it belonged to. For class variables, such as mineral filling - calcite, the fracture would be assigned the value 0 or 1 to reflect absence or presence. As a final stage, all input data are normalized over their actual or theoretical range of values.

An example Kohonen network application is illustrated in Table 3-1. This test case consists of four types of properties: Vector data (orientation), ordinal data (planarity, opening), continuous data (size), and class data (filling).

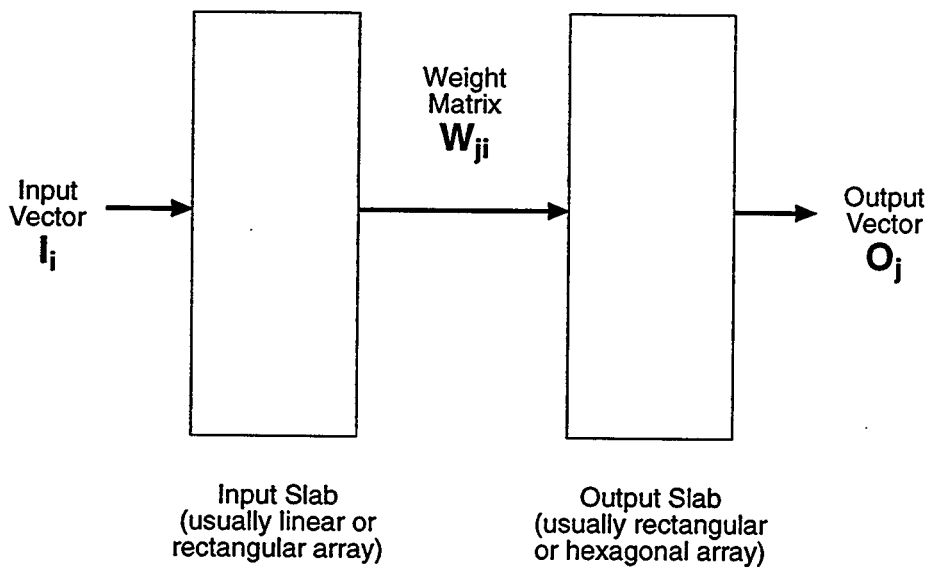

FIGURE **3-1**
SELF-ORGANIZING (KOHONEN) NETWORK MODEL
NPTO

PROJECT NO. 983 1258.521 DRAWING NO. 85004 DATE 7/29/99 DRAWN BY TK

Golder Associates

Set #	Orientation	Planarity	Filling	Size	Open/ Closed
1	Horizontal, Fisher Dispersion $\kappa = 10.0$	Smooth	Calcite	Normal, mean = 15, stdev = 2	Open
2	Mean Pole Trend, Plunge = (0,0) Fisher Dispersion $\kappa = 10.0$	Moderat ely Rough	Calcite	Normal, mean = 7, stdev = 2	Closed
3	Mean Pole Trend, Plunge = (0,45) Fisher Dispersion $\kappa = 10.0$	Rough	None	Normal, mean = 10, stdev = 3	Open

Table 3-1 Example Dataset for Kohonen Network Demonstration

The example dataset was generated from the stochastic properties given in Table 3-1, using FracMan/FracWorks discrete feature network model (Dershowitz et al., 1998). The sets were defined with overlapping parameter distributions of, for example, orientation, size filling and openness. Figure 3-2 is a stereoplot of the three sets, showing the overlap in orientation distributions.

Three parameters must be specified to apply the Kohonen network for heterogeneous reservoir data. For the example network, the following parameters were specified as summarized in Table 3-2.

Parameter	Assumption	Basis
Number of Sets (Clusters)	3	Visual inspection of data
Initial Weighting of Neurons	Uniform Distribution U[0,1]	Lack of conditioning
Neighborhood Scale	2	
Learning Rate	0.6	
Distance Metric	orientation (vector data): euclidean distance on stereonet planarity (ordinal data) infilling (class data) size (continuous data) opening (ordinal data)	

Table 3-2 Kohonen Network for Example Data Set

All 600 fractures were correctly clustered by the net. The classification results maybe expressed as neuron values; the smallest value indicates the closest match to a cluster. For example, fracture #1 had values of 0.054, 1.888 and 3.303 for clusters #1, #2 and #3. The smallest value was for cluster #1, so that is the cluster or set to which it is assigned.

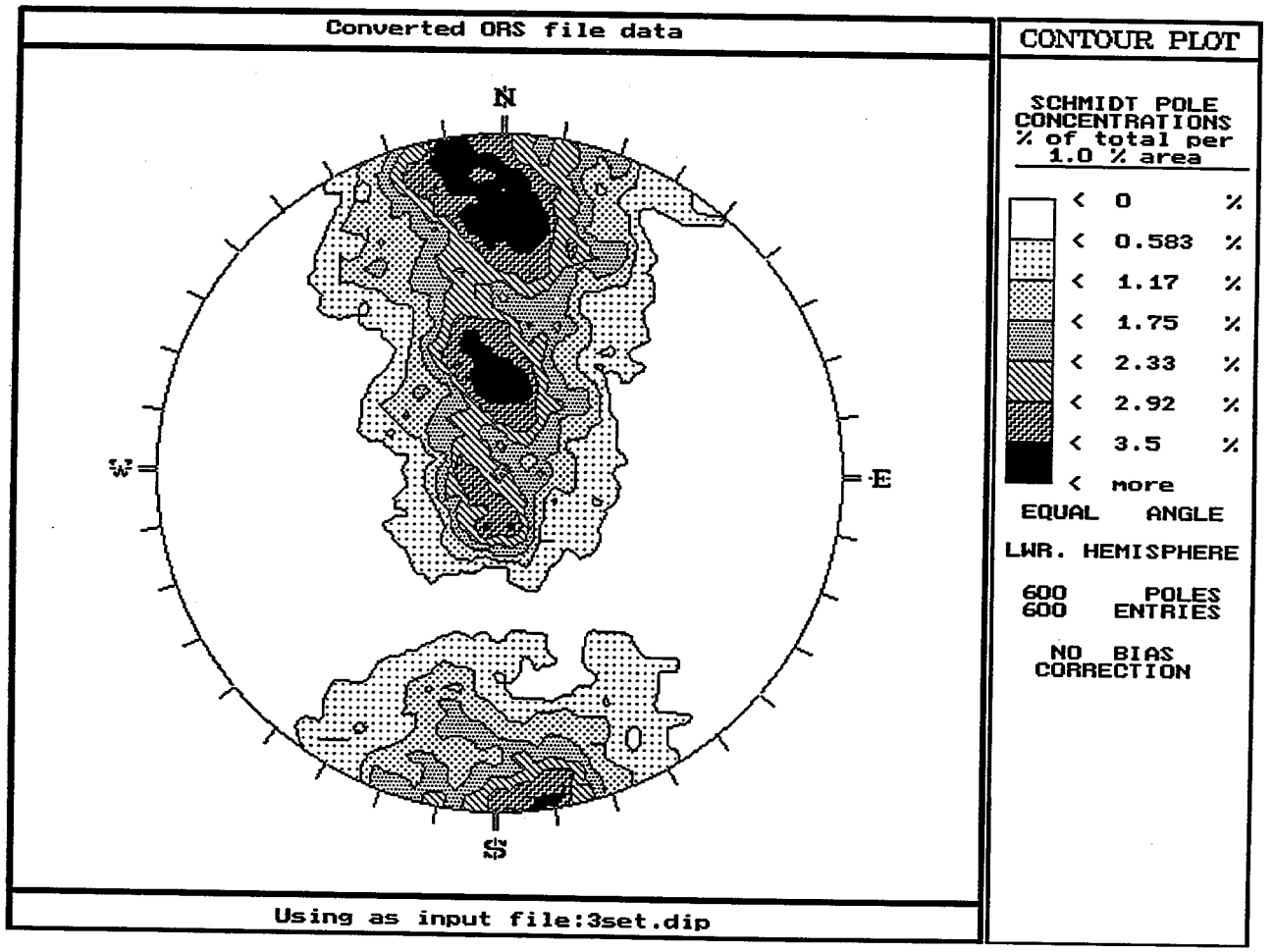

FIGURE **3-2**

CONTOUR PLOT OF TEST DATA WITH THREE FRACTURE SETS

NPTO

PROJECT NO. 983 1258.521 DRAWING NO. 85005 DATE 7/30/99 DRAWN BY TK

Golder Associates

Figure 3-3 shows these neuron probability values for all 600 fractures in the example case. The separation between the three sets of points for the fractures 1-200 and 401-600 show that the net had little problem in distinguishing Set #1 from the other sets, or Set #3 from the other sets; the neuron values for each set are very different from each other. Set #2 is slightly different; while the net had no problem correctly clustering it, the neuron values for the two other sets are similar to each other. This suggests that the characteristics of Set #2 are intermediate between Set #1 and Set #3 (which is also seen by the intermediate position of neuron values for Set #2 for fractures 1-200 and 401-600). Set #1 is more unlike Set #3 than it is unlike Set #2.

3.2.1.4 Algorithm Demonstration, Yates Field Tract 17

The Kohonen neural network was applied using data from Tract 17 in the Yates Field, west Texas, one of the four project study site window areas. This data provides a rigorous test of a self-organizing network's ability to distinguish orientational sets in a complex data set. Figure 3-4 shows the stereoplot of joint orientations from three wells, YU1711, YU1755 and YU2511. An expert structural geologist (T. Cladouhos) was given the stereoplot and asked to identify sets based upon orientation. The geologist's picks are shown in Figure 3-5.

There were five sets identified by the geologist, labeled G1 through G5 on Figure 3-5.

A Kohonen network was applied to the orientation data. The parameters assumed for the Kohonen network are summarized in Table 3-3.

Parameter	Assumption	Basis
Number of Sets (Clusters)	5	Structural geologist
Initial Weighting of Neurons	Uniform Distribution U[0,1]	Lack of conditioning
Neighborhood Scale	4	
Learning Rate	0.6	
Distance Metric	orientation (vector data): euclidean distance on stereonet planarity (ordinal data) infilling (class data) size (continuous data) opening (ordinal data)	

Table 3-3 Kohonen Network for Yates Tract 17 Data Set

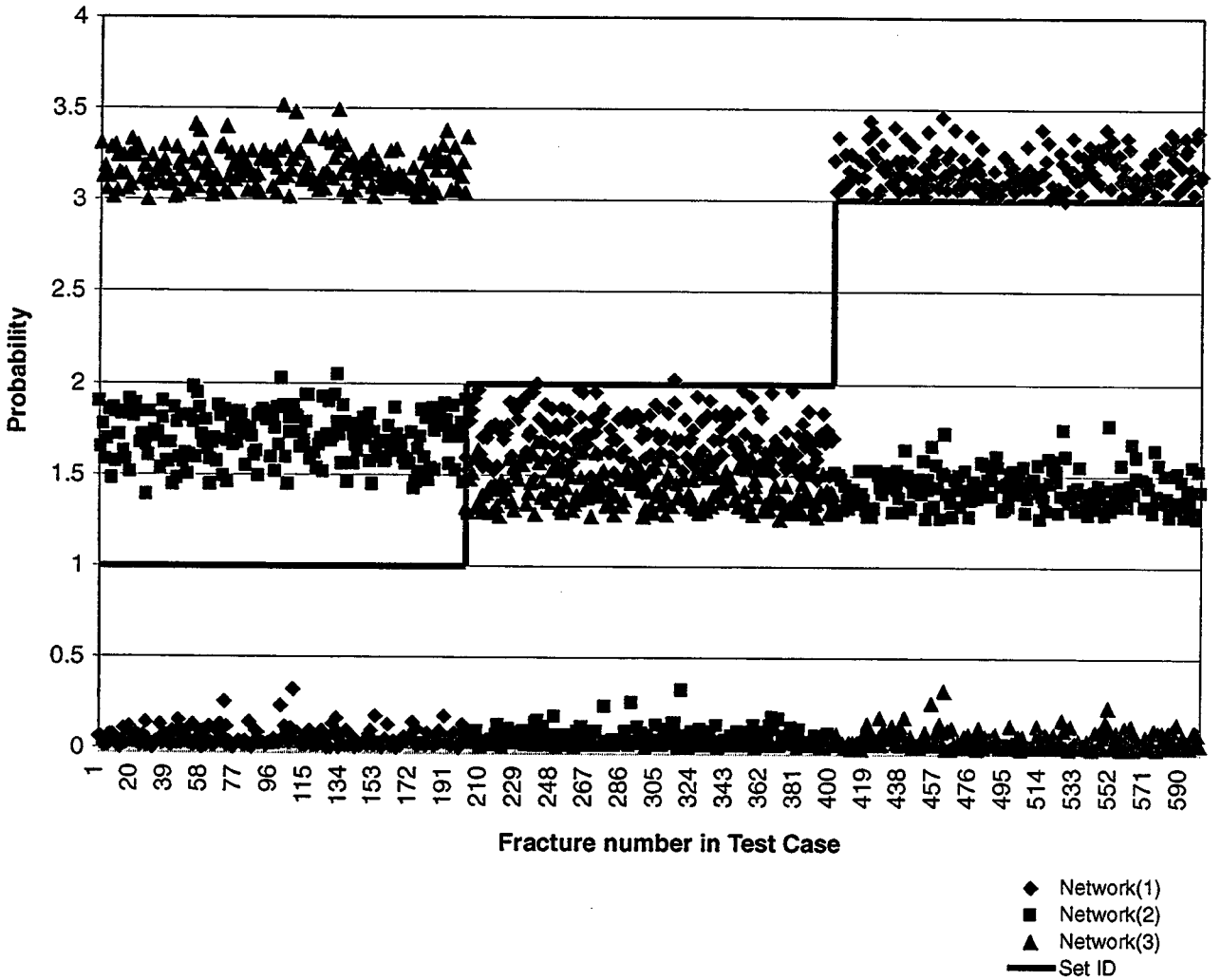

FIGURE **3-3**
NEURAL NET PERFORMANCE RESULTS FOR 3 SET TEST CASE
NPTO/CORRELATIONS

PROJECT NO. 983 1258.521 DRAWING NO. 85006 DATE 8/9/99 DRAWN BY TK

Golder Associates

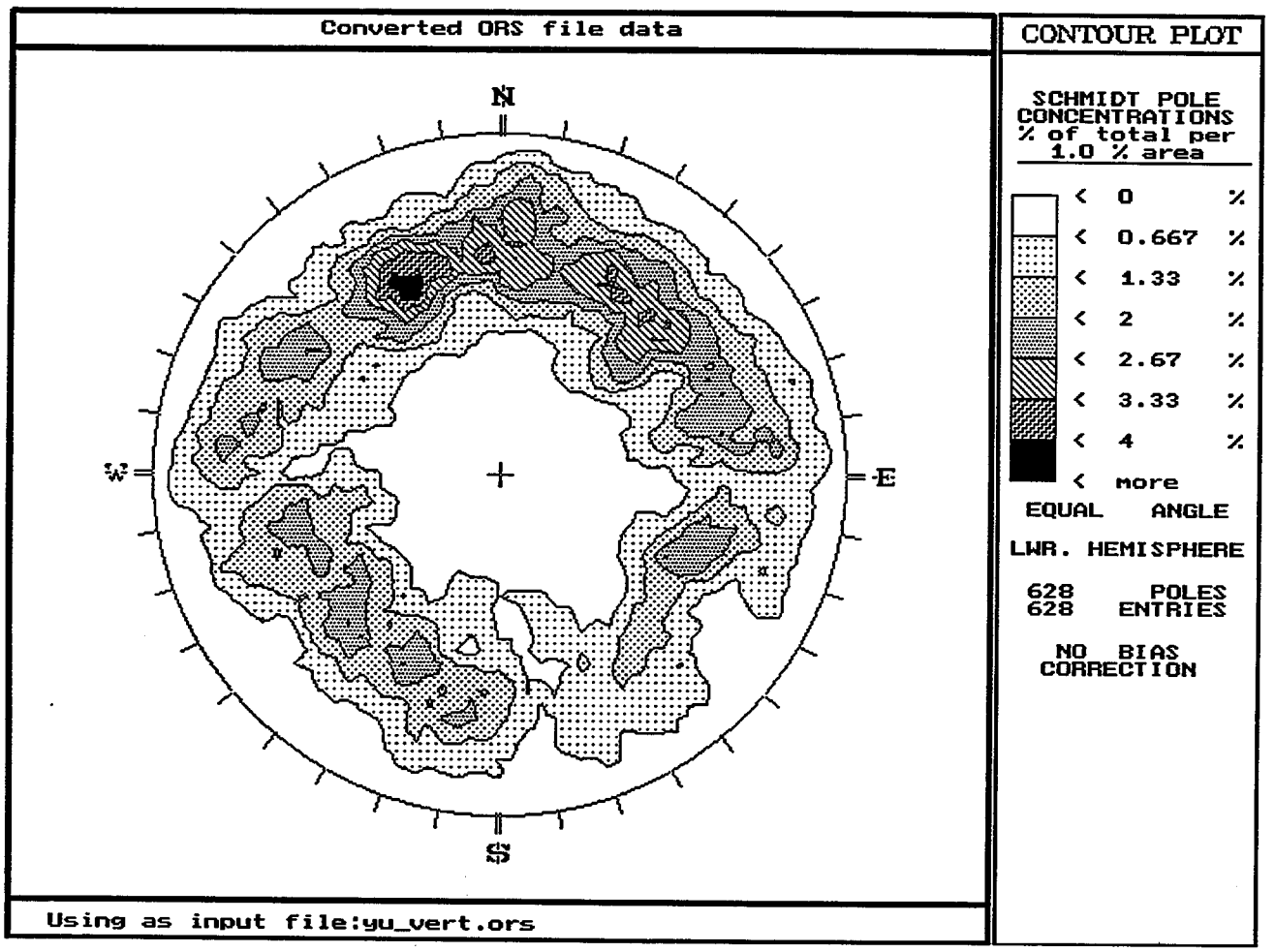

FIGURE **3-4**

CONTOUR PLOT OF JOINT ORIENTATIONS IN THREE YATES WELLS

NPTO

PROJECT NO. 983 1258.521 DRAWING NO. 85007 DATE 7/28/99 DRAWN BY TK

Golder Associates

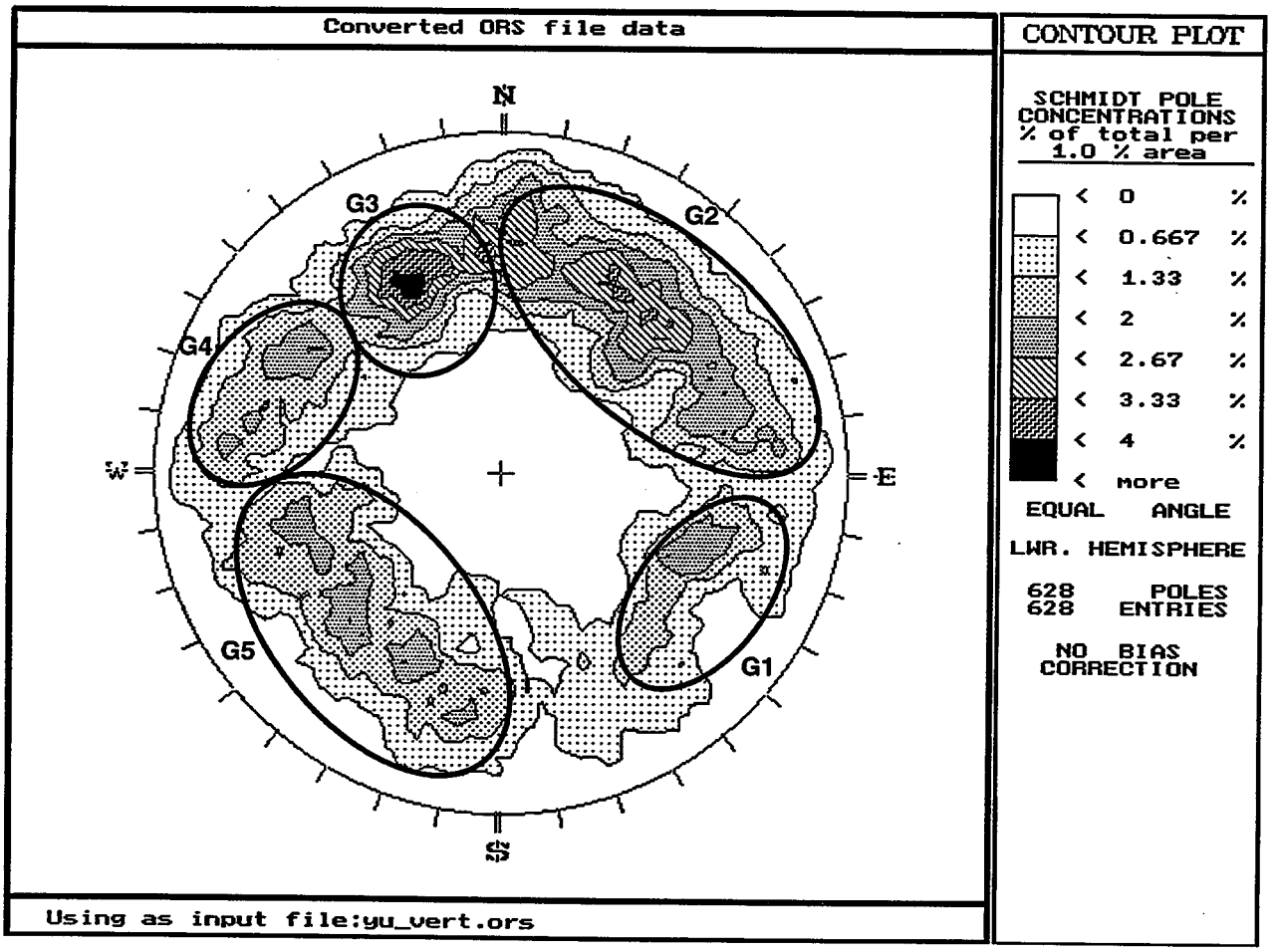

FIGURE **3-5**

CONTOUR PLOT OF SETS IDENTIFIED BY STRUCTURAL GEOLOGIST

NPTO

PROJECT NO. 983 1258.521 DRAWING NO. 85008 DATE 7/29/99 DRAWN BY TK

Golder Associates

The five sets selected by the neural net are labeled as N1 through N5 in Figure 3-6

The G sets and the N sets are very similar. G1 matches N1 exactly. The neural net made a slightly different selection of N2 and N3 versus G2 and G3. The region of the stereoplot covered by the combination of G2 and G3 is the same as that covered by N2 and N3. The difference is in the boundary between the two sets. The boundary between the G2 and G3 is approximately a few degrees west of north, while the boundary between N2 and N3 is about 20 degrees east of north. The difference is that the concentration of orientations represented by poles trending north is included with the N3 set by the neural network, but was included with the G2 set by the geologist.

Likewise, sets N4 and N5 cover the same region of the stereoplot covered by G4 and G5, the difference being where the boundary between the two sets is positioned. The boundary selected by the geologist was taken to be a few degrees south of due west, placing the concentration of poles trending around 250 degrees into G5. The neural net chose a boundary more to the southwest at around 240 degrees, moving this concentration of poles into N4.

Overall, the sets identified by the self-organizing neural net are very similar, but not identical to those picked by the geologist. The differences are minor, and would need to be resolved by either collecting additional parameter data or by considering other information on the tectonic or structural history of the reservoir. For example, the G3 set might have different sizes, fillings or roughness than the other fractures included in N3. Or it might be that the G3 fractures were in the orientation expected for a particular tectonic event, while the additional fractures found in N3 were not.

The fact that the geologist and the neural network came up with slightly different groupings is a useful result in itself. Just as two geologists might define sets differently, and thereby stimulate discussion, the network illustrates alternative interpretations and set definitions. The difference between the neural network's set identifications are useful for focusing further considerations as to the geological origins of each set.

3.2.1.5 Applications for Heterogeneous Reservoir Data

There are several potential applications of neural network technology to heterogeneous reservoirs. The first application is that described above: identification of clusters in the data in order to guide statistical analysis and to stimulate further investigations into the possible geological explanations of the groupings.

Another use of the self-organizing network analysis is as a classification tool for rapidly assigning additional data into the proper sets. This is particularly useful for mature reservoirs where there may be an abundance of data that can require a lot of time for a skilled geologist to classify. Once the self-organizing net has been trained on a small subset of data to the geologist's satisfaction, then the trained net can be used to automatically assign set probabilities to all the remaining data. The assignment is both quick and consistent, and does not require the time of a skilled geologist.

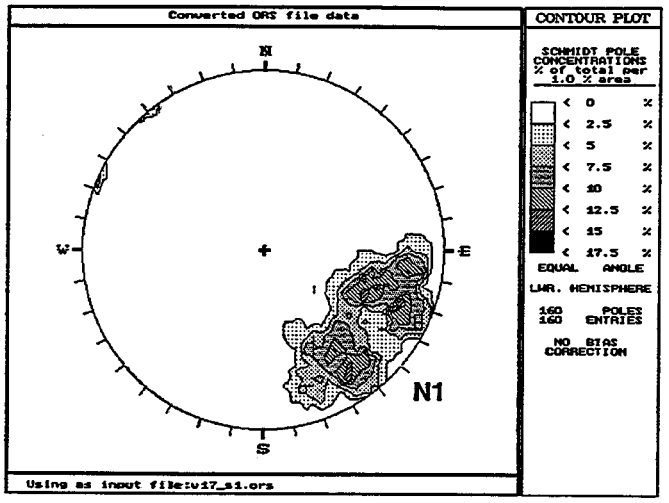

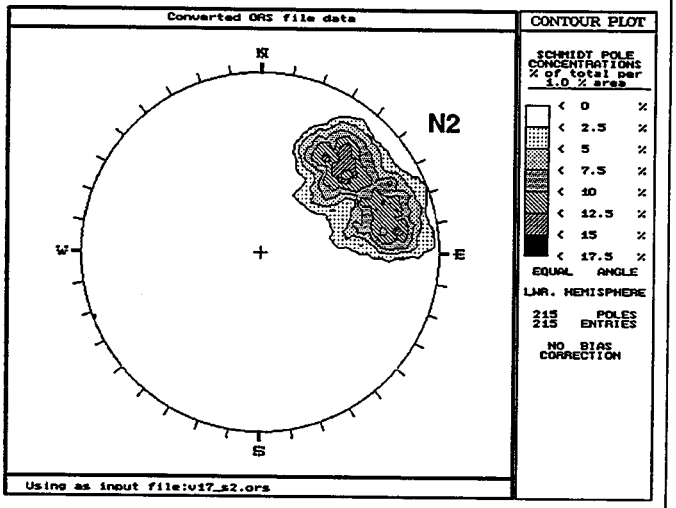

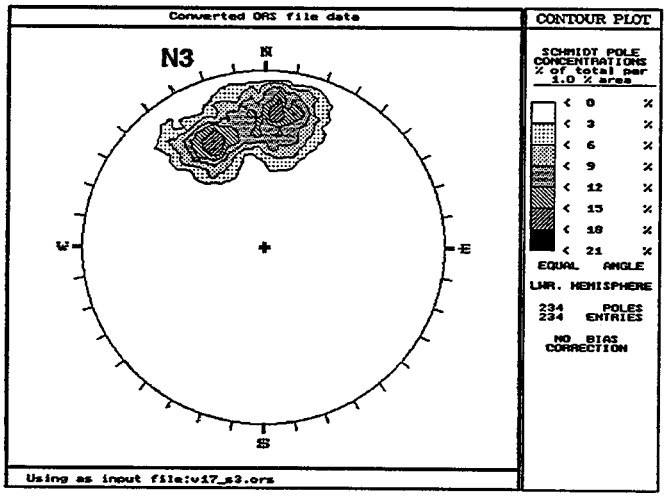

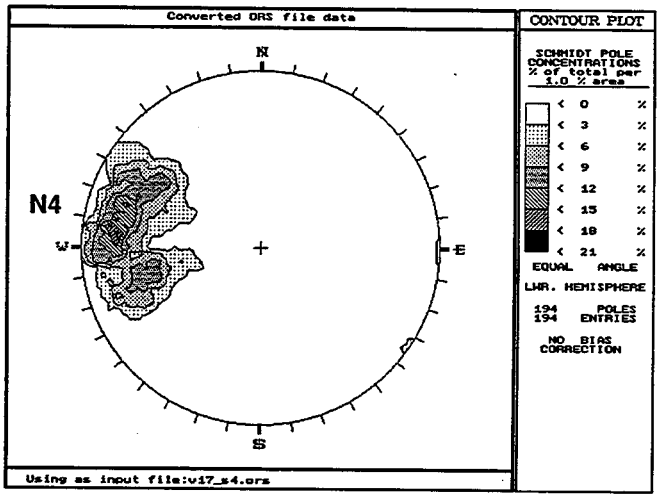

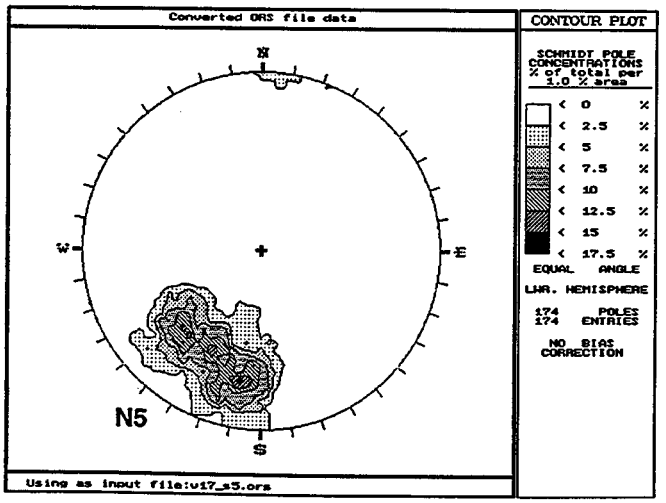

FIGURE **3-6**

CONTOUR PLOTS OF SETS IDENTIFIED BY NEURAL NETWORK

NPTO

PROJECT NO. 983 1258.521 DRAWING NO. 85009 · DATE 7/29/99 DRAWN BY TK

Golder Associates

3.2.2 Task 1.3.1 Hetereogeneous Reservoir Interdisciplinary Database

During the reporting period, significant heterogeneous reservoir data for the project study site window areas was provided by Marathon Oil for posting on the project web site, http://heteroil.golder.com. This data is illustrated in Figures 3-7 through 3-10. The data posted to the project web site during the reporting period is summarized in Table 3-4.

Field	Data	Data Detail	Illustrative Figures
Yates	FMI Logs		
Yates	Core Logs		
Yates	Geological Background		
Stoney Point	Geological Background		
South Oregon Basin	Geocellular Data	depth, porosity, gamma ray, flexure	Figure 3-7
South Oregon Basin	Tracer Test Data	11 breakthrough curves	
South Oregon Basin	Geological Background		
North Oregon Basin	FMI Data	1 well	
North Oregon Basin	Core data	4 wells	Figure 3-10
North Oregon Basin	Geocellular Data	depth, porosity, gamma ray, flexure	Figure 3-8
North Oregon Basin	Tracer Test data	16 breakthrough curves	Figure 3-9
North Oregon Basin	Geological Background		

Table 3-4 Heterogeneous Reservoir Interdisciplinary Database

3.2.3 Tasks 2.X.2 Preliminary DFN Model Development, North Stoney Point

The geologic and development background of the reservoir are reviewed in the first project report (Dershowitz, 1999). The Stoney Point Field produces from a linear trend of dolomitized carbonates in the Trenton and Black River Group of Southern Michigan (Figure 3-11). During the second reporting period, we derived and implemented a preliminary Discrete Feature Network (DFN) model for the Trenton Formation of the Stoney Point Field. This preliminary model will be applied for initial design of IOR projects using techniques such as those demonstrated in Section 3.2.6 below.

3.2.3.1 Task 2.2.2 Derivation of DFN Model Parameters

Discrete Feature Network (DFN) models are derived through a combination of spatial and stochastic distributions for spatial structure, orientation, size, intensity, and mechanical/hydraulic properties of important structural features. These distributions can be derived from any combination of well, surface mapping, geophysical, and geological

information. For the Stoney Point field, we have built the preliminary DFN model based primarily on geological information. This model was designed to focus on compartmentalization issues, and was therefore built at the compartment scale, which is approximately 500 m.

3.2.3.1.1 Spatial Model, Reservoir Structure, and Conceptual Model

The compartments or sub-reservoirs at Stoney Point are controlled by a set of *en echelon* shear faults above a basement strike-slip fault. Hurley and Budros (1990) interpreted synclinal sags on seismic data to delineate the faults along which carbonate dissolution and dolomitization has taken place (Figure 3-12). This map was used to develop an initial conceptual DFN model of a fault pair. Reservoir compartments along each fault are hypothesized to be formed by fracturing along Riedel shears in ~200 m (~750′) wide zones (Figure 3-13). Riedel shears form at an angle of ~15° to the shear plane (Twiss and Moores, 1992). The areas between faults tips are also hypothesized to be zone of intense fracturing. In the fault step-over region, fractures would be related to tension rather than shear and thus have an EW orientation (Figure 3-13).

3.2.3.1.2 Orientation

Three fracture sets are hypothesized for the Stoney Point site based on the geological conjecture described in the previous section:

- Riedel Shears along the faults,
- Tension fractures in fault step-overs, and
- Background fractures.

The mean pole of the Riedel shears along the strike-slip faults is assumed to have a trend of 30° and a plunge of 0°. The dispersion coefficient (κ) was set to 20 to produce a range of orientations from 10 to 50°.

The mean pole of the tension fractures in the step-over region is assumed to have a trend of 0° and a plunge of 0°. The dispersion coefficient (κ) was set to 30 to produce a range of orientations from -15 to 15°.

Background fractures were assumed to be defined by a uniform orientation distribution (Fisher $\kappa=0$). Locations for background fractures are distributed with uniform intensity in space by a Poisson process.

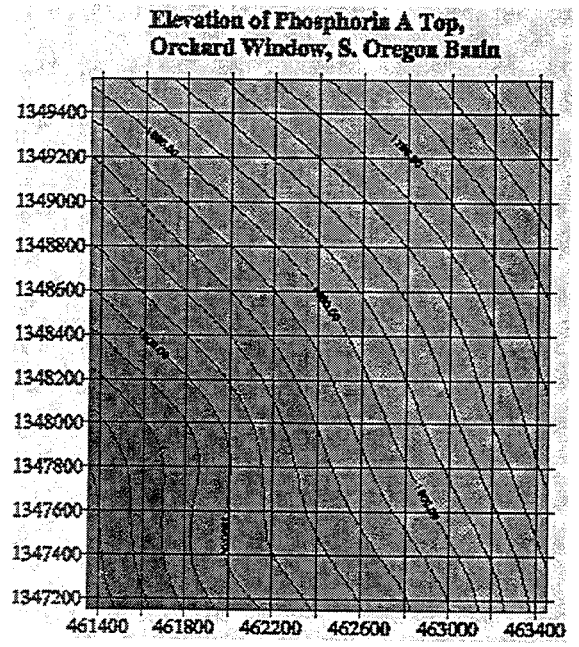

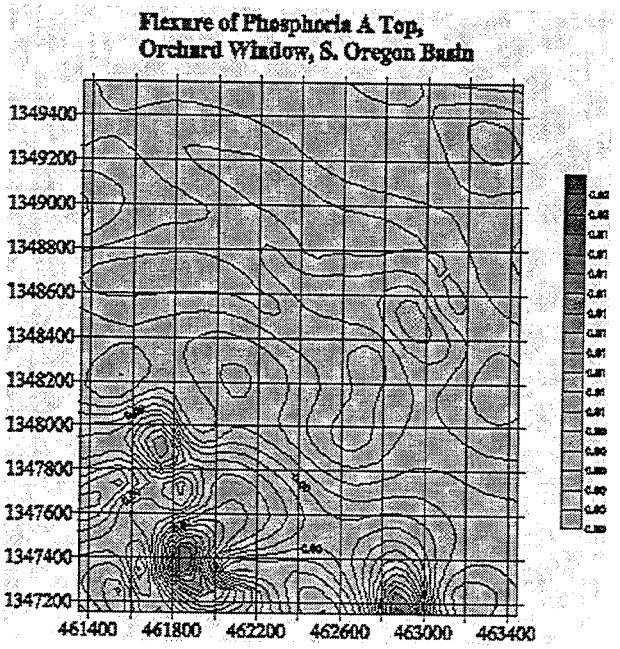

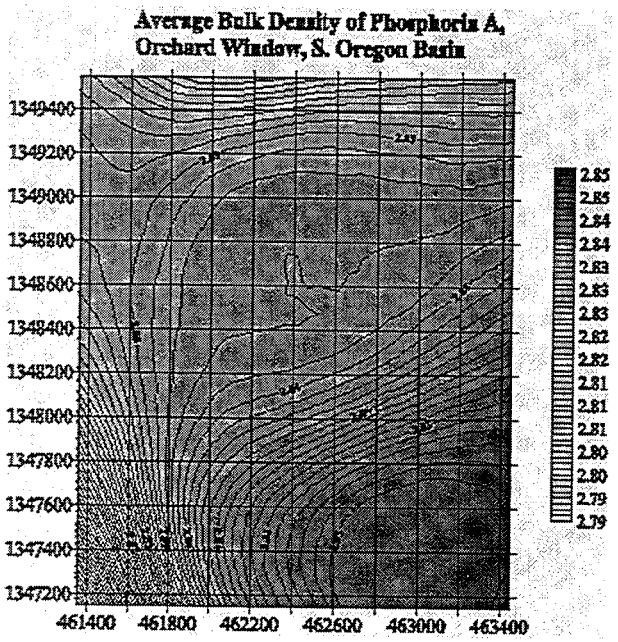

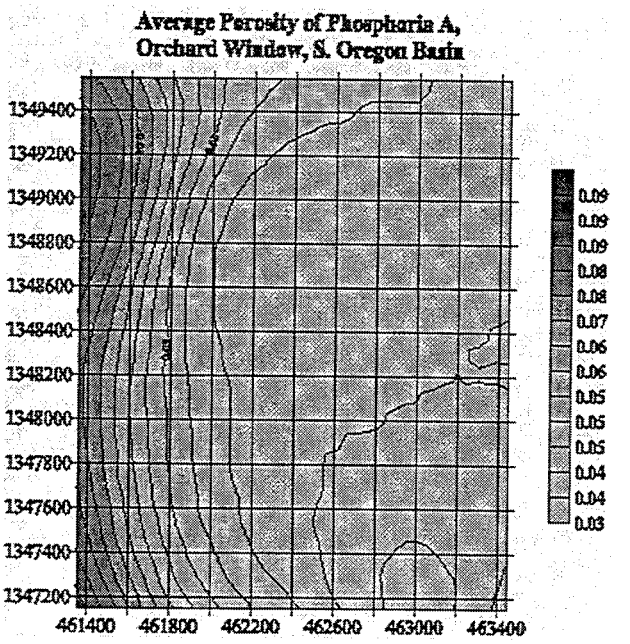

FIGURE **3-7**

EXAMPLE STRATAMODEL DATA FROM SOUTH OREGON BASIN

NPTO

PROJECT NO. 983 1258.521 DRAWING NO. 85010 DATE 7/29/99 DRAWN BY TK

Golder Associates

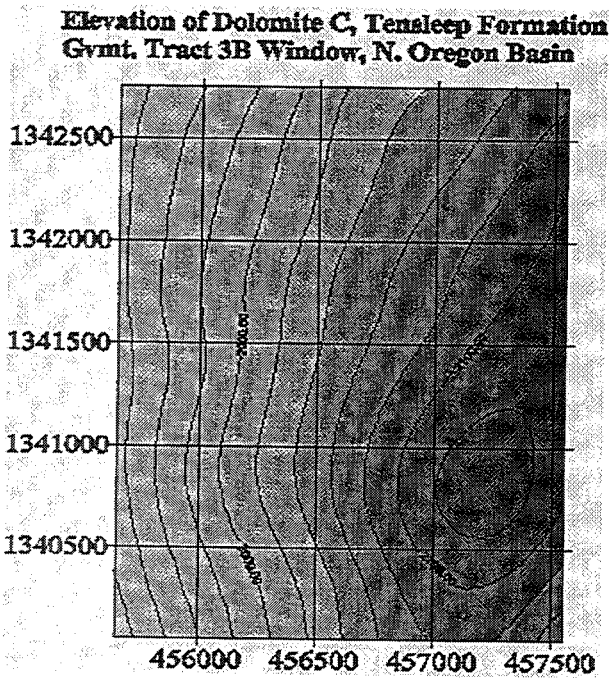

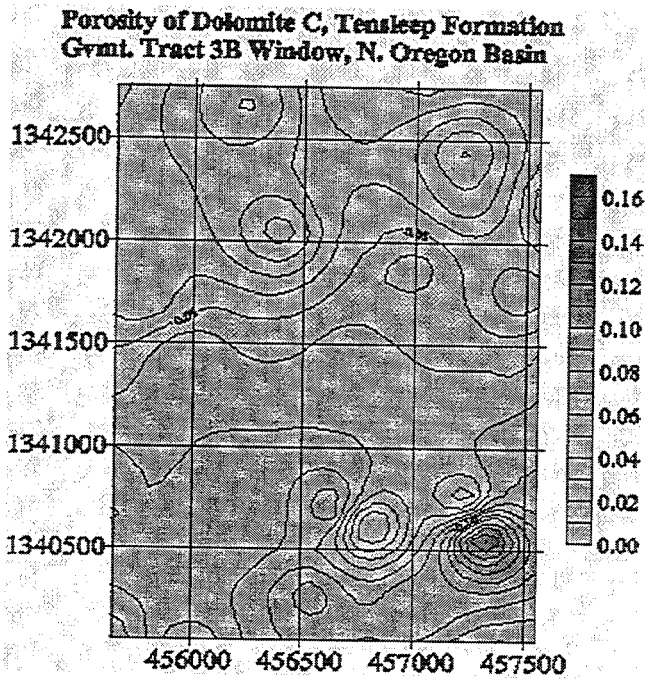

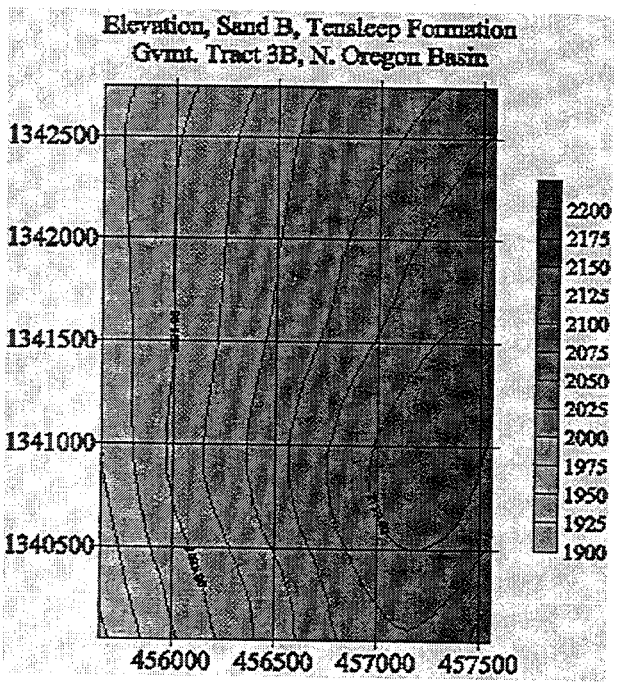

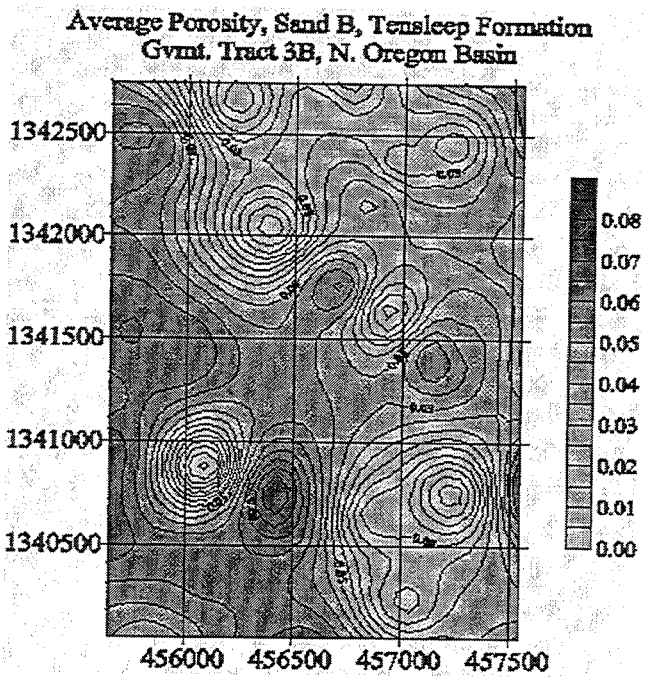

FIGURE **3-8**

EXAMPLE STRATAMODEL DATA FROM NORTH OREGON BASIN

NPTO

PROJECT NO. 983 1258.521 DRAWING NO. 85011 DATE 7/29/99 DRAWN BY TK

Golder Associates

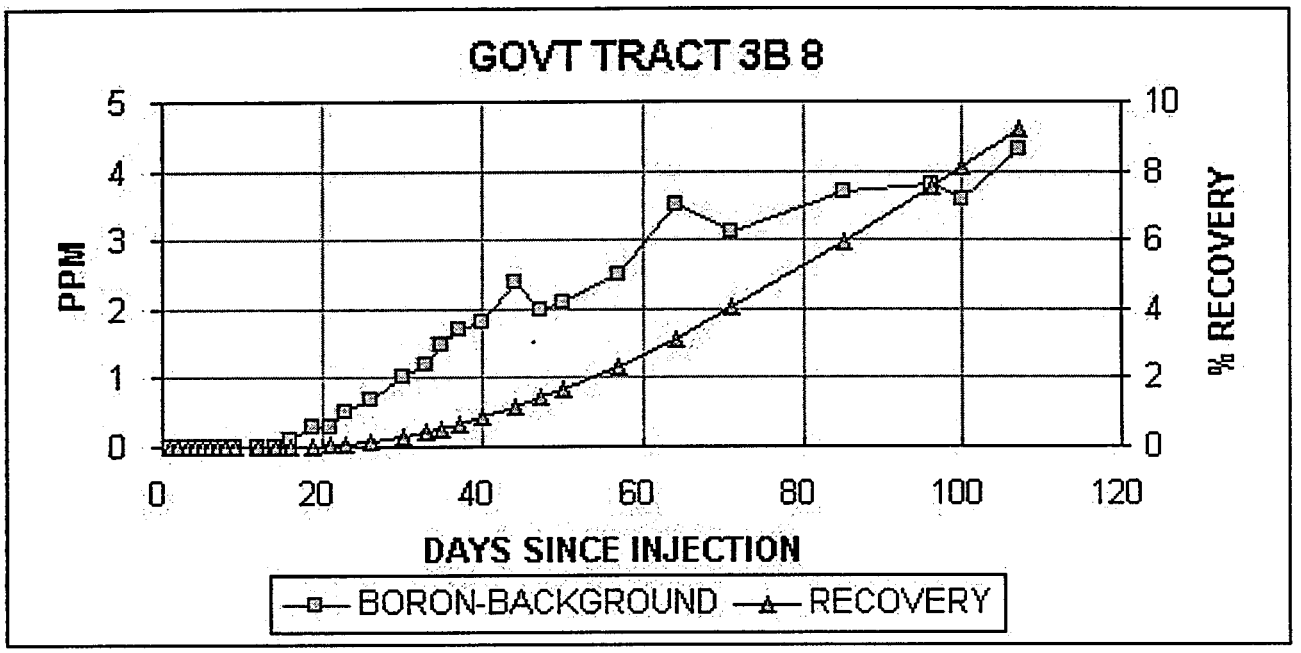

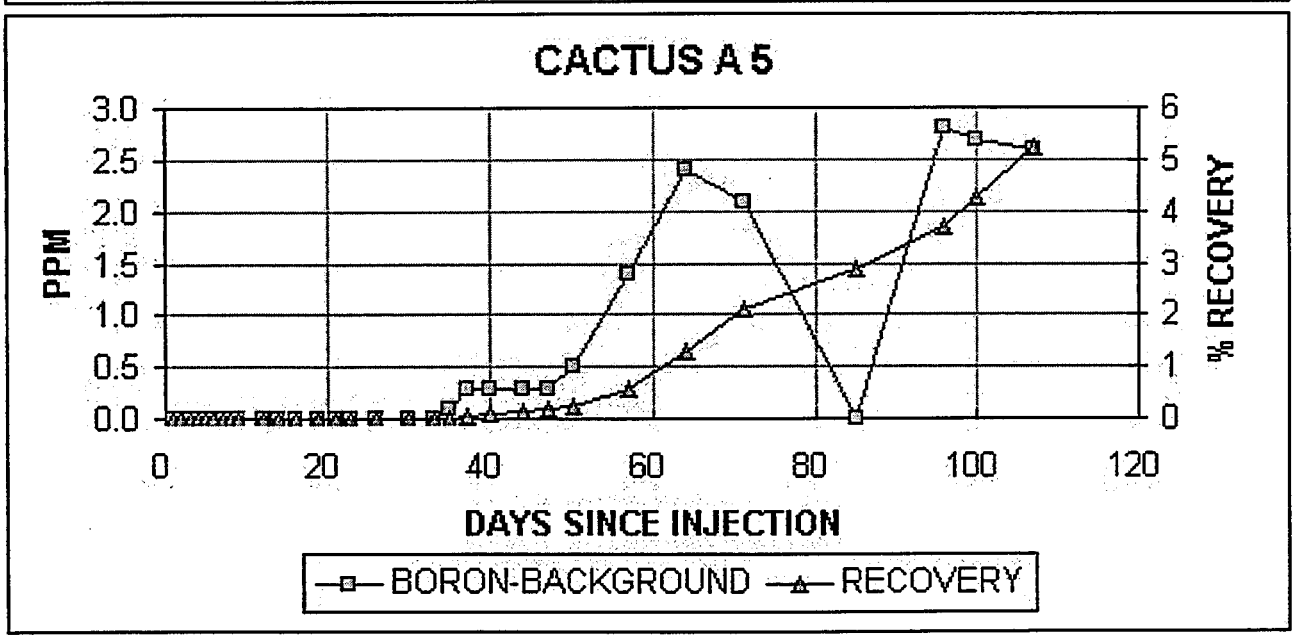

FIGURE **3-9**
EXAMPLE TRACER BREAKTHROUGH CURVES FROM NORTH OREGON BASIN
NPTO

PROJECT NO. 983 1258.521 DRAWING NO. 85012 DATE 7/29/99 DRAWN BY TK

Golder Associates

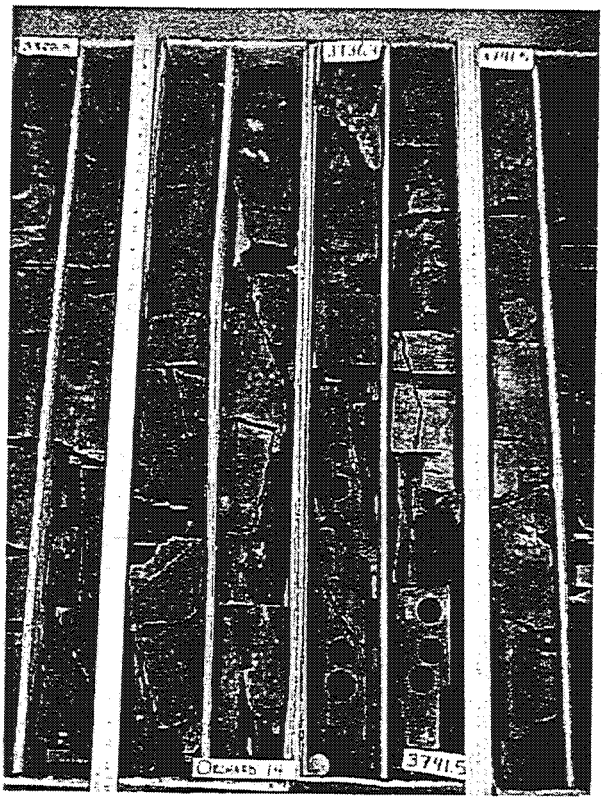

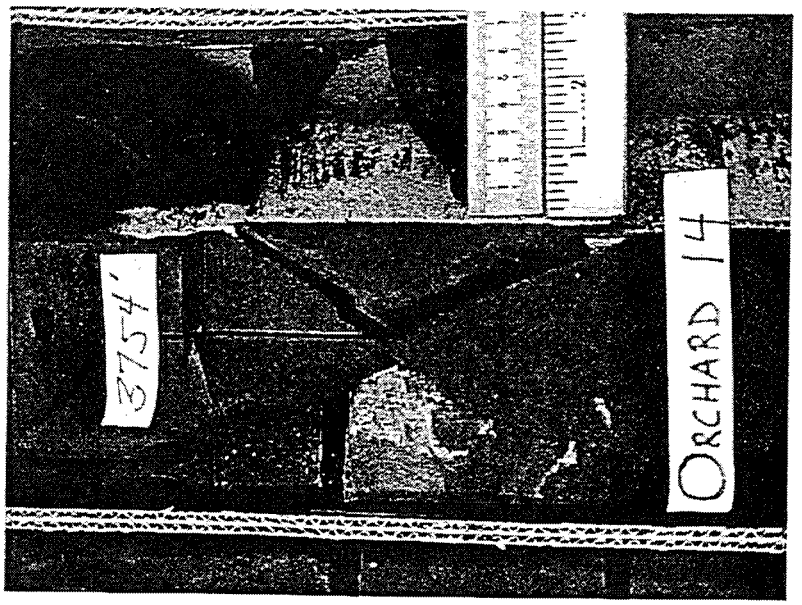

FIGURE **3-10**
CORE PHOTOS FROM ORCHARD 14, NORTH OREGON BASIN
NPTO

PROJECT NO. 983 1258.521 DRAWING NO. 85013 DATE 8/9/99 DRAWN BY TK

Golder Associates

3.2.3.1.3 Size and Intensity

Unfortunately, no definitive data on fracture size or conductive fracture intensity have yet been identified for the Stoney Point site. Fracture size and intensity was therefore studied through sensitivity studies. Once fracture size distribution case, and four intensity cases were developed, in order to produce DFN models with a range of connectivities. These cases are listed in Table 3-5.

The fracture size distribution assumed was based on the scale of model being considered. Since the model being considered is on the scale of 500 feet, the fractures which controls flow should be larger than approximately 10% of the model scale. The fracture size distribution was therefore defined assuming a truncated exponential fracture size with a mean radius of 66 feet (20 m). All fractures with radii less than the mean (66 feet) were excluded in the preliminary modeling. The same distributional assumption was used for all three sets.

Intensity in DFN modeling is expressed in terms of volumetric intensity P_{32}, the total feature area (m^2) per volume (m^3). The four fracture intensity cases varied from intensities of 0.001 m^2/m^3 to 0.3 m^2/m^3 per set, where. The highest fracture intensity model had a volumetric fracture intensity (P_{32}) of 0.01 m^2/m^3 in the Riedel shear set and an intensity of 0.3 m^2/m^3 in the tension fracture set. These values translate to 1228 and 1030 fractures in each set, respectively. The lowest fracture intensity model had a volumetric fracture intensity (P_{32}) of 0.001 m^2/m^3 in the Riedel shear set and an intensity of 0.03 m^2/m^3 in the tension fracture set. A 90% reduction in intensity results in a 90% reduction in fracture numbers; therefore, the lowest intensity set has 124 and 106 fractures in each set, respectively. All models have the same intensity of background fractures away from the faults: an intensity of 0.005 m^2/m^3 for a total of about 650 background fractures.

3.2.3.2 Task 2.3.2 DFN Model Implementation

Four preliminary DFN models of the Trenton formation at the Stoney Point Field were constructed using the parameters derived above and summarized in Table 3-5. Three-dimensional views of this conceptual model are shown in Figure 3-14 and Figure 3-15. The orientations of the fractures in the model are illustrated in the stereoplots of Figure 3-16. These models were used in preliminary compartmentalization calculations in support of IOR projects as described in Section 3.2.6 below.

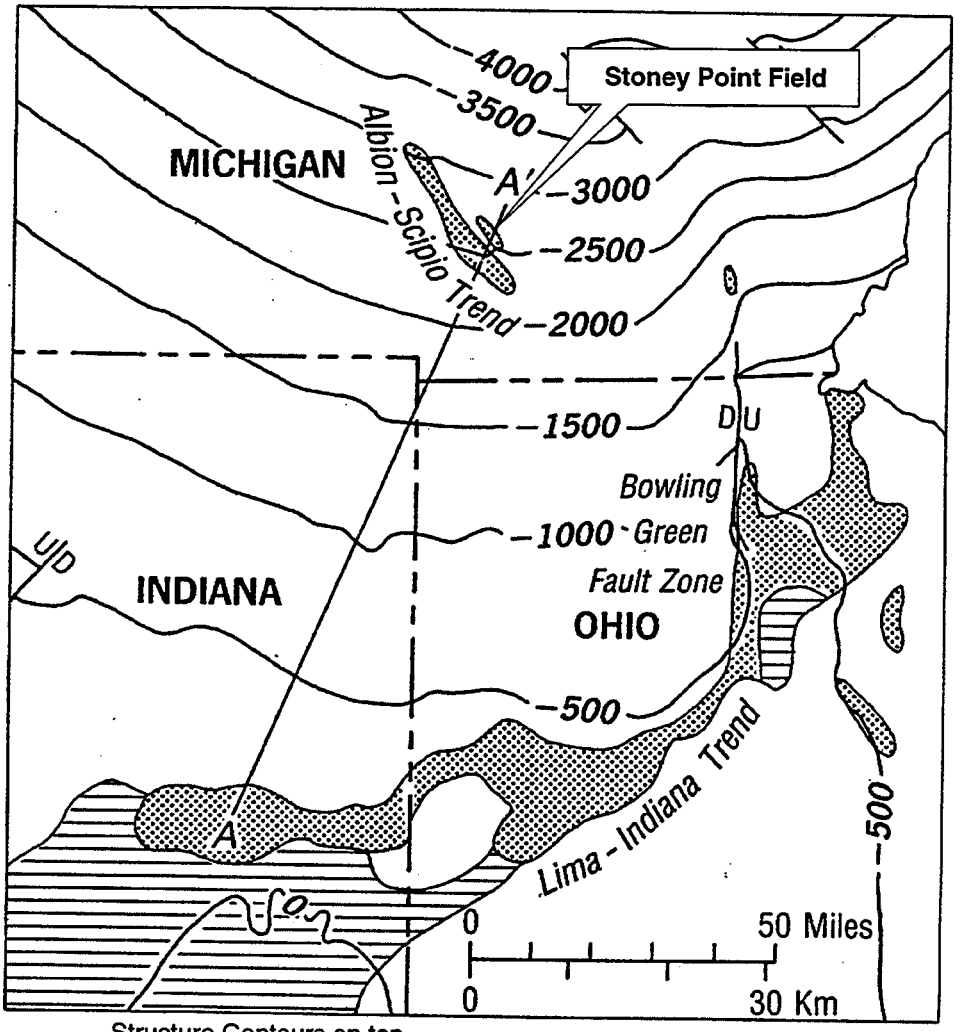

Structure Contours on top of the Trenton Limestone

UPPER ORDOVICIAN PRODUCTION

Oil Gas

FIGURE **3-11**

LOCATION MAP OF STONEY POINT FIELD

NPTO

PROJECT NO. 983 1258.521 DRAWING NO. 85014 DATE 7/29/99 DRAWN BY TK

Golder Associates

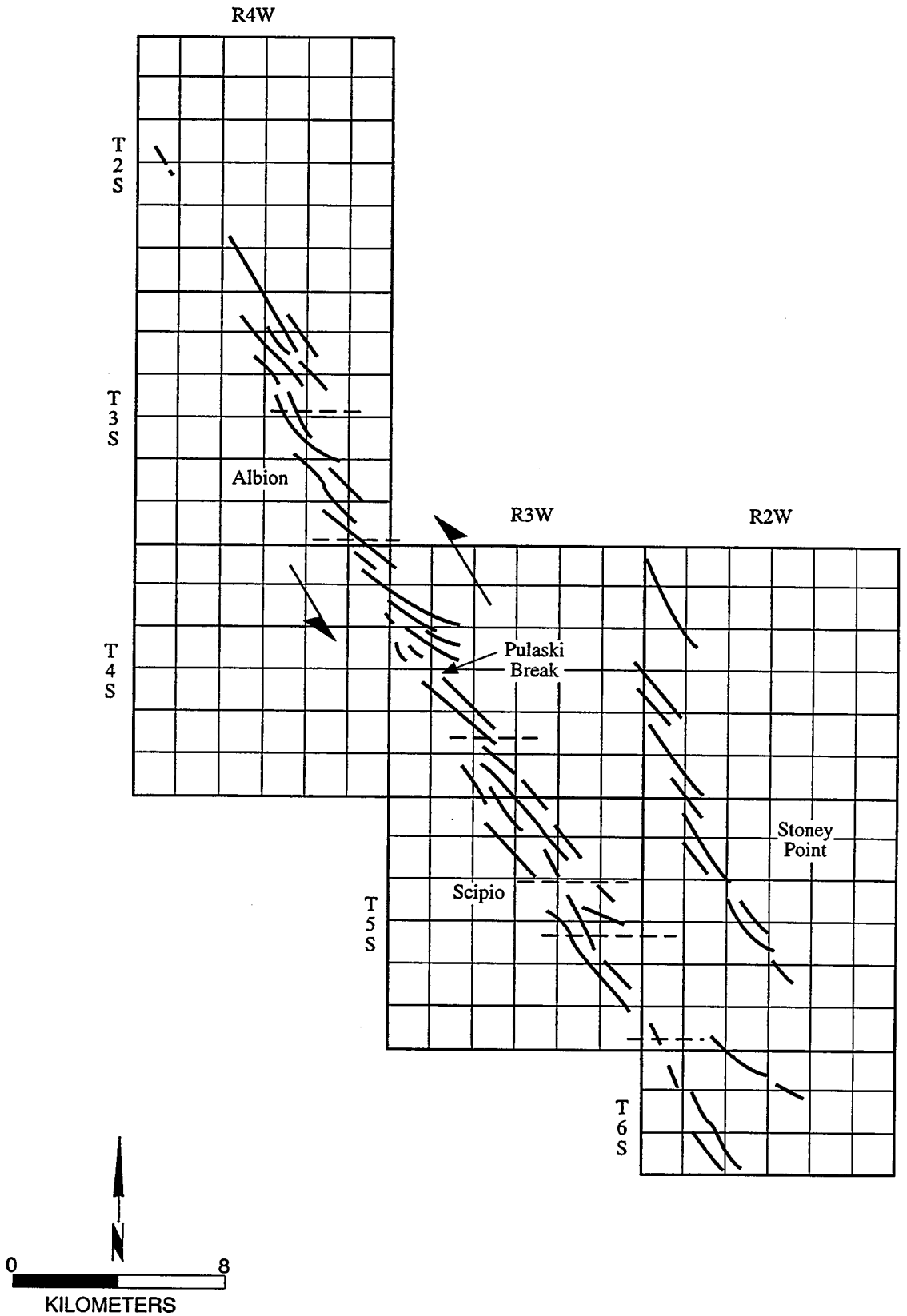

After Hurley and Budros, 1990

FIGURE **3-12**
FAULTS INTERPRETED AT STONEY POINT FIELD
NPTO/STONEY POINT

PROJECT NO. 983 1258.521 DRAWING NO. 85015 DATE 7/29/99 DRAWN BY TK

Golder Associates

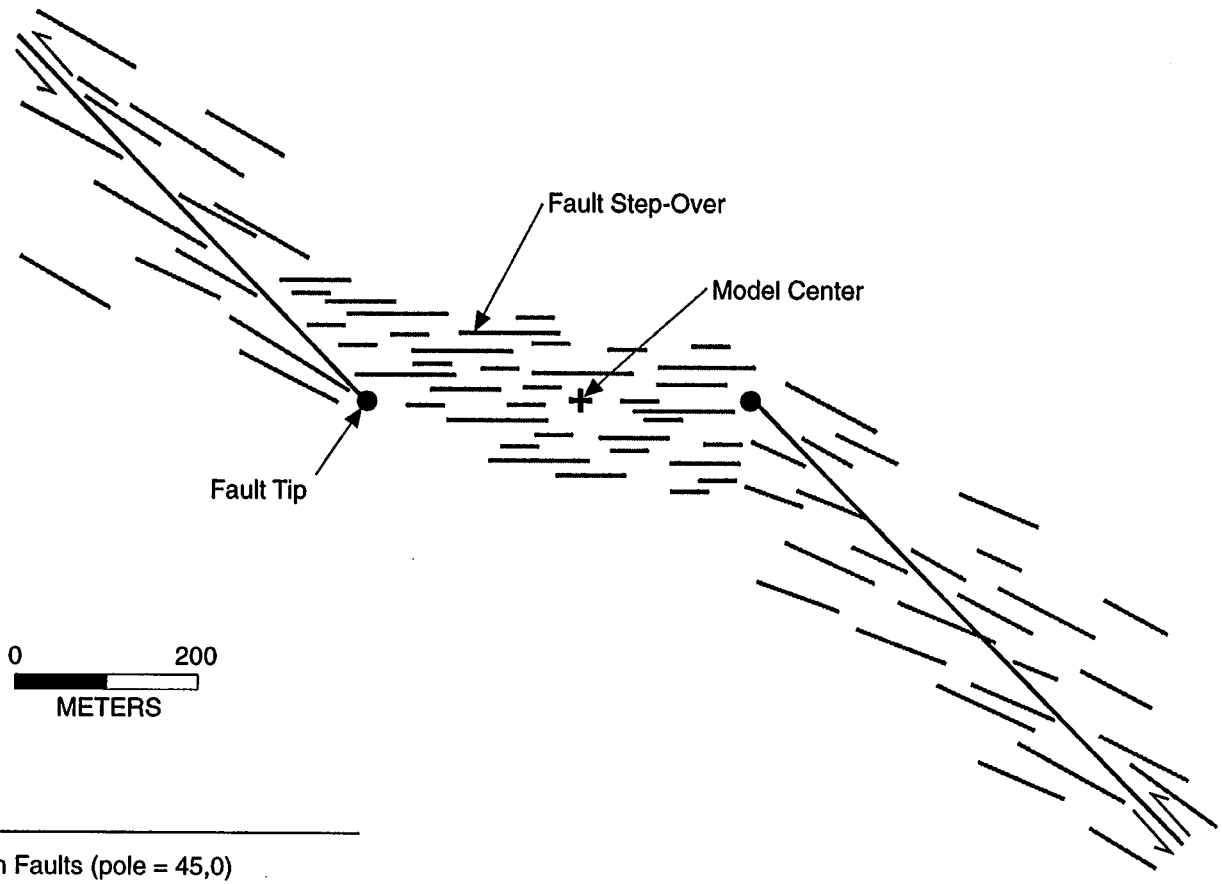

LEGEND

- Main Faults (pole = 45,0)
- Riedel Shears (pole = 30,0 K = 20)
- Tension Fractures in Step-Over Slab Region (pole = 0,0 K = 30)

FIGURE **3-13**

STONEY POINT CONCEPTUAL MODEL

NPTO

PROJECT NO. 983 1258.521 DRAWING NO. 85016 DATE 7/26/99 DRAWN BY EA

Golder Associates

	Parameter	Basis
Fault Model DFN		
Generation Region	Adjacent to deterministic faults only	Figure 3-13
Conceptual Model	Nearest Neighbor, Exponent=10^7	Conceptual Model
Fracture Orientation	Fisher Distribution Mean Pole (Trend,Plunge)= (30,0) Dispersion $\kappa = 20$	Conceptual Model
Fracture Size	Exponential Mean = 20 m, Min. =20 m	Conceptual Model
Fracture Intensity	$P_{32} = 0.01\ m^{-1}$ (N=1228) $P_{32} = 0.005\ m^{-1}$ (N=615) $P_{32} = 0.0025\ m^{-1}$ (N=316) $P_{32} = 0.001\ m^{-1}$(N=125)	Sensitivity Assumption
Fracture Aperture	$1x10^{-6}$ m	Sensitivity Assumption
Fracture Transmissivity	$1x10^{-6}\ m^2/s$, LogNormal Distribution Standard Dev. = $5x10^{-7}\ m^2/s$	Sensitivity Assumption
Fault Tip Model DFN		
Generation Region	700 m x 250 m x 165 m 0.4 mile x 0.15 mile x 550 feet	Figure 3-13
Conceptual Model	Enhanced Baecher	Conceptual Model
Fracture Orientation	Fisher Distribution Mean Pole (Trend, Plunge)= (0,0) Dispersion $\kappa = 30$	Conceptual Model
Fracture Size	Exponential Distribution Mean = 20 m, Min. = 20 m	Conceptual Model
Fracture Intensity	$P_{32} = 0.3\ m^{-1}$ (N=1030) $P_{32} = 0.15\ m^{-1}$ (N=542) $P_{32} = 0.075\ m^{-1}$(N=246) $P_{32} = 0.03\ m^{-1}$(N=106)	Assumption
Fracture Aperture	$1x10^{-6}$ m	Assumption
Fracture Transmissivity	$1x10^{-6}\ m^2/s$ LogNormal Distribution Standard Dev. = $5x10^{-7}\ m^2/s$	Assumption
Background Fractures		
Generation Region	2000 m x 2000 m x 165 m ~1.2 mile x ~1.2 mile x 500 feet	Figure 3-13 and thickness of Trenton Formation
Conceptual Model	Enhanced Baecher	Conceptual Model
Fracture Orientation	Fisher Distribution Mean Pole (Trend, Plunge)= (0,0) Dispersion $\kappa = 0$ (Uniform)	Conceptual Model
Fracture Size	Exponential Distribution Mean = 20 m, Min. = 20 m	Conceptual Model
Fracture Intensity	$P_{32} = 0.005m^{-1}$ (N=~649)	Assumption
Fracture Aperture	$1x10^{-6}$ m	Assumption
Fracture Transmissivity	$1x10^{-6}\ m^2/s$ LogNormal Distribution Standard Dev. = $5x10^{-7}\ m^2/s$	Assumption

Table 3-5 Stoney Point DFN Model Parameters, Trenton Formation

3.2.4 Tasks 2.X.3 Preliminary DFN Model Development, South Oregon Basin (Phosphoria)

At South Oregon Basin (SOB) the window area chosen for the demonstration of the Discrete Feature Approach for production enhancement is the Orchard lease on the northeast flank of the dome (Figure 3-20). The target formation for increased oil recovery (IOR) is the Phosphoria, and the discrete features of the most importance are fractures. During the reporting period, extensive research was carried out on the geological background of both the South and North Oregon basins to support DFN model development. Section 3.2.4.1 below is applicable to both the South and North Oregon Basin sites. Sections 3.2.4.2 and 3.2.4.3 below describe derivation and implementation of the DFN model for the South Oregon Basin. The North Oregon Basin DFN model derivation is described in Section 3.2.5.

3.2.4.1 Task 2.2.3 Geological Background, North and South Oregon Basins

The Oregon Basin Oil Field consists of two domes separated by a small saddle. Production from a Paleozoic oil pool in the Phosphoria Formation carbonate, Tensleep Sandstone, and the Madison limestone has been over 350 MMBO since the discovery of oil in 1927 (Stone, 1984). Reservoir heterogenieties effect the improved oil recovery (IOR) programs at both the North Dome and the South Dome.

3.2.4.1.1 Tectonic Setting

The Oregon Basin Field is the largest of many oil-producing anticlines in the Big Horn Basin of northwestern Wyoming and southwestern Montana (Figure 3-17). These fields produce from the Paleozoic section, which includes the marine Phosphoria carbonate and the eolian Tensleep sandstones as well as the Madison limestone. The Big Horn Basin is both a topographic and structural basin surrounded by the Big Horn, Owl Creek, Abasaroka, and Beartooth Mountains. The basin is a foreland fold-thrust belt formed by northeast-southwest Laramide compression during the Late Cretaceous.

The Oregon Basin field is an asymmetric, anticline with over 5000′ total relief. The anticline is evident at surface (Figure 3-18) and the discovery of the field was based entirely on geologic mapping (Hewett, 1926). The northeast flank of the anticline is bounded by the Oregon Basin thrust, a fault with approximately 20,000 feet of displacement (Figure 3-19). In the footwall of this thrust is the syncline at the axis of Big Horn valley. The southwest flank of the field anticline is bound by the Wiley Reverse fault, a backthrust with ~1500 feet of displacement (Figure 3-19).

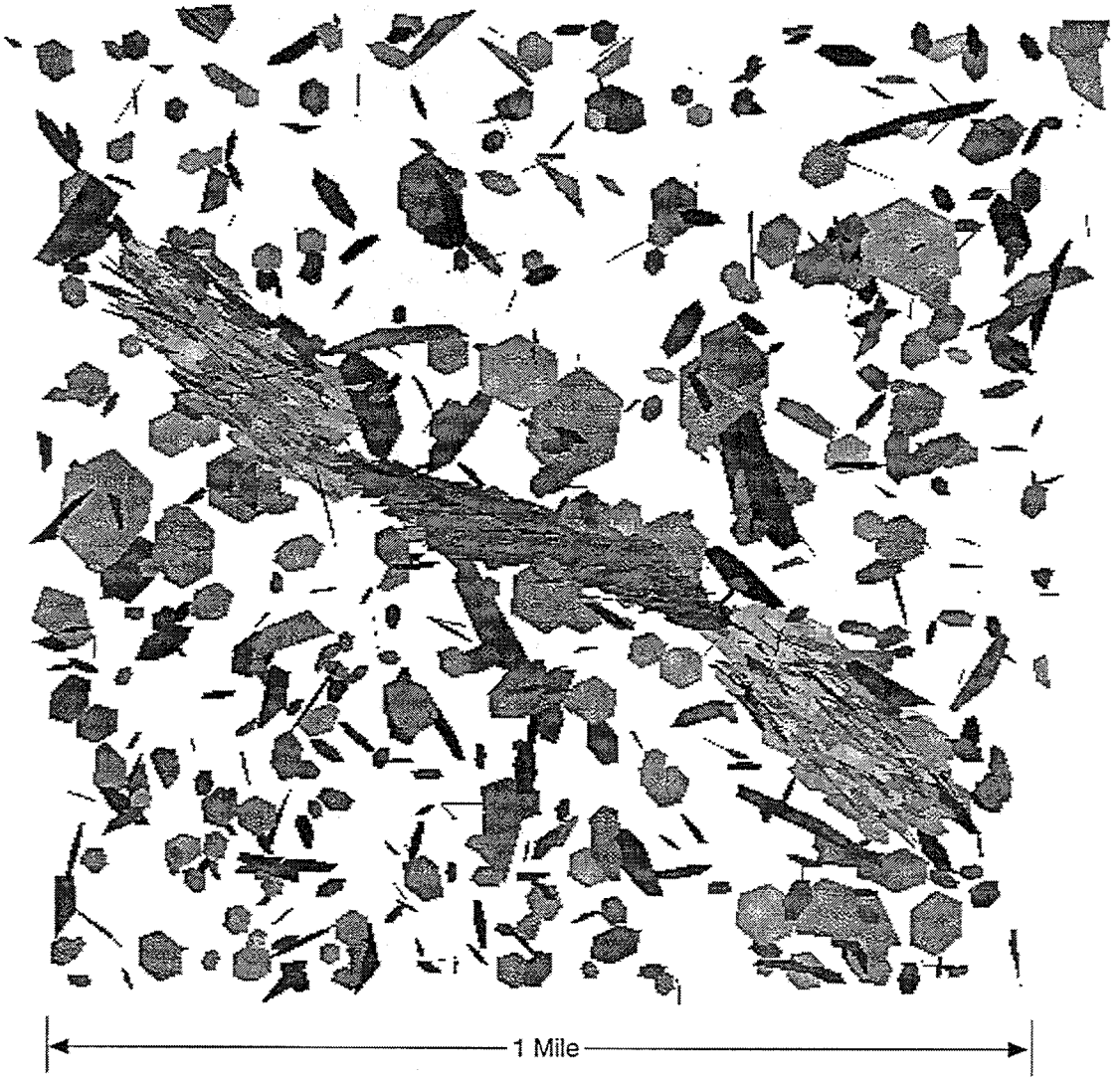

FIGURE **3-14**

CONCEPTUAL DFN MODEL AT STONEY POINT
TOP VIEW
NPTO

PROJECT NO. 983 1258.521 DRAWING NO. 85017 DATE 7/29/99 DRAWN BY EA

Golder Associates

FIGURE **3-15**

CONCEPTUAL DFN MODEL AT STONEY POINT
SIDE VIEW
NPTO

PROJECT NO. 983 1258.521 DRAWING NO. 85018 DATE 7/29/99 DRAWN BY EA

Golder Associates

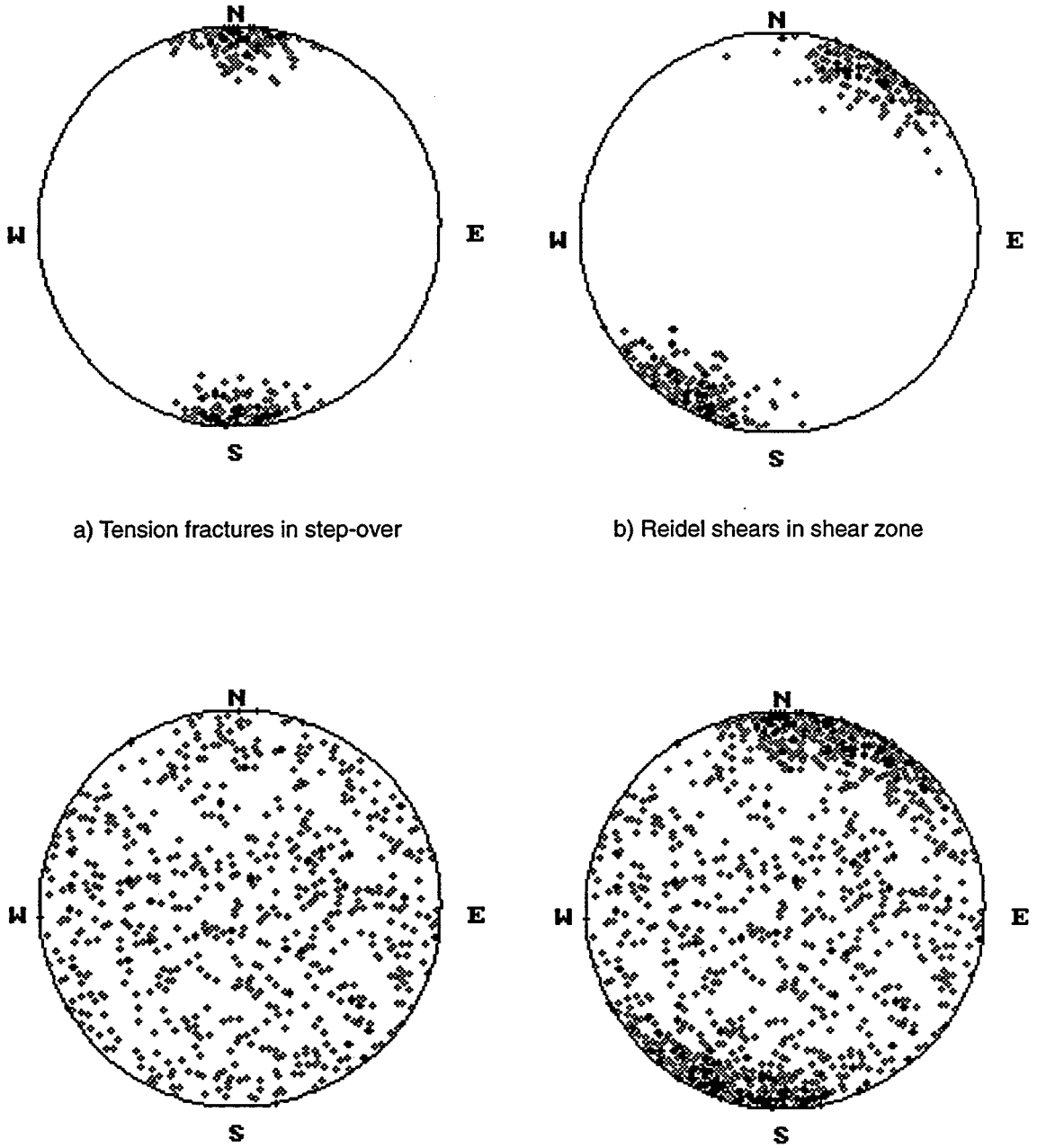

a) Tension fractures in step-over

b) Reidel shears in shear zone

c) Background fractures

d) All fractures

FIGURE **3-16**
FRACTURE ORIENTATIONS IN STONEY POINT CONCEPTUAL DFN MODEL
NPTO

PROJECT NO. 983 1258.521 DRAWING NO. 85019 DATE 7/29/99 DRAWN BY EA

Golder Associates

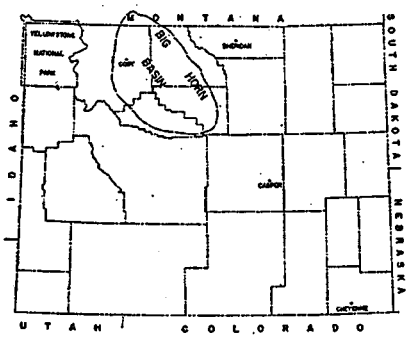

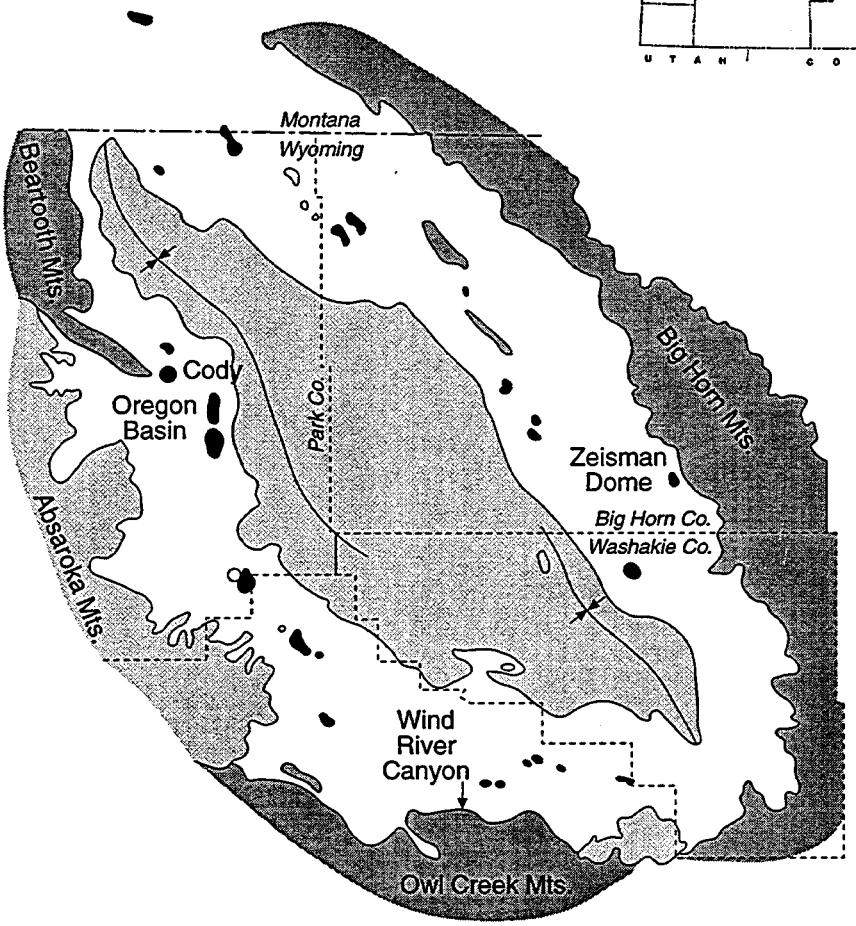

Eocene and Later Tertiary Beds

Paleocene and Mesozoic Fms.

Paleozoic and Older Rocks

Oil and Gas Field

Gas Field

from Walton, 1947

FIGURE **3-17**

MAP OF BIG HORN BASIN SHOWING LOCATION OF OREGON BASIN FIELDS

NPTO

PROJECT NO. 983 1258.521 DRAWING NO. 85020 DATE 7/29/99 DRAWN BY TK

Golder Associates

from Pierce, 1997

FIGURE **3-18**
SURFACE GEOLOGIC MAP OF OREGON BASIN FIELDS
NPTO/NOB

PROJECT NO. 983 1258.521 DRAWING NO. 85021 DATE 7/29/99 DRAWN BY TK

Golder Associates

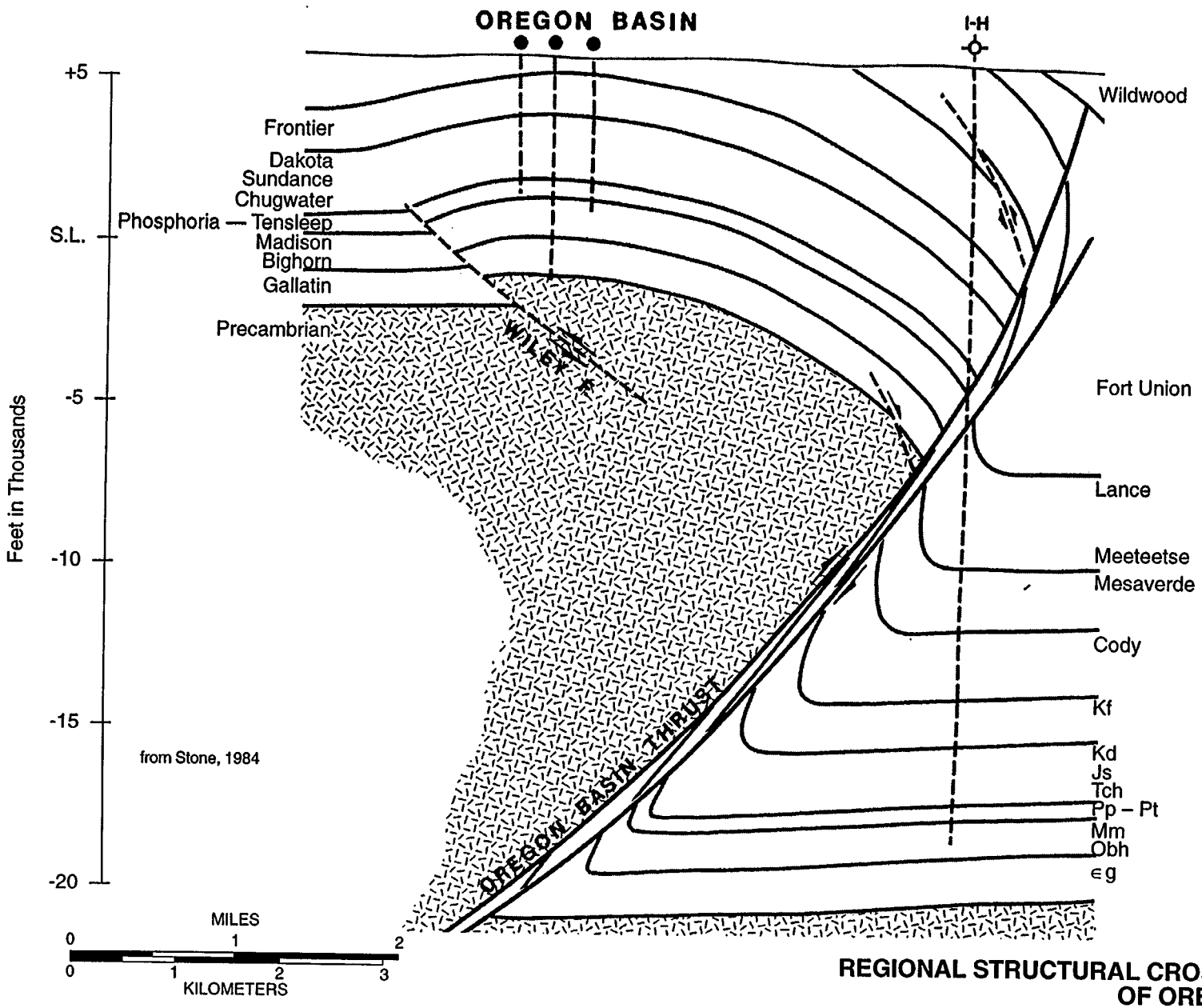

FIGURE **3-19**

REGIONAL STRUCTURAL CROSS-SECTION OF OREGON BASIN

NPTO

PROJECT NO. 983 1258.521 DRAWING NO. 85022 DATE 7/29/99 DRAWN BY TK

Golder Associates

3.2.4.1.2 Data Sources and References

A significant portion of the effort this reporting period was devoted to collecting, compiling, and analyzing well and seismic data for the Oregon Basin fields. Data was transmitted to Golder by Brendan Curran of Marathon Oil Company's Cody office. The data includes Formation Microimager® (FMI) logs for seven wells, seismic data for South Oregon Basin, and tracer test results for both fields (Table 3-6). The FMI logs were the primary source for developing the preliminary DFN models. In late June 1999, Golder personnel visited Cody, Wyoming to meet with Marathon geologists and geophysicists and investigate outcrops of the reservoir rocks. The information collected on this trip will provide further refinement of the current DFN models. Cyclic validation, iteration of data analysis, DFN model construction, flow simulations and sensitivity analysis, is always an important aspect of the DFN approach.

FMI	
FMI interpretations (paper)	Not available yet
FMI interpretations (files)	fracture orientations and depths in tables in report 2 wells in South Oregon Basin 5 wells in North Oregon Basin (one horizontal)
FMI reports	by Neil Hurley for individual wells and field
Location Maps for FMI logs	yes
Neutron porosity & FracView logs	2 wells in South Oregon Basin, 5 wells in North Oregon Basin
Seismic (South Oregon Basin only)	
Basemap	yes
Seismic Lines w/ interps	6 lines, 6 traces
stratamodel	eventually
maps	Gros Ventre and Phosphoria edge
magnetic field maps	raw, bougier, and edge
Tracer Tests	**30 in South Oregon Basin, 20 in North Oregon Basin**
Well locations	map for each test
Breakthrough curves	~300
Injection Curves	Not currently available
Pumping/Injecting Rates	Not currently available
Tracers used	phpa, bromide, rhodamine

Table 3-6 North and South Oregon Basin Data sources

In addition to the proprietary data provided by Marathon, a literature search of Big Horn Basin references was performed. Hewett (1926) and Walton (1947) provided important information on field discovery, early development, and stratigraphy. Although the data is now 20 years old, two articles by Marathon engineers and geologists, Morgan et al. (1977) and Cordiner & Livingston (1977) provide important information on reservoir characterization and engineering development plans. Finally, interpretation of a deep seismic line across the

Oregon Basin by Stone (1984) provides important information on the structural setting of the field.

In addition to the above journal published articles, recent abstracts and reports of research performed under the direction by Dr. Thomas Dunn of the University of Wyoming and Dr. Bryan Tapp of the University of Tulsa, will provide further information on the heterogenities in the Oregon Basin reservoirs. Dunn (1997) describes a DOE funded research project on the permeability structure of the Tensleep reservoir. Kerr and Tapp (1998) and Aviantara (1996) describe a cross-disciplinary study involving characterization of the deposition and deformation (including fracturing) of the Tensleep from surface outcrops at Ziesmann Dome. Both studies are ongoing and we anticipate collaboration with both professors and their students.

3.2.4.1.3 Stratigraphy

The Big Horn basin was part of a stable shelf throughout the Paleozoic and most of the Mesozoic. Overlying the Precambrian basement are Cambrian shales and interbedded limestones of the Gallatin and Gros Ventre formations (Table 3-7). These are relatively weak layers which can serve as a zones of thrust detachment (Stone, 1984). The Gallatin is followed by a lower Paleozoic section dominated by three, massive cliff forming marine carbonates (Big Horn, Jefferson, and Madison formations) with a total thickness over 1000 feet. After Madison time, the stable marine environment gave way to a more varied depositional environment in which the area was near sea level and sedimentation alternated between shallow marine and subariel. The upper Paleozoic formations above the Madison are the Amsden, Tensleep and Phosphoria formations. The latter two formations are the targets for increased oil recovery programs at the North and South Oregon Basins, respectively, and are described in more detail below.

The Tensleep formation is the most important reservoir rock of the Oregon Basin. Initially, the sandstones with minor interbedded carbonates were interpreted as marine (i.e. Walton, 1947; Todd, 1964). However, the most recent work (Dunn, 1997) interprets the Tensleep formation as recording six transgression-regression cycles. The regionally extensive marine carbonates represent high stands and the sandstones were deposited in crescentic dunes during times of falling relative sea level. The key to "Geologic map of the Cody 1x2 degree Quadrangle" (Pierce, 1997) described the Tensleep Sandstone as "(upper and Middle Pennsylvanian) - Light gray, well-sorted, crossbedded and massive sandstone; thin beds of gray limestone and dolomite in lower part. Thickness 40-75 m [130-250 feet]."

The Phosphoria formation is considered the hydrocarbon source rock in Oregon Basin. In the early days there was confusion about the name and age of this strata, confusion that has persisted. In 1947, Walton used the name Embar for an interbedded sequence of gray, finely crystalline, vuggy limestone and light bluish gray dolomite from an interval of both Triassic and Permian strata (Walton 1947). The term Phosphoria was introduced to denote the limestone portion of the section but as Walton pointed out ".. it is herein suggested that the term Embar is too well established among geologists and oil men to consider abolishing it when it is applied in its present usage .." Furthermore, on the *Geologic map of the Cody Quadrangle* (Pierce 1997), these strata are called the "Park City Formation (Lower Permian) – Siliceous limestone and dolomite, nodular chert, and tan and gray shale. Formerly called Phosphoria Formation in this area. Thickness 15-50 m."

The cap rocks for the Phosphoria reservoir are the Dinwoody Formation, 6-15 m of siltstone, gypsum, and dolomite, and the very thick (180-250 m) Chugwater Formation which is

siltstone, shale and sandstone. The remainder of the stratigraphy at the Oregon Basin is summarized in Table 3-7 and on the regional structural cross section (Figure 3-19).

3.2.4.1.4 Field Structure

The primary structure at the Oregon Basin fields is an asymmetric, west-verging anticline. The anticline is bound on the west by the Wiley thrust and on the east by the Oregon Basin thrust (Figure 3-19 and Figure 3-20). While total relief of the fold is over 5000 feet, relief in the field is about 1000´. Maximum bedding dips are 20º on the west limb of the fold; the east limb dips are around 10º. The two domes are separated by a small saddle 800 feet lower than the apex of the north dome and 1000 feet lower than the south dome (Morgan et al., 1977).

Secondary field structures in the Oregon Basin field are vertical tear faults. G.L. Brown's structure map of the fields (Figure 3-20) shows three NW-SE trending tear faults near the center of the North Oregon Dome and three NE-SW trending tears in on the south side of South Oregon Dome. Meanwhile, maps in Morgan et al. (1977) show general agreement in the South Oregon basin but four NE-SW (a change of orientation of 90° compared to Brown's map) trending faults in the North Oregon Basin. Because the Government Tract 3B window area (Figure 3-20) is in the vicinity of the faults mapped it will be very important to decide which structural setting for the window area is more accurate. Golder and Marathon discussed the discrepancy between the North Dome structure maps at a meeting in June 1999, and decided to use the structural model from Morgan et al. (1977).

In the South Oregon Basin, the Orchard lease window is far from the tear faults mapped on either map (Figure 3-20). 3D seismic data, which has been collected across the entire South Dome, will be instrumental in developing the DFN model at the Orchard lease. In particular, edge enhancement maps provided by Marathon (Figure 3-21 and Figure 3-22) are thought to provide information on the locations and sizes of tear faults in South Oregon Basin. The lineament on Figure 3-22 is quite pronounced, indicating that a major tear fault may cross the northern portion of the Orchard lease.

Symbol	Formation	thickness (south dome)	Lithology	Sed.Envir-onment
FRON	Frontier	490-600′	Massive sandstones	
MOWR	Mowry Shale	310-360′	Siliceous Shale	
KMR	Thermopolis	430′	Black, fissile shale	
MUDD	Lower Cretaceous Cloverly	180′	Siltstone, shale, and sandstone	Marine or littoral
DAKO	Upper Jurrassic Morrison	480-515′	Mudstone and shale with conglomeratic sandstone lenses	Flood-plain
SUND	Upper Jurrassic Sundance	410′	Glauconitic sandstone, calcareous shale, and mudstone and shale	Flood-plain
GYPS	Upper Jurrassic Gypsum spring	240′	Anhydrite and mudstone	Evaporite flats
Disconformity				
CHUG	Triassic Chugwater	625	Sandstones and siltstones interbedded with shale and mudstone	Estuarine
DINW	Triassic Dinwoody	30-45′	Shale and anhydrite	Marine or estuarine
PHOS	Triassic-Permian Phosphoria	250′	Limestone (also called Embar or Park City)	Marine
erosional unconformity				
TENS	Penn. Tensleep	20-190′	Cross-bedded and massive, well-sorted sandstone with dolomitic intervals	Marine/ eolian (coastal dune)
AMSD	Penn. Amsden	210′	Dolomite, shales and anhydrite. Basal sandstone	
erosional unconformity				
MADI MADB	Lower Miss. Madison	740′	Marine limestone, lower part dolomitized	Marine
	Devonian Jefferson	205'	Marine limestone	Marine
	Ordovican Big Horn	330′	Marine limestone and dolomite	Marine
	Cambrian Gallatin, Gros Ventre, and Flathead Sandstone			
unconformity, Precambrian Basement				

Table 3-7 Stratigraphy from Walton modified after Dunn

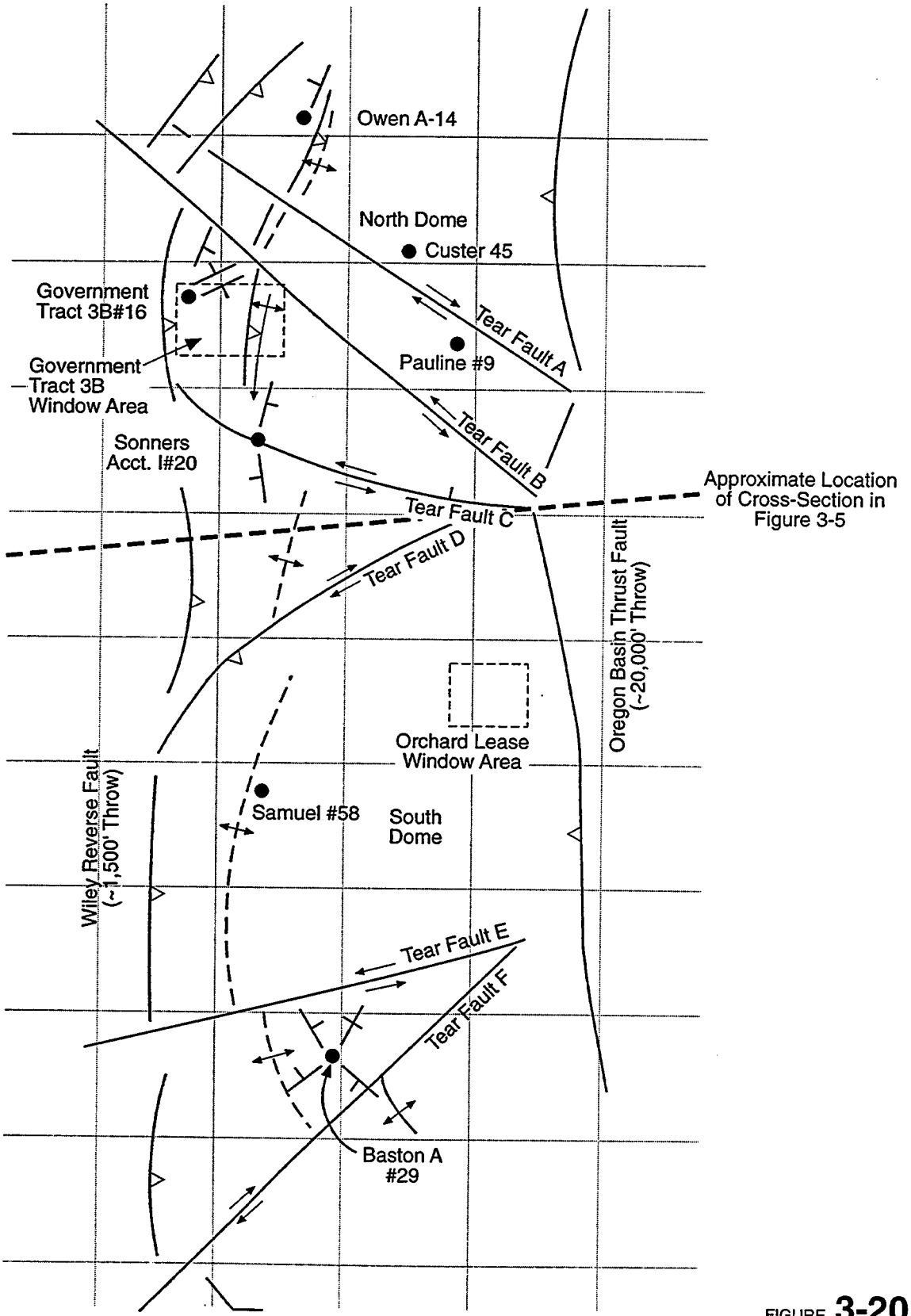

by G.L. Brown, 6/91

FIGURE **3-20**

PHOSPHORIA RESERVOIR STRUCTURE MAP WITH STRIKE AND DIP OF FMS FRACTURES SHOWN AT WELLS

NPTO

PROJECT NO. 983 1258.521 DRAWING NO. 85023 DATE 7/30/99 DRAWN BY TK

Golder Associates

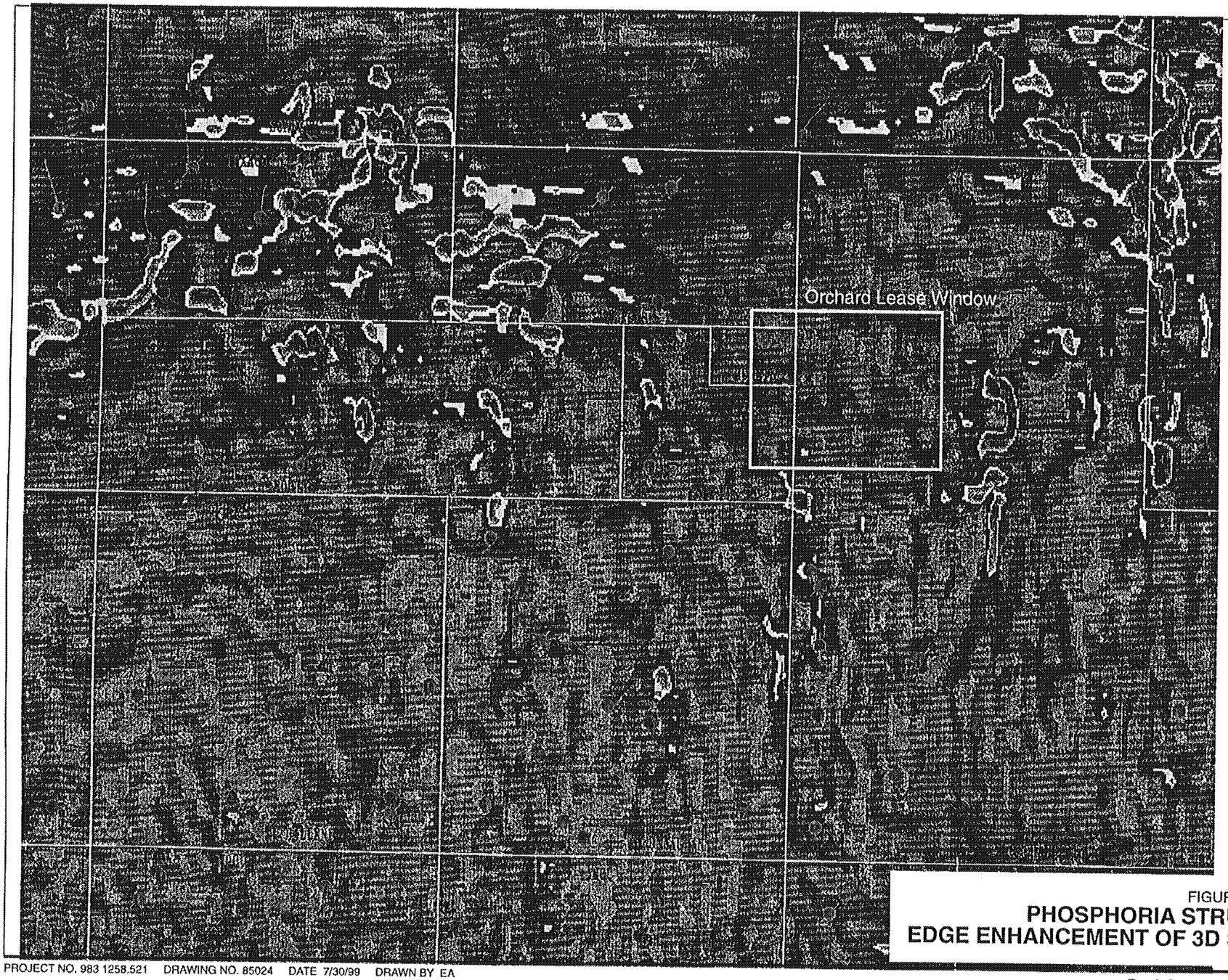

FIGURE **3-21**
PHOSPHORIA STRUCTURE
EDGE ENHANCEMENT OF 3D SEISMIC
NPTO

PROJECT NO. 983 1258.521 DRAWING NO. 85024 DATE 7/30/99 DRAWN BY EA

Golder Associates

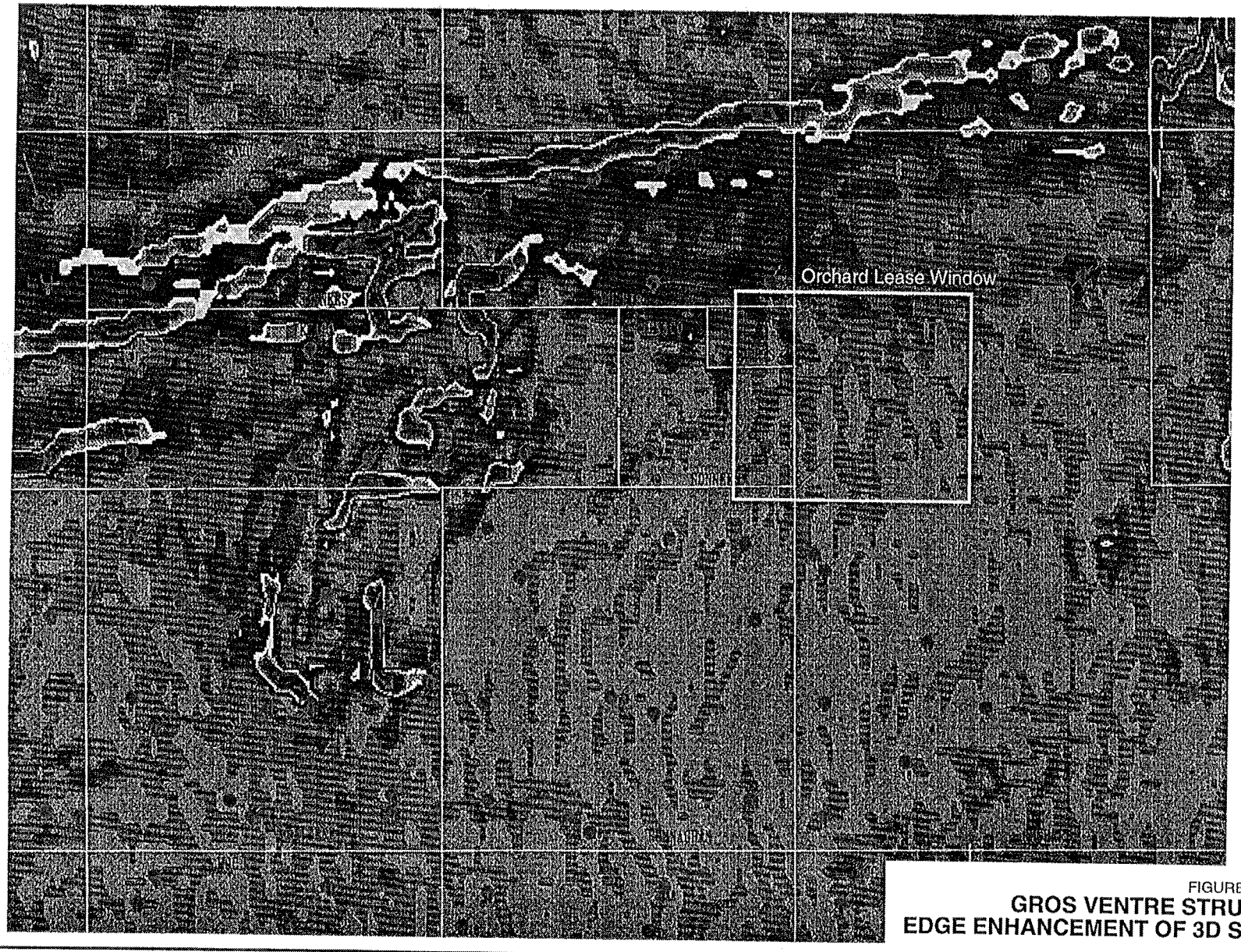

FIGURE **3-22**
GROS VENTRE STRUCTURE
EDGE ENHANCEMENT OF 3D SEISMIC
NPTO

PROJECT NO. 983 1258.521 DRAWING NO. 85025 DATE 7/30/99 DRAWN BY EA

Golder Associates

3.2.4.1.5 Reservoir Background

Gas was first discovered in the Dakota formation in South Oregon Basin in 1912. In 1927, oil was discovered at a depth of 3350' in the Embar (AKA Phosphoria) formation in the North Oregon Basin. This discovery was the first to produce the upper Paleozoic common pool in the Oregon basin which includes the Phosphoria, Tensleep, and Madison formations with a total oil column of 1500 feet (Walton, 1947; Stone, 1967). By 1984, the total production was over 350 MMBO with production at 10 MMBO per year at that time (Stone, 1984).

Both fields were unitized in 1947 with Marathon as the operator (Cordiner & Livingston, 1977). Water injection started in 1960's and until 1968, increased water brought increased oil production. At the peak, 50,000 B/D of water were injected and 9,000 B/D of oil produced (Cordiner & Livingston, 1977). In 1968 production dropped when water breakthroughs occurred in wells near the water-oil contact.

3.2.4.1.6 June 1999 Field Visit Report

Drs. Paul La Pointe and Trenton Cladouhos of Golder Associates visited Marathon's Cody, Wyoming office on June 21-23,1999, in order to visit with engineers, geologists, and geophysicists familiar with Oregon Basin. On the first day, Dr. Cladouhos presented the preliminary DFN models and results. This was followed by discussions with Oregon Basin engineers about reservoir architecture and the role of DFN models in enhanced oil recovery programs. On the second day, morning meetings with Richard Rosencrans, the geophysicist responsible for much of the interpretation of the South Oregon Basin 3D seismic, resulted in Golder receiving important new data on seismic lineament orientations and sizes in the window area of the South Dome. In the afternoon, Golder explored the South Dome geocelluar model (Stratamodel®) with Muriel Behrens and extracted data and graphics. On the final day, Brendan Curran of Marathon Oil, led a field trip to Zeismann Dome, the Wind River Canyon, and the Oregon Basin Field. Preliminary observations and conclusions from the meetings and field trip are discussed below. Because of the timing of the trip, these ideas have not yet been incorporated into the DFN models presented below, but are currently being used to update the DFN models.

3.2.4.1.6.1 Meeting with Reservoir Engineers

The Oregon Basin reservoir engineers made the following observations and comments in response to questions raised by Golder's preliminary analysis:

- Dolomite intrabeds in the Tensleep have tight matrix but are shattered. The dolomites may cause the water sheeting observed in the upper Tensleep wells.

- Equal amounts of lost returns were observed throughout the Tensleep. In other words, large conductive fractures are not confined to a particular layer or position within the formation.

- Eolian laminations in the Tensleep are thought to be important for reservoir performance.

- The Phosphoria is divided into an upper bench and a lower bench based on a gamma ray streak. The gamma ray streak is probably due to migration of Uranium-rich fluids at this contact.

- Horizontal well length does not seem to correlate with production.

3.2.4.1.6.2 Meeting with Geophysicists

On Tuesday morning, Golder personnel met with Richard Rosencrans. Mr. Rosencrans has used the 3D seismic data in the South Oregon Basin to create 2D attribute maps. Attributes mapped include average peak amplitude and instantaneous frequency. By interactively adjusting the color mapping, it is possible to identify lineaments, which may correspond to subseismic faults. Figure 3-23 shows a tracemap of lineaments mapped in this way overlain on the average peak amplitude attribute map in the Orchard window area. However, it is difficult on a static figure to appreciate the robustness of the method. Figure 3-24 and Figure 3-25 shows preliminary analysis of the tracemap. This data and analysis will be critical for conditioning the next scale of DFN models.

On Tuesday afternoon, Golder met with Muriel Behrens. Ms. Behrens is responsible for the South Oregon Basin Stratamodel® geocellar model. The Stratamodel® contains the following data:

- Porosity,
- Gamma ray,
- Matrix density,
- Bulk density, and
- Water saturation vs. time.

The horizontal dimension of the cells is 100x100 feet, and the cell thickness is 1.7 feet. The window area portion was extracted from the field-wide Stratamodel® as well as data at four wells within the window area. As an example of the data, a fence diagram of porosity between Orchard 10 and Orchard 14 is shown in Figure 3-26.

3.2.4.1.6.3 Field Trip

On Wednesday, Golder visited outstanding outcrops of the Tensleep and Phosphoria formations at Zeismann Dome and Wind River Canyon (see Figure 3-17 for locations). Observations made at the Amphitheater (Kerr and Tapp, 1998) of Zeisman Dome include the following:

- The primary fracture set has an azimuth of 65° and a spacing of approximately 5 m (Figure 3-27a). This orientation, which is widespread in the amphitheater, cuts the anticlinal structure obliquely.
- A secondary fracture set with a 90° azimuth is localized to the southern portion of the amphitheater where the anticlinal axis plunges to the south. The intensity of this set increases markedly toward the south. Some of these fractures show evidence of right lateral shear. This set may be related to a NE-trending right-lateral fault mapped by Kerr and Tapp (1998).

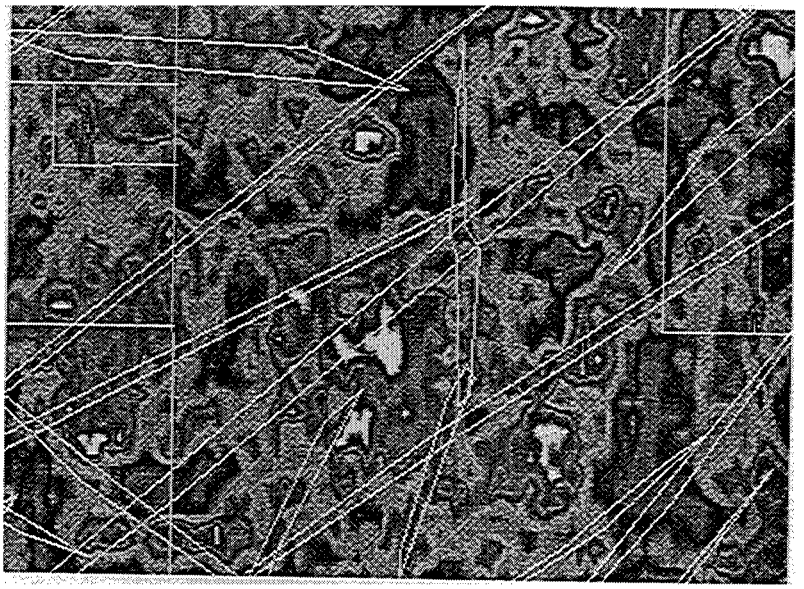

FIGURE **3-23**

SUBSEISMIC LINEAMENTS MAPPED FROM AVERAGE PEAK AMPLITUDE WITHIN ORCHARD WINDOW OF SOUTH OREGON BASIN

NPTO

PROJECT NO. 983 1258.521 DRAWING NO. 85026 DATE 7/30/99 DRAWN BY TK

Golder Associates

a)

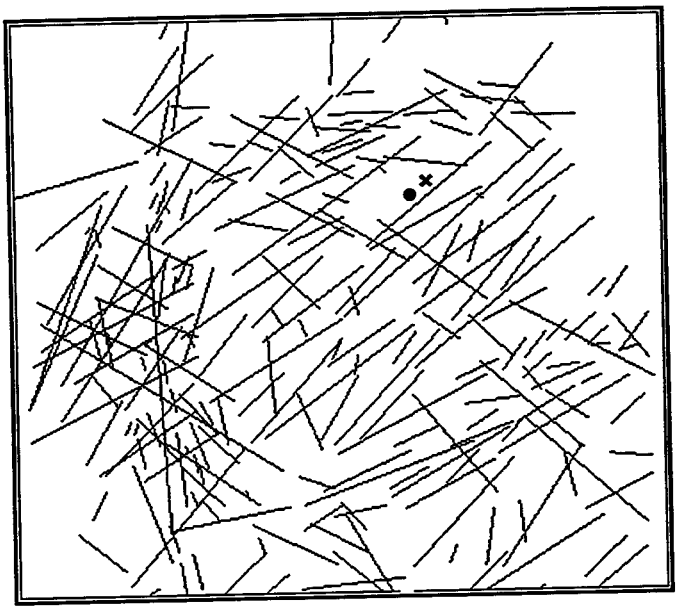

× Orchard 16

● T. Sommers B1

b)

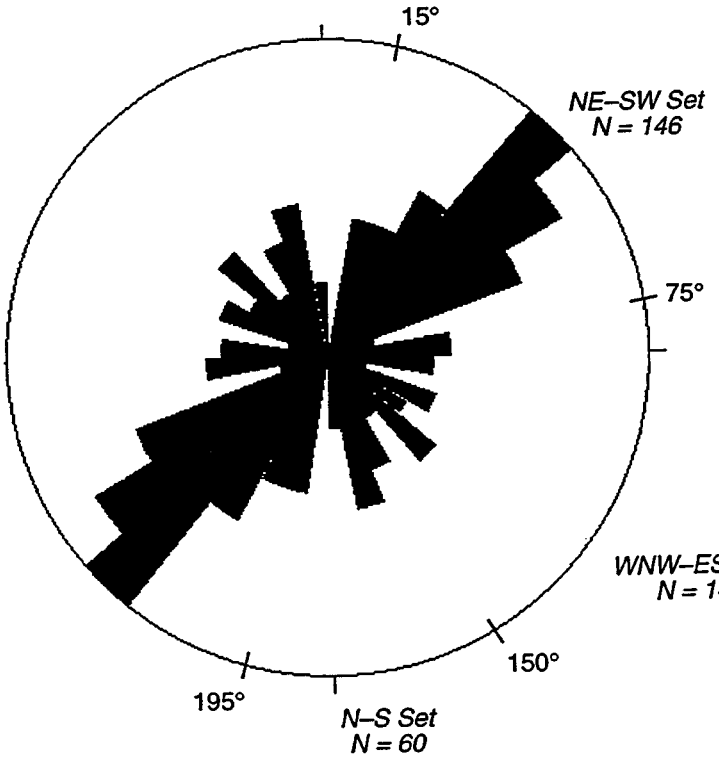

n = 287
Largest petal: 39 values
Largest petal: 13% of all values

FIGURE **3-24**
TRENDS OF SEISMIC LINEAMENTS
NPTO

PROJECT NO. 983 1258.521 DRAWING NO. 85027 DATE 7/30/99 DRAWN BY TK

Golder Associates

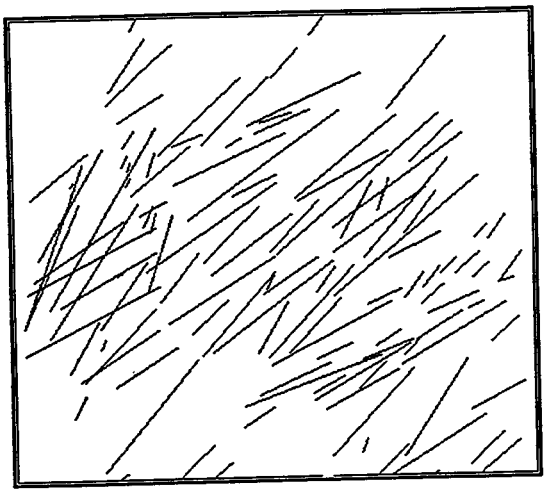

1000'
1000'

a) NE–SW Set

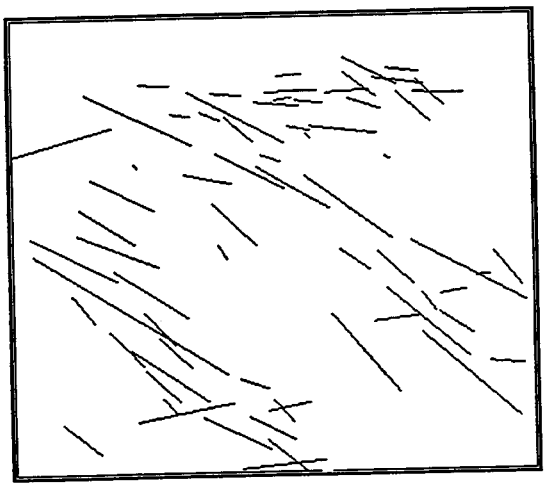

1000'
1000'

b) WNW–ESE Set

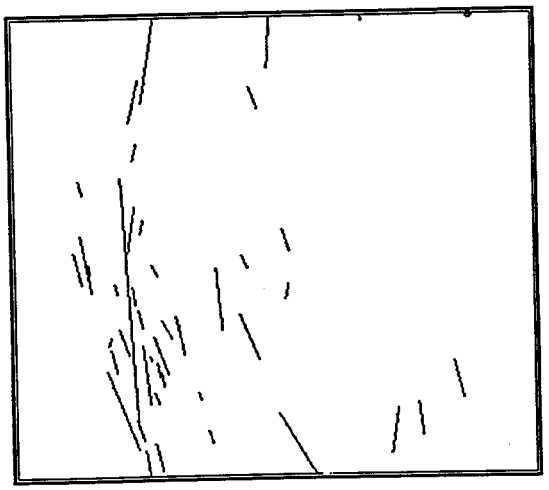

1000'
1000'

c) N–S Set

FIGURE **3-25**
FRACTURE SUBSETS ON SUBSEISMIC LINEAMENT MAP
NPTO

PROJECT NO. 983 1258.521 DRAWING NO. 85028 DATE 7/30/99 DRAWN BY TK

Golder Associates

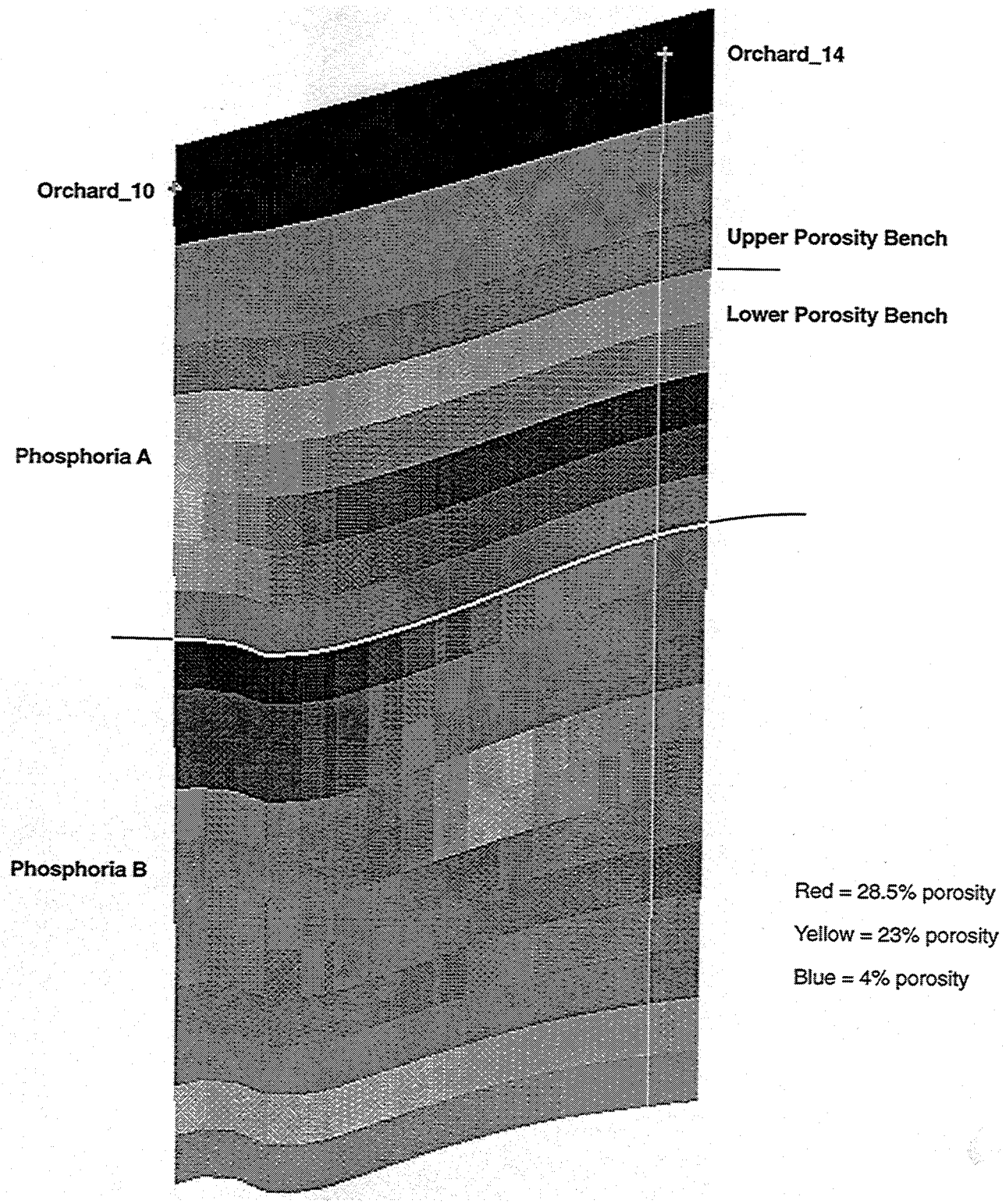

FIGURE **3-26**

EXAMPLE POROSITY FENCE DIAGRAM

NPTO

PROJECT NO. 983 1258.521 DRAWING NO. 85029 DATE 7/30/99 DRAWN BY TK

Golder Associates

- There is evidence of a significant tear fault with an azimuth of 55° crossing the center of the Amphitheater. The evidence includes erosion of the fault surface itself and increased fracturing adjacent to the fault.
- Mechanical layering plays an important role on fracture style and intensity. Large fractures in the upper cross-bedded dune facies truncate downward into the horizontally bedded intradune facies (Figure 3-27b).
- In contrast to the less fractured intradune facies, the marine facies is highly fractured with two perpendicular sets and ~0.3 m spacing (Figure 3-27c).

The Wind River Canyon provides a spectacular exposure of the Paleozoic section of the Big Horn Basin (Figure 3-28a). The Phosphoria formation is exposed at the mouth of the canyon (Figure 3-28b). Observations made at these outcrops include:

- There are at least two fracture sets. The dominant set is perpendicular to the cliff face and the road (70° azimuth) and the secondary set is parallel to the cliff face (160° azimuth).
- A hierarchy of fracturing can be observed at the outcrop. Fractures which cut the entire Phosphoria formation have a spacing of ~10 m (Figure 3-28c). Between these large fractures are smaller, bedding confined fractures. The size and intensity of these fractures are controlled by the thickness of the mechanical layer (Figure 3-28d).

Further up canyon are ~300 foot cliffs of Tensleep formation. The same two fracture sets observed at the Phosphoria outcrops are also present here. Additional observations made at the Wind River Canyon Tensleep outcrops include:

- Vertical fractures that cut the entire Tensleep have a spacing of roughly 20 m (Figure 3-29a). These fractures can have large mechanical apertures (Figure 3-29b).
- Between the major fractures are bedding confined fractures with spacings down to 1 m; however, these smaller fractures are not as numerous or continuous as similar fractures in the Phosphoria.
- The major fractures cut through the dolomite intrabeds in the Tensleep formation (Figure 3-29c).
- The dolomite intrabeds are heavily fractured (Figure 3-29d); however, the fractures are very small and thin. Except where the major fractures cut though the dolomites, the dolomite would serve as a barrier between the matrix of adjacent sandstones.

3.2.4.1.6.4 Conclusions from Field Visit

There are several implications of the field visit that will affect the next phase of DFN model implementation. The preliminary DFN models described below are entirely based upon data from the well bores. New data collected on this trip are at the larger scale necessary for reservoir scale models. In the next round of DFN models, the well bore models of this report will be nested, instead of using larger models derived from data of the type collected on the field visit.

The well bore data, field data, and seismic data agree in one important aspect: all have major fracture sets that obliquely cut the folds. The most prominent orientation of fractures of this type is the ENE to NE fractures. In addition, these fractures seem to be open, as NE

permeability trends are also evident in tracer tests and production tests (Brendan Curran, pers. comm.). It seems likely that this fracture set is regional and younger than the folding in the Big Horn Basin. Golder will further investigate the tectonic cause of these fractures in future reporting periods.

A significant improvement in the fracture size models will be possible using the data collected in the field and from seismic data. Fracture size is very difficult to estimate from well bore data and it is usually a non-robust value. This is partly due to the fact that widely spaced, vertical fractures are unlikely to be intersected by a well. Fortunately, observations at the Wind River Canyon and Zeismann dome provide information on the largest, most important fractures. At the Wind River Canyon, we observed very large fractures that entirely cut the Tensleep and Phosphoria formation with a spacing of approximately 10 m. Fractures appeared to be smaller and closer spaced at Zeismann Dome.

Lastly, observations of the dolomites intrabeds in the Tensleep formation provide important clues on how to incorporate these features into the DFN models. The dolomites are heavily fractured, but the fractures have small apertures and are discontinuous, making it is unlikely that they provide paths across the layer. However, the major fractures, which cut the sandstones also, cut the dolomites, indicating that these provide localized paths across the layers.

3.2.4.2 Task 2.2.3 Derivation of DFN Model Parameters

Preliminary discrete feature network (DFN) models were derived during the reporting period to model fractures in the South Oregon Basin Phosphoria formation. These preliminary DFN models are designed to support design of IOR techniques to improve access to oil in the upper Phosphoria, which has 80% oil saturation, as compared to the lower Phosphoria which has only 30% saturation.

3.2.4.2.1 Spatial Model

The first step in DFN model development is the determination of the appropriate spatial model. The fracture spatial model is derived by statistical and fractal analysis of spatial patterns observed in borehole logs, geophysical logs, and outscrops. Figure 3-30 illustrates spatial distributions of fracture intensities from FMI logs (Table 3-8). Preliminary analysis of these logs indicate that:

- There may be a trend of increased fracture intensity with depth. However, this trend is not present in all wells, and
- Spatial correlation and clustering are generally weak.

Based on this analysis, it was decided to use the simple, Poisson process Baecher Model (Dershowitz et al., 1999) for fracture location in the preliminary DFN model.

Future models will be based on a more rigorous analysis of fracture location data, and will consider implementation of spatial models such as fractal clustering, interaction zones between faults, damage zones of faults, and fold-related fracturing.

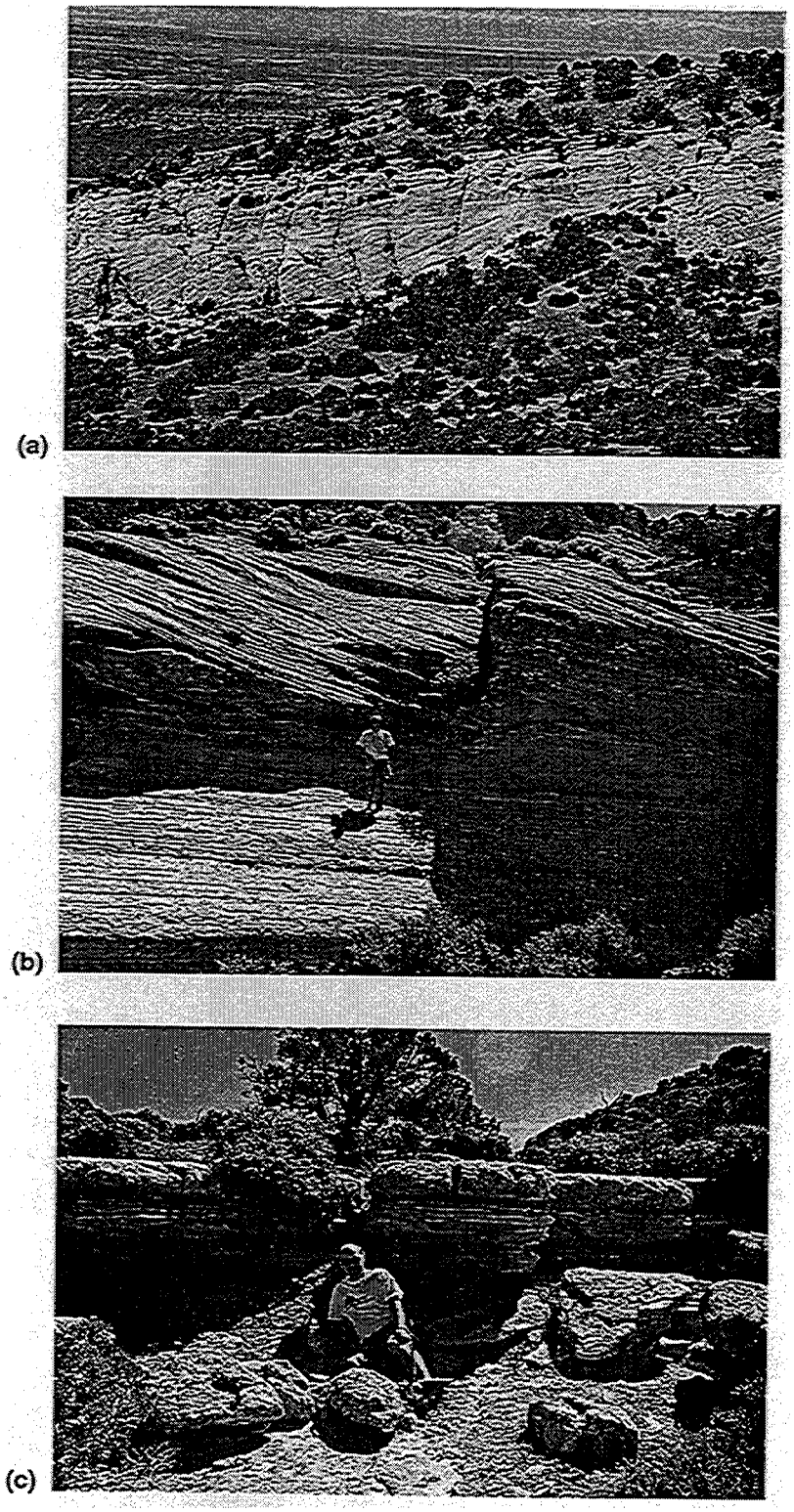

FIGURE **3-27**
ZEISMAN DOME OUTCROP PHOTOS
NPTO

PROJECT NO. 983 1258.521 DRAWING NO. 85030 DATE 7/30/99 DRAWN BY TK

Golder Associates

(a)

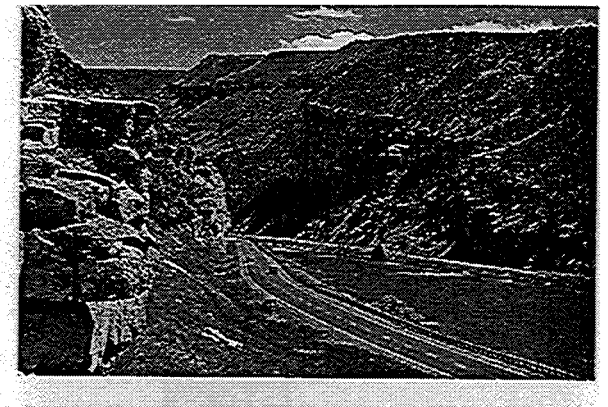

(b)

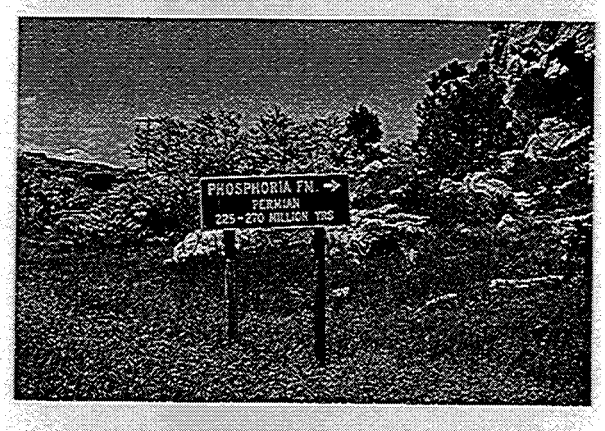

(c)

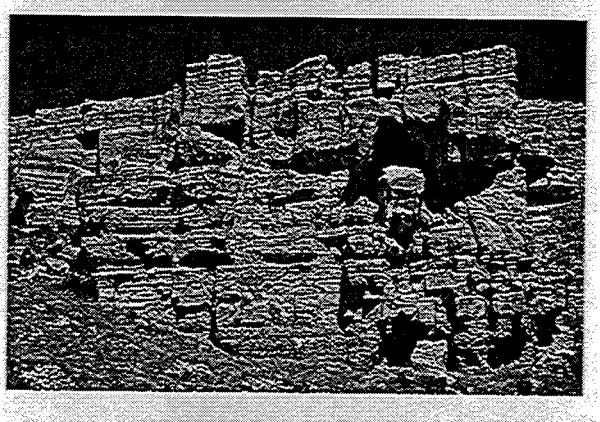

(d)

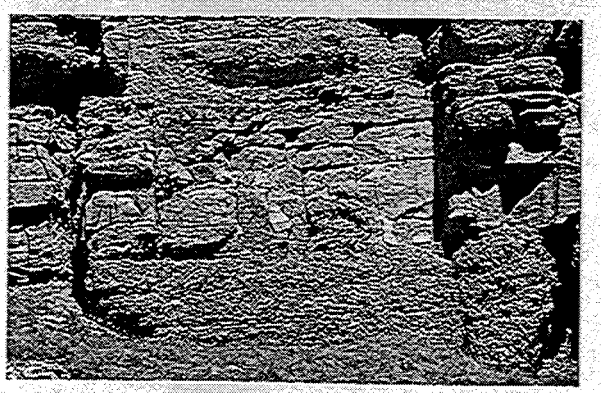

FIGURE **3-28**

WIND RIVER CANYON PHOTOS: PHOSPHORIA FORMATION

NPTO

PROJECT NO. 983 1258.521 DRAWING NO. 85031 DATE 7/30/99 DRAWN BY TK

Golder Associates

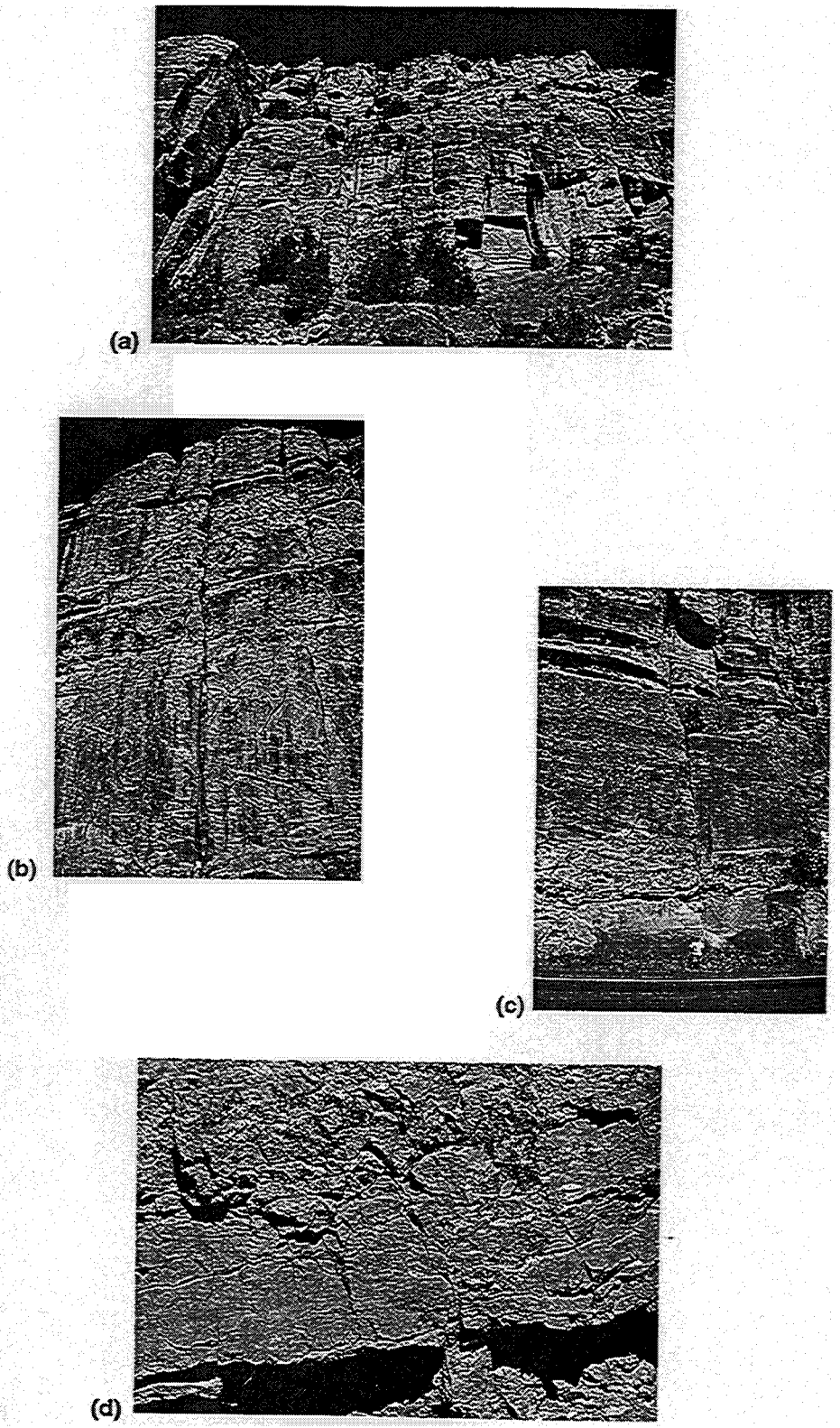

FIGURE **3-29**
WIND RIVER CANYON PHOTOS: TENSLEEP FORMATION
NPTO

PROJECT NO. 983 1258.521 DRAWING NO. 85032 DATE 7/30/99 DRAWN BY TK

Golder Associates

3.2.4.2.2 Orientation

Fracture orientation distributions for the preliminary DFN were derived from FMI logs of four wells, two of which are in the South Oregon Basin (Baston A #29 and Samuel 58) and two of which are in the North Oregon Basin (Pauline #9 and Government Tract 3B #16) (Table 3-8). This dataset combines vertical and horizontal wells, and should provide a good sample of the Phosphoria fracture population.

Well	Geological Setting	Length in Phosphoria		Bedding (strike, dip)	Intensity	
		feet	m		Fractures	4 pad Fractures
Samuel #58 Vertical **South Dome**	SE flank of dome, 1800' from fault	230	70	50, 6.5 SE	27	100%
Baston A #29 Vertical **South Dome**	NW edge of dome crest, no faults	220	67	342, 5 NE	19	68%
Pauline #9 Horizontal **North Dome**	E limb of North Oregon Basin anticlinal crest, 800' from tear fault, horizontal well trend, plunge = 78,80	538	164	180,15 E	149	97%
Governmen t Tract 3B #16 Vertical **North Dome**	near crest of North Oregon Basin dome, vertical well	150	46	28, 8NW	14	50%

* used to estimate fracture size

Table 3-8 Phosphoria wells

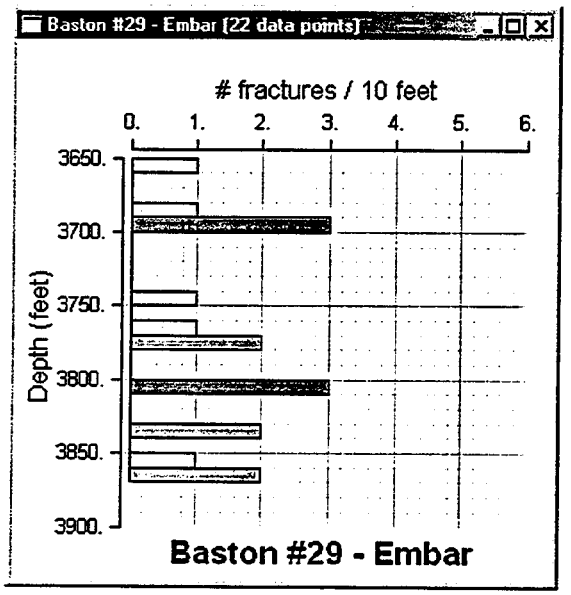

a

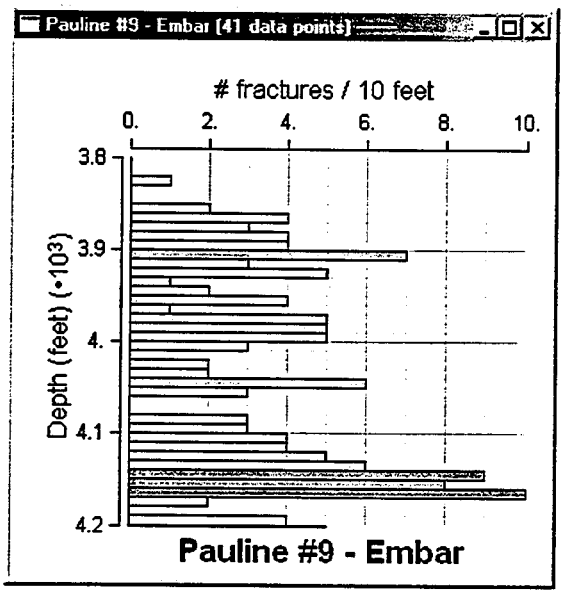

b

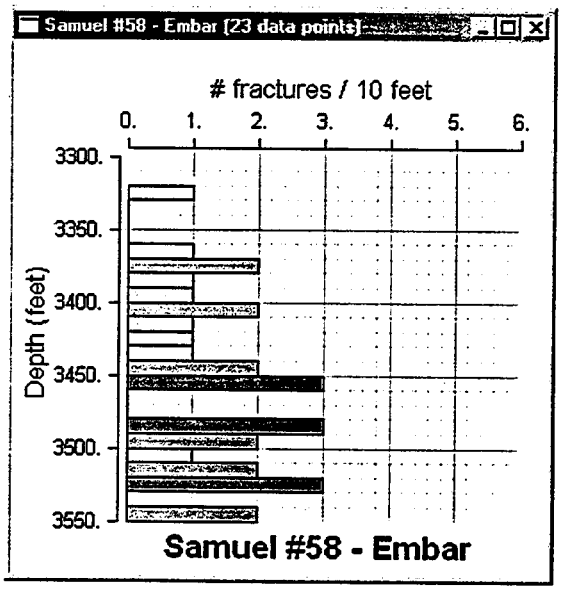

c (North Dome)

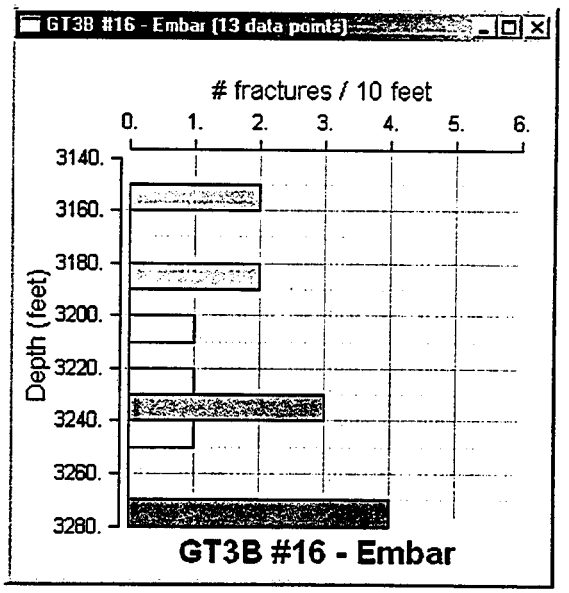

d (NOB)

FIGURE **3-30**

FRACTURE INTENSITIES IN PHOSPHORIA (AKA EMBAR) FROM FMI WALLS

NPTO

PROJECT NO. 983 1258.521 DRAWING NO. 85034 DATE 8/9/99 DRAWN BY TK

Golder Associates

Figure 3-31 shows fracture orientations of 46 fractures from the two vertical wells in South Oregon Basin, 149 fractures in the horizontal Pauline #9 well, and 14 fractures in a vertical North Oregon Basin well. Although Neil Hurley interpreted four fracture sets in Baston A #29, we prefer to interpret all fractures as belonging to one set with high dispersion in trend and low dispersion in plunge, similar to the data seen in the horizontal well (Pauline #9).

To derive an orientation model for the FMI fractures in the Phosphoria formation, the data from the Pauline #9 well in the North Dome (Figure 3-31b) was used. This data was considered to be the most reliable because it is from a horizontal well which intersects the vertical fractures most prevalent in the Phosphoria formation. This assumes that the Phosphoria fracturing in the North and South Dome are similar. The assumption is supported by the gross similiarity of the fracture orientations in the vertical wells in the North and South Dome (i.e. compare Figure 3-31a and Figure 3-31c to Figure 3-31d). This assumption will be further evaluated after the field data collected in June and additional core data still to be provided by Marathon are evaluated.

Fracture data from Pauling #9 were analyzed for fracture orientation distribution using the FracMan/ISIS algorithm. The best fit orientation distribution for data from the Pauline #9 well is a sub-vertical set defined by a Bivariate Bingham distribution with a mean pole of 135°, 9.4° a major axis of 340°, 80°, and dispersion coefficients of κ_1=-13.3, κ_2= -7.0. The significance of the fit is relatively low (15%); future models may employ bootstrapping rather than an orientation model.

3.2.4.2.3 Intensity

The interpretation of the FMI logs in the South Dome show 19 to 27 fractures within the ~220 foot thick Phosphoria formation which gives an average fracture spacing of 8-11 feet (Table 3-8). The horizontal Pauline #9 well shows a fracture intensity three times higher; however, it is to be expected that a horizontal well will intersect more subvertical fractures.

Fracture intensities in the four wells were calculated in 10-foot intervals in order to evaluate the variability with depth in each well (Figure 3-30). The three vertical wells show no trends or clustering of fractures. In contrast, the fracture intensity in the horizontal Pauline #9 appears to be increasing with depth. It is possible that this well is approaching a subseismic fault, which is responsible for the increased fracturing.

Well	Number (total)	Length (ft)	P_{10} (#/ft)	P_{10}(#/m)	P_{32} (m^2/m^3)
Baston A #29	19	220	0.09	0.28	1.04
Samuel 58	27	230	0.12	0.39	1.45
Pauline #9	149	538	0.28	0.91	1.67
Government 3B #16	14	150	0.09	0.31	1.15

Table 3-9 Phosphoria Fracture Intensities

The stereological fracture intensity measure (P_{32}) shown on Table 3-9 is a scale and direction independent measure. P_{32} intensity is used to generate fractures in three-dimensional space without reference to well locations or orientations. P_{32} is derived from P_{10} by calculating the conversion constant $C_{31} = P_{32}/P_{10}$, by simulating the intersections with a specified orientation distribution and wells of specified orientations.

The P_{32} values shown in Table 3-9 were calculated by simulating the four specified wells in DFN models with the orientation distribution derived in the previous section. The resulting P_{32} values vary from 1.04 m^2/m^3 to 1.67 m^2/m^3. The highest P_{32} value derived from the subhorizontal Pauline #9 well is used as the upper bound on geological fracture intensity for the preliminary DFN modeling.

Geologic fracture intensity provides an upper bound for DFN models used for flow simulations. Normally 10-25% of fractures observed at the well bore are conductive for a conductive fracture intensity P_{32c} of approximately 0.15 m^2/m^3 to 0.42 m^2/m^3.

3.2.4.2.4 Size

Fracture size (radius) is normally a difficult parameter to determine from well data. La Pointe et al. (1993) developed a method using the percentage of fractures which intersect all four FMI pads to derive fracture size. The basic idea is that if fractures are on average small compared to the size of the borehole, the FMI interpreter would see many fracture tips due to fractures which only partially cut the well bore. If fractures are large compared to the well bore then few fracture tips will be seen and the 4-pad intersection probability would be near 100%.

Employing the method of La Pointe et al. (1993) requires forward models to be run and sampling simulated using a FMI-like sampling tool. This procedure was carried out using the known borehole geometries and fracture parameters derived so far (orientation and intensity). The simulation results were then compared to the 4 pad percentages for the Phosphoria FMI wells (Table 3-8). The results are shown in Figure 3-32. In the Pauline well 97% of fractures were reported to cut the entire well corresponding to a mean fracture radius of 20 m or 66 feet. This is larger than expected based on geological observations. In the Baston 29 well, 68% of the fractures were reported to cut the entire well, corresponding to a mean fracture radius of about 3 m or 10 feet. This is a much more likely fracture size and will be used below.

3.2.4.3 Task 2.3.3 DFN Model Implementation

For the preliminary DFN model of the Phosphoria formation at the South Oregon basin, well-scale models were constructed using the parameters derived above and summarized in Table 3-10. Sensitivity analysis was run on conductive fracture intensity by creating models with 50%, 25%, 18%, and 12% of the geologic fracture intensity. A 3D view of the 25% geologic fracture intensity model is shown in Figure 3-34 and tracemap views are shown in Figure 3-34. The orientations of the fractures in the model and the fractures intersected by a horizontal and vertical well are shown as stereonets in Figure 3-35. These simulated stereonets can be compared to the actual orientation data in Figure 3-31.

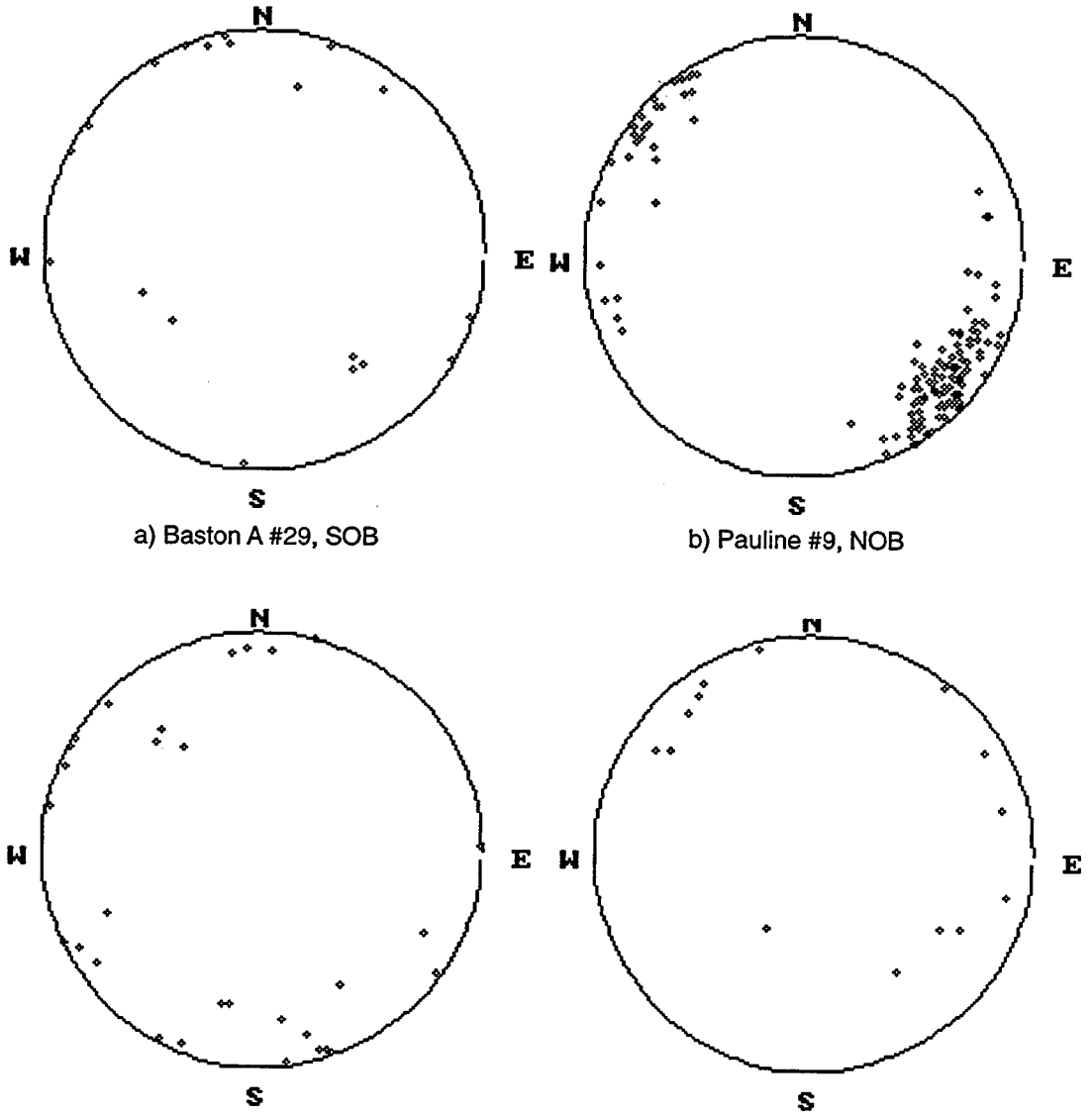

a) Baston A #29, SOB

b) Pauline #9, NOB

c) Samuel #58, SOB

d) Government Tract 3B #16, NOB

FIGURE **3-31**
PHOSPHORIA FRACTURE ORIENTATIONS
NPTO

PROJECT NO. 983 1258.521 DRAWING NO. 85033 DATE 8/9/99 DRAWN BY EA

Golder Associates

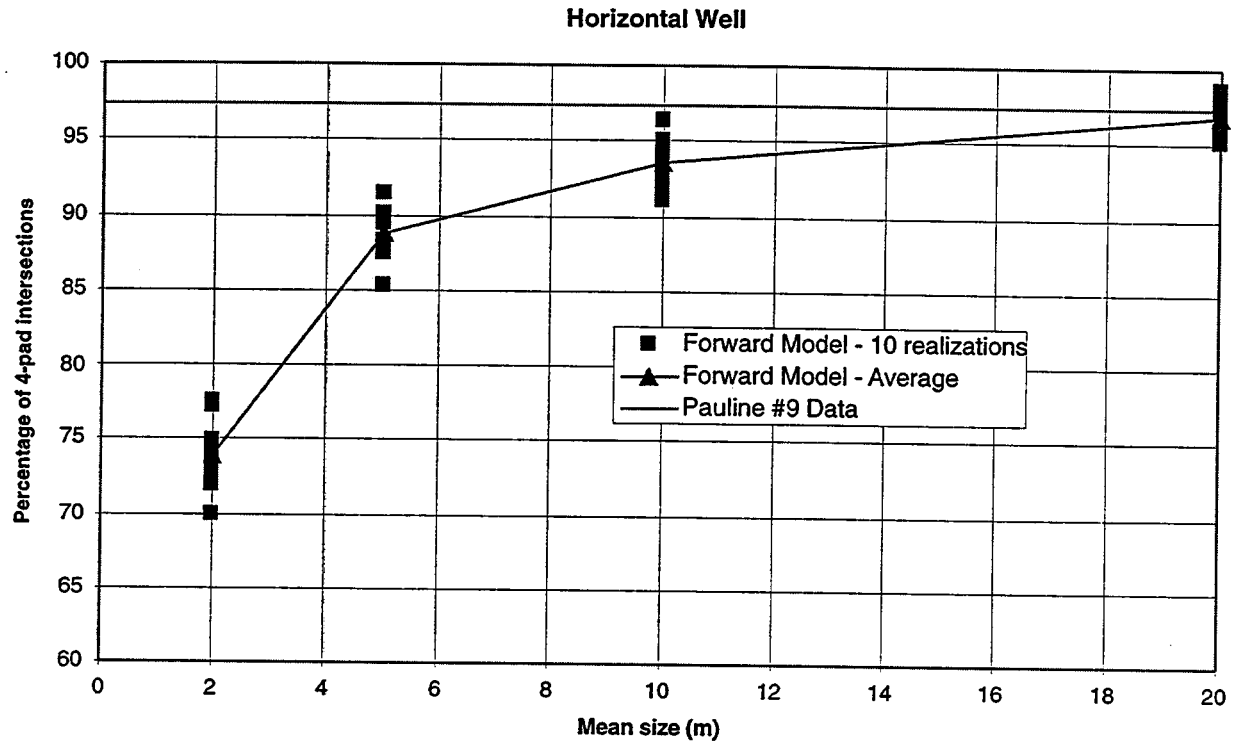

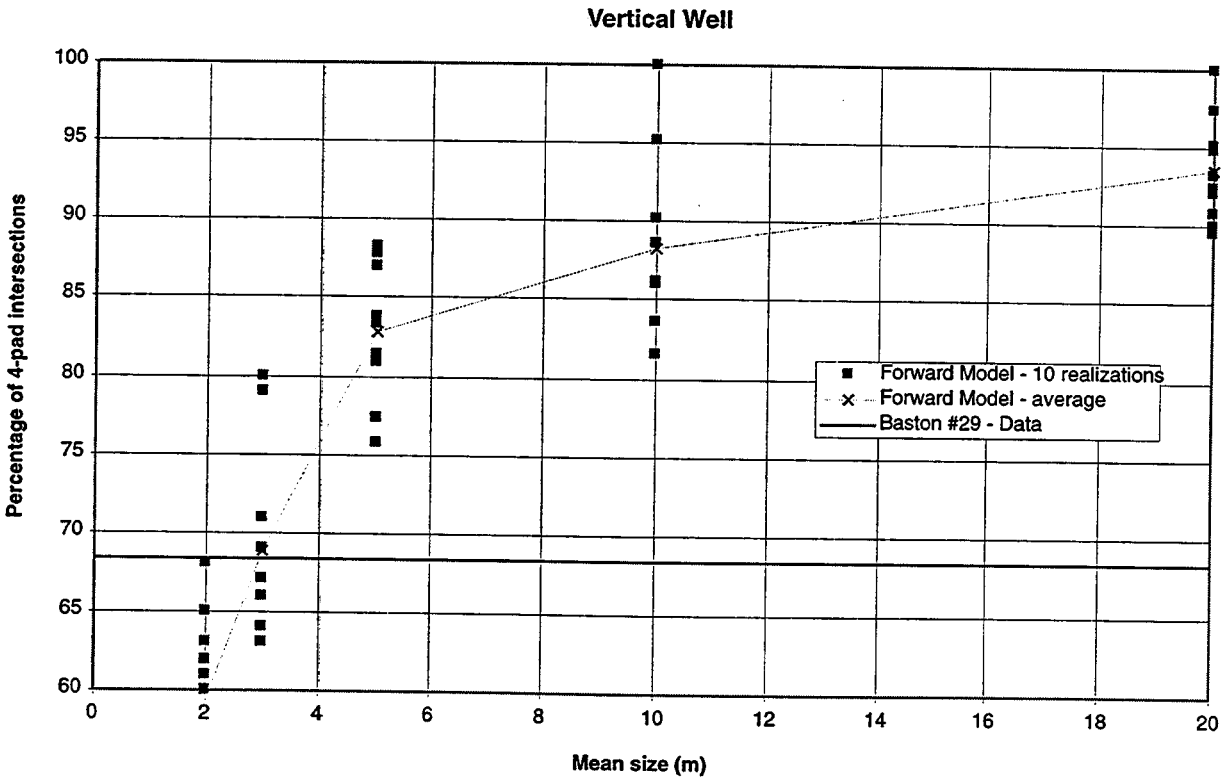

FIGURE **3-32**
FORWARD MODELING FOR FRACTURE SIZE: SOB
NPTO

PROJECT NO. 983 1258.521 DRAWING NO. 85035 DATE 7/30/99 DRAWN BY TK

Golder Associates

Parameter	Assumption	Basis
Generation Region	Cylinder, H=70 m, D=50 m	220' thickness of Phosphoria at South Oregon Basin FMS wells: Baston A #20 and Samuel #58
Conceptual Model	Enhanced Baecher	fracture spacing from FMI wells
Fracture Orientation	Bivariate Bingham Mean Pole =135, 9.4 Major Axis 340, 80 K1=-13.3, K2= -7.0	Terzaghi Corrected Orientations in Pauline #9 Horizontal Well in North Dome
Fracture Size	Lognormal Mean = 3 m StDev = 1.5	Calibrated to 68% 4 pad FMS intersection in Baston well
Fracture Intensity	Geologic Intensity P32 = 1.6 m^{-1} Sensitivity Analysis P32 = 0.8, 0.4, 0.3, 0.2 $^{m-1}$	P10 intensities in Pauline #9 (hz) and Baston A #29 (vt)
Fracture Aperture	Normal Distrib., Mean =0.2 mm = $2x10^{-4}$ m, stdev=0.05 mm = $5x10^{-5}$ m	0.1 to 0.3 mm estimate from Hurley
Fracture Transmissivity	$1x10^{-6}$ m^2/s	Assumption

Table 3-10 DFN Model Parameters, South Oregon Basin

3.2.4.4 Task 2.4.3 DFN Model Calibration

During the reporting period, initial data was collected to support DFN model calibration. It is currently anticipated that DFN model calibration will be based on tracer test simulation.

Over thirty tracer tests have been run in the South Oregon Basin, three of which are in the Orchard lease window area (Table 3-11). The most interesting tracer test is the Bromide injection test at Orchard 16 (Figure 3-33). In this test, the connection between Orchard 16 and Texas Sonners B1, ~1000 feet SW of the injector, seems to be very strong. Initial breakthrough occurred after 10 days and peak breakthrough at 80 days. The orientation of the recovery contours (Figure 3-36) and the rapid breakthrough indicate that this tracer path may be fracture controlled. Currently, Golder is gathering more information about the boundary conditions of this test in preparation for simulation.

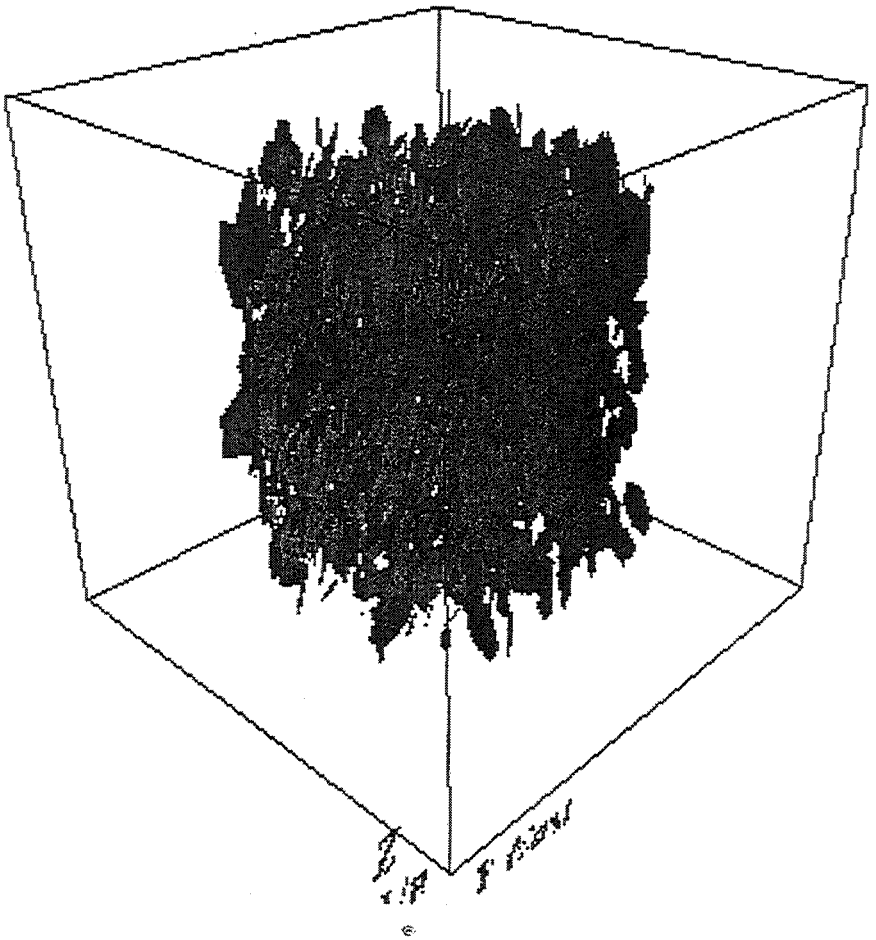

FIGURE **3-33**
NORTHEAST VIEW OF DFN MODEL OF PHOSPHORIA AT SOB (P_{32} = 0.4M^{-1})
NPTO/SOB

PROJECT NO. 983 1258.521 DRAWING NO. 85037 DATE 8/9/99 DRAWN BY TK

Golder Associates

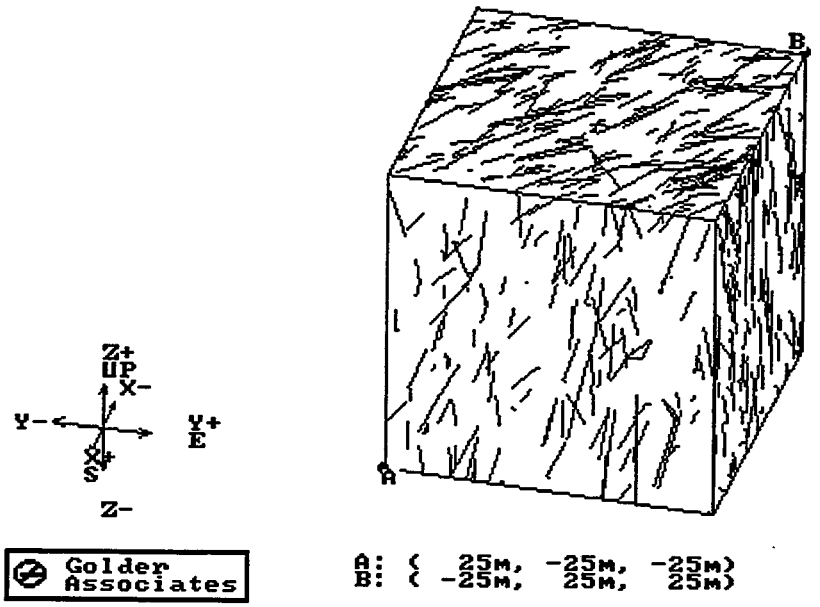

(a) Block View

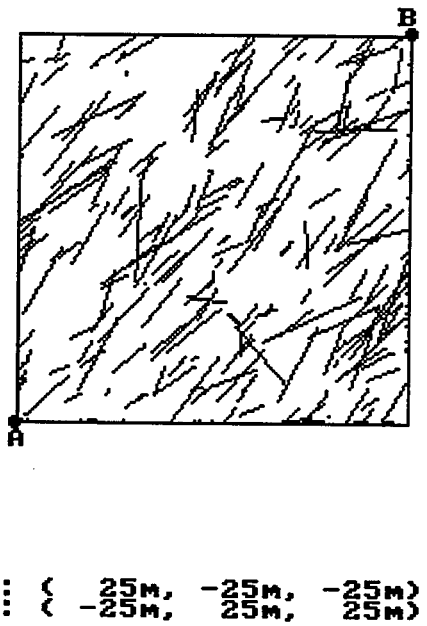

(b) Top View

FIGURE **3-34**
TRACE MAP VIEWS OF DFN MODEL OF PHOSPHORIA AT SOB
NPTO

PROJECT NO. 983 1258.521 DRAWING NO. 85038 DATE 8/9/99 DRAWN BY TK

Golder Associates

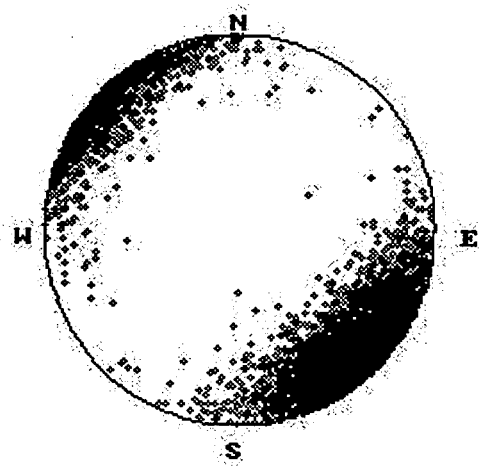

(a) All fractures in model

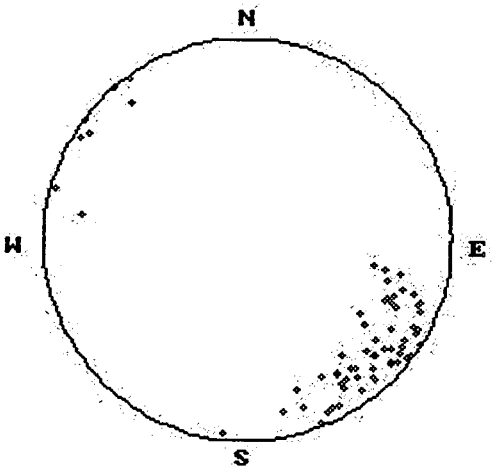

(b) Fractures intersected by 240' long horizontal well (i.e. compare to Pauline orientation data in Figure 3-30b)

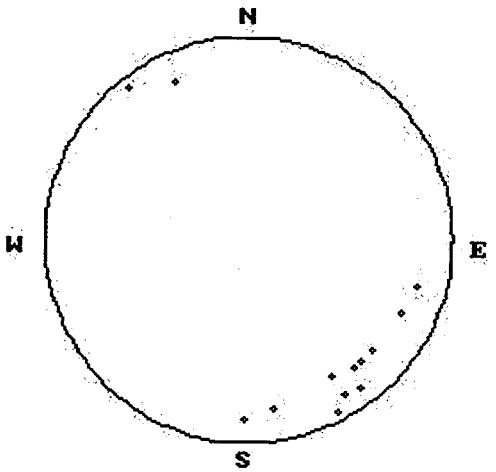

(c) Fractures intersected by vertical well

FIGURE **3-35**
FRACTURE ORIENTATIONS IN PHOSPHORIA MODEL
NPTO/SOB

PROJECT NO. 983 1258.521 DRAWING NO. 85039 DATE 8/9/99 DRAWN BY TK

Golder Associates

Test	6/15/92	6/15/92	7/2/93
Injector	Orchard 16	Orchard 16	Orchard 16
Tracer(s)	Bromide	Rhodamine	PHPA
Duration (days)	150 +	90	45+
# Monitoring Wells	9 or 10?	11	7
Recovery Wells (Top 5)	Conn 3ET 1.5% Morris 6ET 4% Orch. 19 ET 1.5% Tx. Sn B1 ET 27% Tx. Sn B2 ET 2%	Fortin 2 0.3% Orch. 14 E 0.4% Tx. Sn B1 ET 0.1% Orch. 10 ET .07% Morris 6 ET .035%	

Table 3-11 Tracer Tests, South Oregon Basin

3.2.5 Tasks 2.X.4 Preliminary DFN Model Development, North Oregon Basin (Tensleep)

At North Oregon Basin (NOB) the window area chosen for the demonstration of the Discrete Feature Approach for production enhancement is the Government Tract 3B lease near the center of the dome (Figure 3-20). The target formation for IOR is the Tensleep Formation, an eolian sandstone with dolomite intrabeds. The dolomite intrabeds divide the reservoir sandstones into separate zones (Figure 3-37). Two types of discrete features impact IOR efforts: dolomite layers and fractures.

3.2.5.1 Task 2.2.4 Derivation of DFN Model Parameters

In the North Oregon Basin, discrete feature network models were developed during the reporting period to model fractures and dolomite intrabeds in the Tensleep formation. The IOR issue at the North Oregon Basin is how to displace the bypassed oil in the matrix of the upper eolian sandstones. In this case, DFN models will provide insight into the shapes and volumes of the reservoir not connected to a fracture compartment.

3.2.5.1.1 Geological Background, Tensleep Formation

The Tensleep sandstone is composed of a series of nine subarielly-deposited eolian sandstones separated by marine dolomites and dolomitic sandstones (Figure 3-37). This formation was deposited during near sea level during a time of cyclic relative sea level changes (Dunn, 1997). Many of the dolomitic intervals can be correlated across the entire Bighorn Basin. At North Oregon Basin, nine dolomites have been correlated across the field, dividing the reservoir sandstones into nine subreservoirs, labeled A through I (Morgan et al. 1977). The current IOR efforts are concentrated in the top three sandstones: A, B, & C.

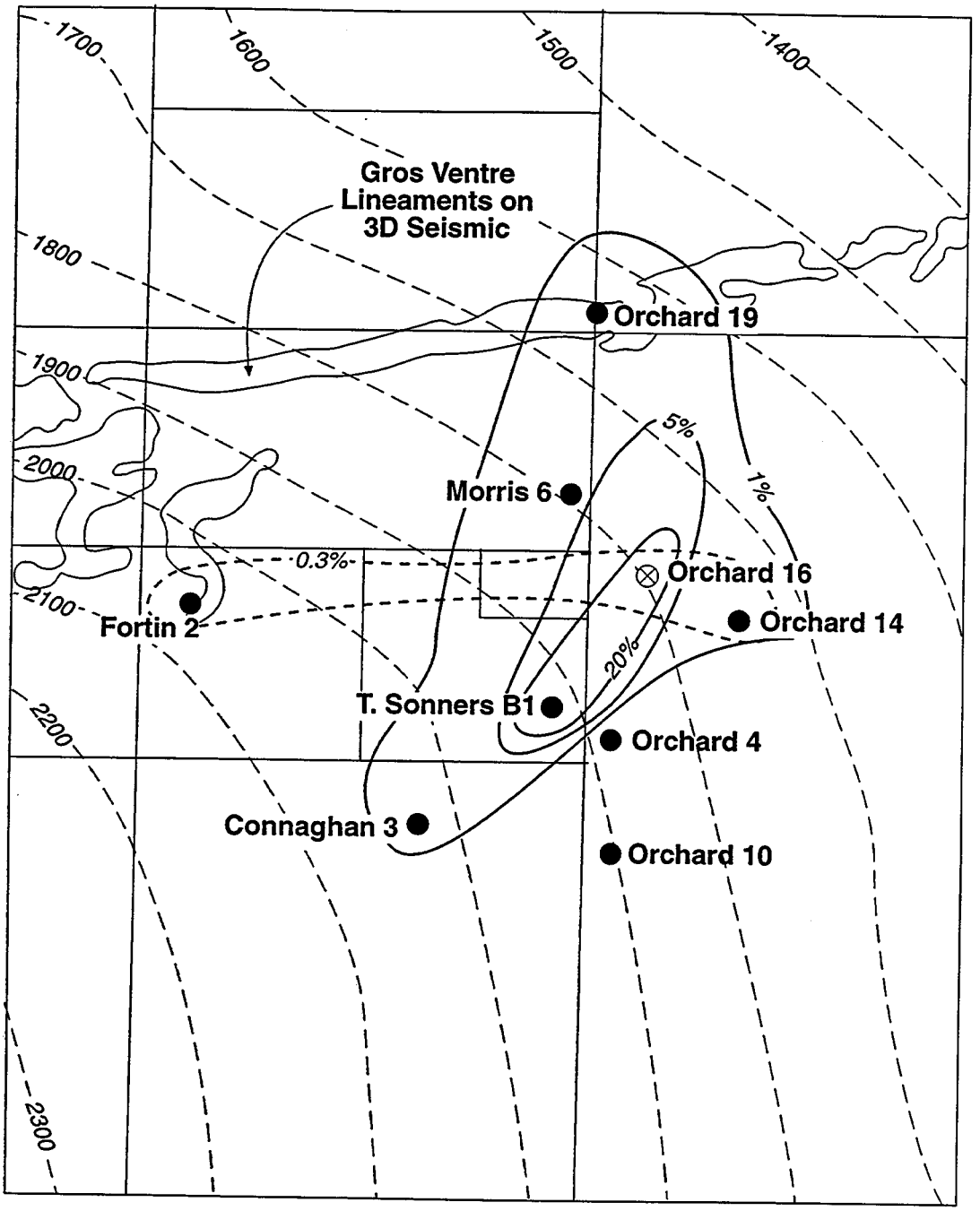

- - - -2000- Contours on top of Phosphoria

——5%—— Contours of cumulative recovery for Bromide tracer test

- - - 0.3%- - Contours of cumulative recovery for Rhodamine tracer test

⊗ Injection well

● Pumping well

FIGURE **3-36**

SOUTH DOME TRACER TEST RESULTS

NPTO

PROJECT NO. 983 1258.521 DRAWING NO. 85036 DATE 8/9/99 DRAWN BY EA

Golder Associates

The eolian sandstones display cross-bedding typical of deposition within a dune environment. Dunn (1997) has extensively studied the effects of the cross bedding on the permeability of the Tensleep sandstones. Depending on the type of bounding surface, directional anisotropies across surfaces as high as 10:1 were estimated (Figure 3-38). Also studied is the orientation and dip of cross beds in the Tensleep (Figure 3-39). The orientation distribution shown is this figure is useful to support development of DFN models. Although the eolian sedimentary structures within the Tensleep are important for reservoir engineering, their scale is smaller than the fractures which cut the entire Tensleep (Figure 3-29). Thus, the preliminary DFN model developed below concentrates on the fracturing only.

3.2.5.1.2 Spatial Model

The spatial model for fracturing in the North Oregon Basin Tensleep can be derived from the distribution of intensity as observed in FMI logs. Intensity on 10-meter intervals from FMI logs of the North Oregon Basin Tensleep is summarized in Table 3-12. Each of the wells shows a slight increase in fracture intensity in the top 30-40 feet of the formation. This may be due to two factors; fracturing during subariel exposure and erosion prior to deposition of the Phosphoria formation or increased bending stresses at the contact between the two different mechanical layers. However, as in the Phosphoria analysis reported in the previous section, no strong spatial correlation or trend in intensity is evident to justify the use of a complex spatial model (Figure 3-40). Consequently, the Baecher spatial model was selected for preliminary DFN modeling.

Well	Geological Setting	Length in Tensleep	Bedding (Strike,dip)	# fractures	Percentage 4 pad Fractures
Gov. Tract 3B #16	In window area near dome crest	200'	28, 8 NW	40	65%
Owens A-14	1.5 miles north of dome crest	190'	60, 12NE	7	43%
Custer #45	NE flank of dome	240'	11, 9.5 NE	25	24%
Sonners #20	1 mile south of dome crest near possible tear fault	220'	70, 8 SW	11	73%

Table 3-12 Tensleep Formation in North and South Oregon Basins

3.2.5.1.3 Orientation

Orientation distributions were evaluated for bedding structures and for fractures. Figure 3-41 illustrates the orientation distributions for bedding within the Tensleep. Bedding in Government Tract 3B Well #16 is dipping slightly to the NW as expected for this position on the structure.

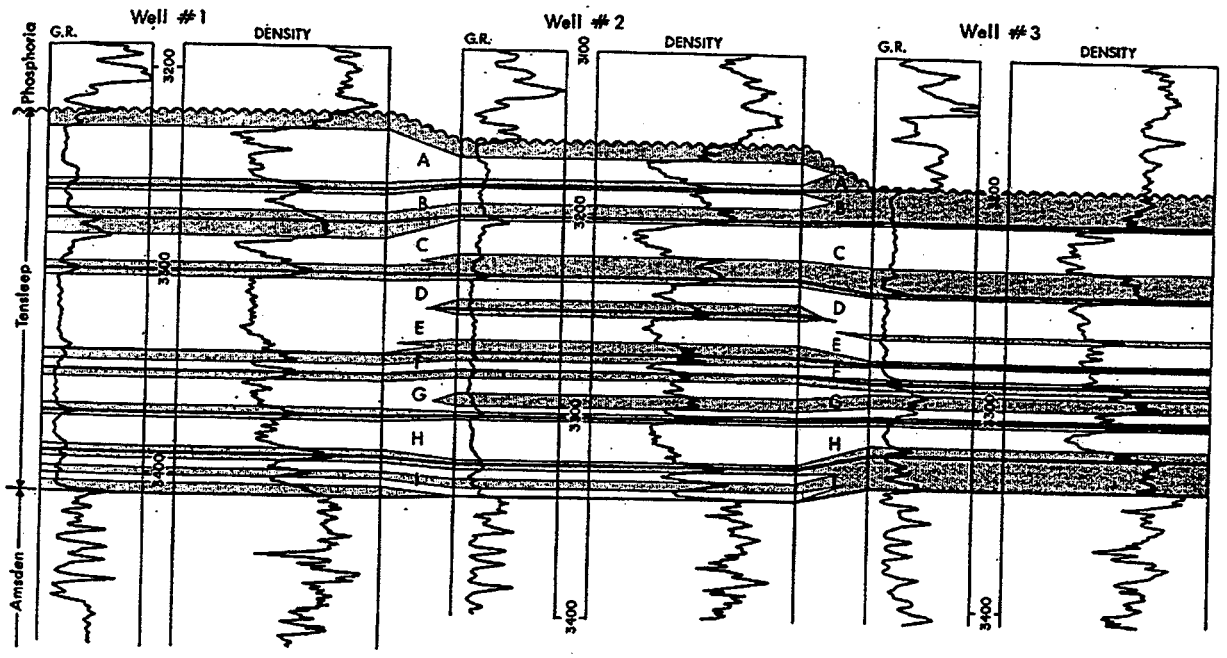

Source: Morgan et al 1977.

FIGURE **3-37**
STRATIGRAPHIC CORRELATIONS IN NORTH OREGON BASIN
NPTO

PROJECT NO. 983 1258.521 DRAWING NO. 85040 DATE 7/30/99 DRAWN BY EA

Golder Associates

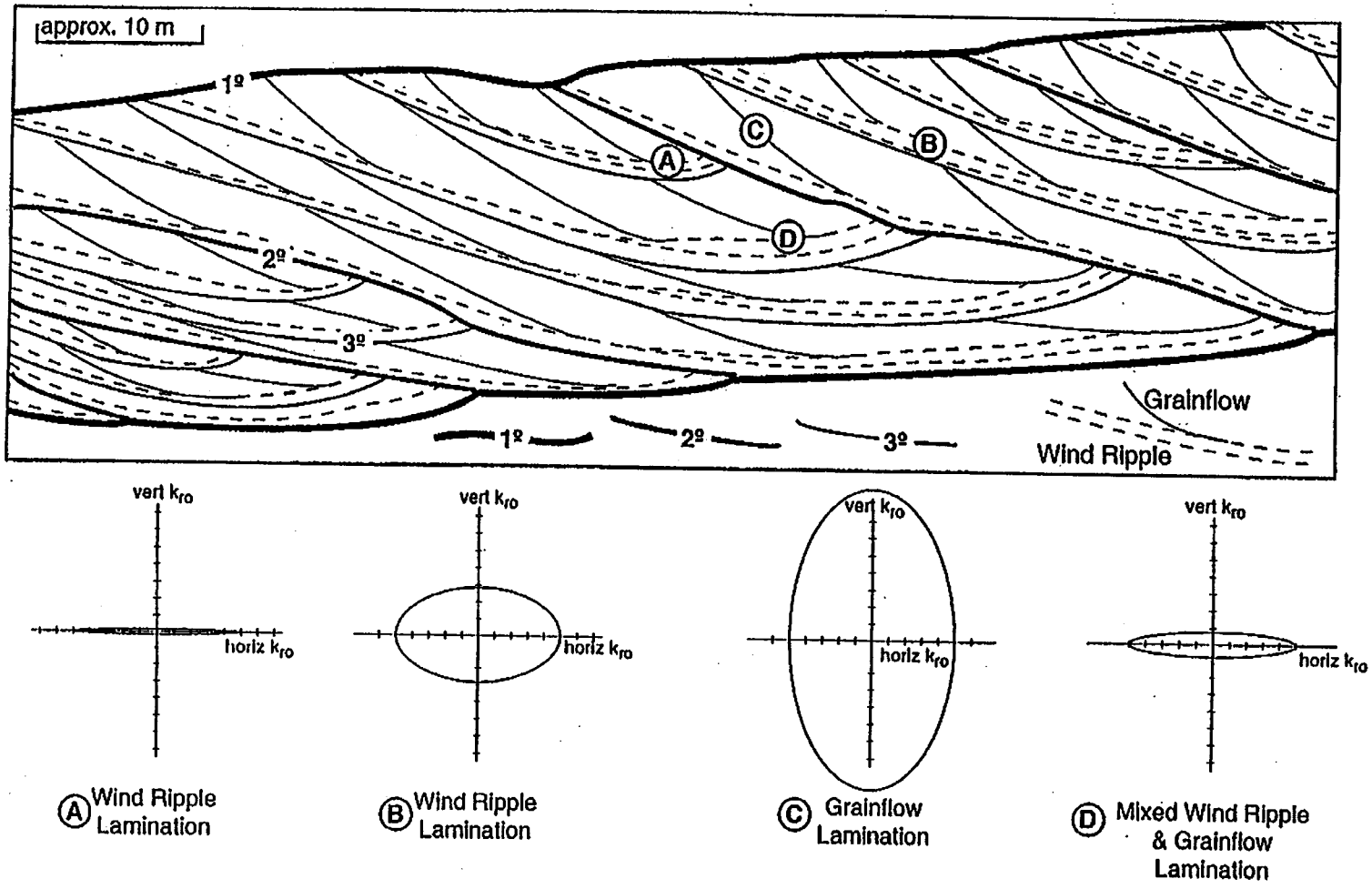

Source: Dunn, 1997.

FIGURE **3-38**
ANISOTROPY ASSOCIATED WITH EOLIAN LAMINATIONS IN THE TENSLEEP
NPTO

PROJECT NO. 983 1258.521 DRAWING NO. 85041 DATE 7/30/99 DRAWN BY EA

Golder Associates

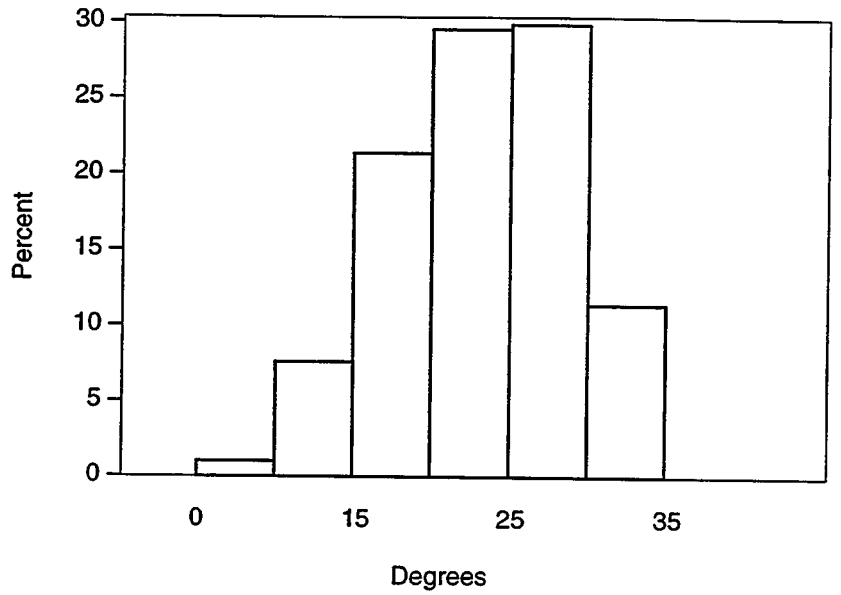

a) Dip of Crossbeds in Tensleep Sandstone

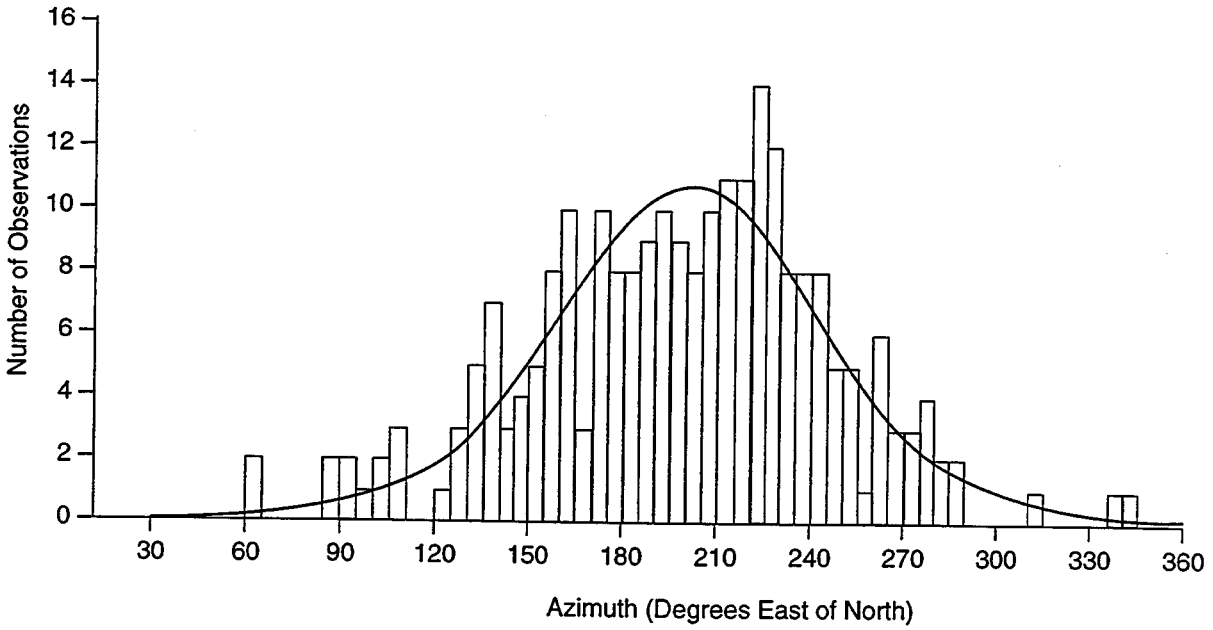

b) Dip Azimuth of Crossbeds in Tensleep Sandstone

Source: Opdyke and Runcorn, 1960

FIGURE **3-39**
CROSS BEDDING ORIENTATION IN TENSLEEP FORMATION
NPTO

PROJECT NO. 983 1258.521 DRAWING NO. 85042 DATE 7/30/99 DRAWN BY EA

Golder Associates

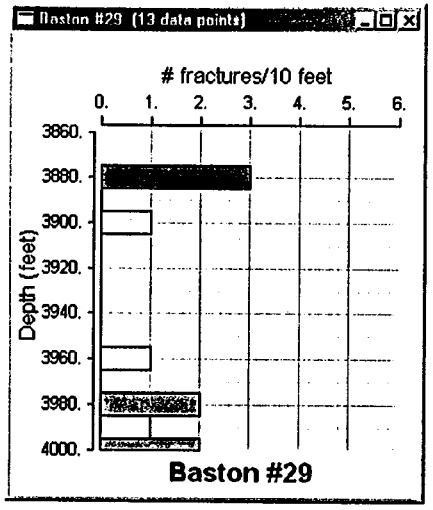

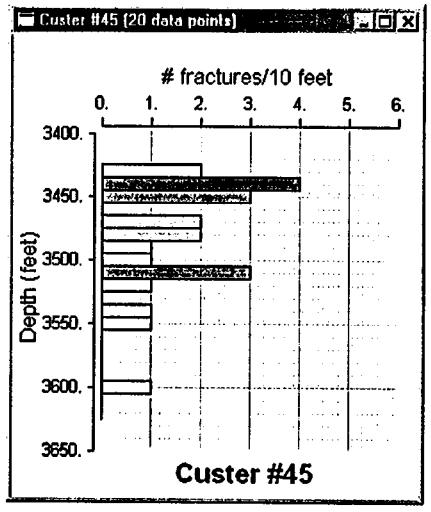

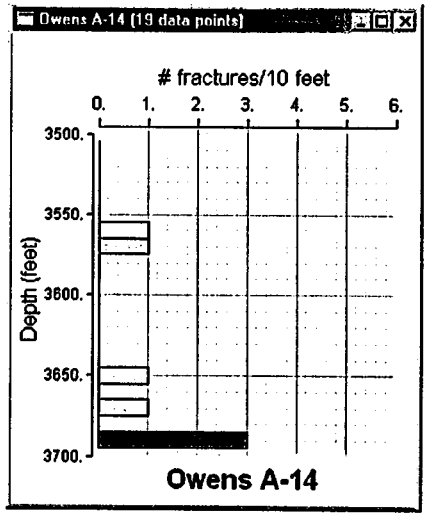

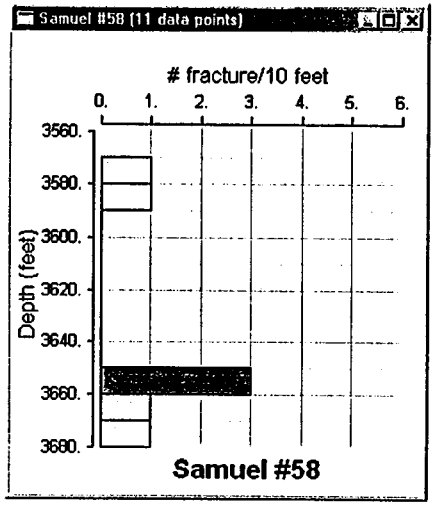

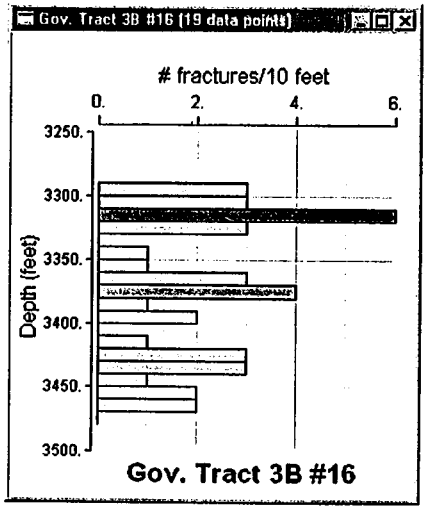

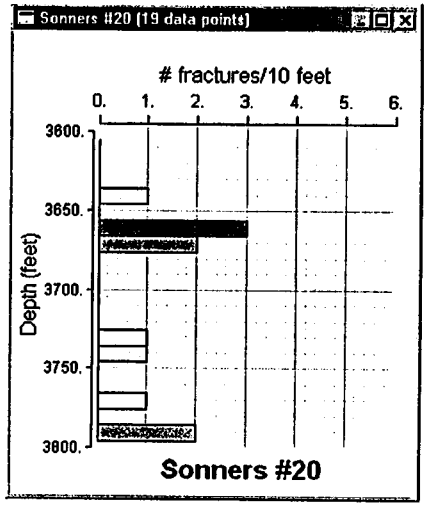

FIGURE **3-40**

FRACTURE INTENSITIES IN TENSLEEP FROM FMI WELLS

NPTO

PROJECT NO. 983 1258.521 DRAWING NO. 85045 DATE 8/9/99 DRAWN BY EA

Golder Associates

The best fit for the bedding orientation data set shown in Figure 3-41 is a Fisher Distribution with a mean pole (trend, plunge) of (117°, 85.8°) and a dispersion κ of 23.5. The significance of this fit is 34.8%, which indicates a good match to observed data.

Figure 3-42 shows fracture orientations of 91 fractures in the Tensleep formation in both the North Dome and South Dome. To derive an orientation model for the FMI fractures, all of orientation data from the Tensleep formation (Figure 3-42g) was used. To combine fracture data from different positions of the fold, one must assume that:

- The fractures are younger than the folding and thus cross-cutting the field structure, or
- The slight change in bedding orientations across the structure (16°) are small compared to the errors of measurement.

The best fit of this orientation data set is a Fisher Distribution with a mean pole of 127°, 0.8° and a dispersion of 3.3. The significance of this fit is 74.3%, which is considered very good, indicating that this orientation model will create a DFN model with fracture orientations similar to the combined data set.

3.2.5.1.4 Intensity

The FMI logs (Table 3-12) in the Tensleep show 7 to 40 fractures within the ~200 foot thick formation which gives an average fracture spacing of 11 feet. However, there is significant variability in fracture intensity across the field. In the Government Tract 3B #16 well the fracture intensity is twice the average, and in the Owens it is A-14 half the average. The reason for this variability will be investigated based on reservoir scale models in future reporting periods.

The volumetric fracture intensity P_{32} was derived for the Tensleep using the same approach used for the Phosphoria in the Section 3.2.3.1.3 above. Results of this analysis are reported in Table 3-13. The Tensleep data fits an average volumetric fracture intensity P_{32} of 0.35 m^2/m^3, while the well within the Government Tract 3B window has a much higher volumetric intensity P_{32} of 0.8 m^2/m^3. Geologic fracture intensity provides an upper bound for DFN models used for flow simulations. Normally 10-25% of fractures observed at the well bore are conductive, corresponding to a conductive fracture intensity P_{32c} of 0.03 m^2/m^3 to 0.2 m^2/m^3.

Well	Number of Fractures	Interval Length	P_{10} (#/ft)	P_{10} (#/m)	P_{32} (m^2/m^3)
Gov. Tract 3B #16	40	200	0.20	0.66	0.80
Owens A-14	7	190	0.04	0.12	0.14
Custer #45	25	240	0.10	0.34	0.41
Sonners #20	11	220	0.05	0.16	0.19
Samuel 58	7	150	0.05	0.15	0.18
Baston #29	11	130	0.08	0.28	0.34
Average	101	1130	0.09	0.29	0.35

Table 3-13 Summary of Tensleep Fracture Intensities

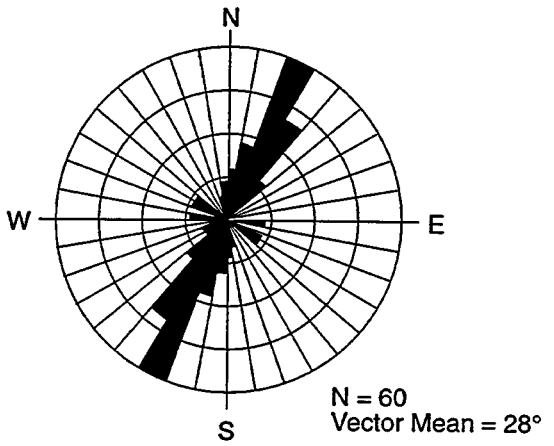

a) Bedding Strikes

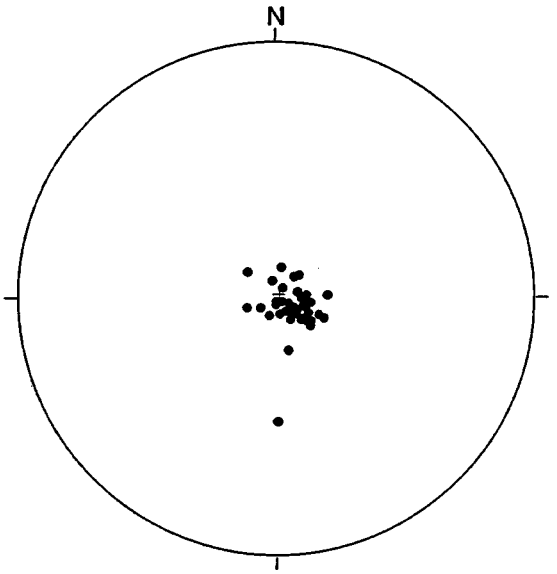

b) Stereoplot of Poles to Bedding

FIGURE **3-41**
BEDDING ORIENTATIONS IN GOVERNMENT TRACT 3B #16
NPTO

PROJECT NO. 983 1258.521 DRAWING NO. 85043 DATE 8/9/99 DRAWN BY EA

Golder Associates

3.2.5.1.5 Size

The La Pointe et al. (1995) method described in Section 3.2.4.1.5 was used to derive fracture size for the Tensleep based on the 4 pad percentages for the Phosphoria FMI wells (Table 3-12). The results are shown in Figure 3-43. The preferred size model for the Tensleep formation is a mean fracture radius of 2 m (6.6 feet) with a standard deviation of 1 m (3.3 feet).

3.2.5.2 Task 2.3.4 DFN Model Implementation

The preliminary DFN model for the Tensleep formation was designed to facilitate simulation of the compartmentalization observed in the Tensleep formation (Livingston and Cordiner, 1977). The preliminary DFN model is implemented at the 32 m scale in order to focus on a series of layers of sandstone and dolomite designated "A", "B" and "C". The layer positions are taken from the stratigraphic correlation shown in Figure 3-37 (Table 3-14).

Parameters for the preliminary Tensleep DFN model are provided in Table 3-15. The fracture intensity of the layers was assigned according to rock type: the dolomites have conductive fracture intensities 50% as great as the sandstone layers. This relationship was chosen in order to place the dolomites barriers between the sandstones, and is supported by field observations that while geologic fracturing in the dolomites may be high, very few of the fracture are large enough to be significant conductors. The DFN model also features fracture truncation on layer boundaries, also chosen to ensure that the dolomites are barriers. This is supported by field observations. All other fracture parameters for the two layers types are the same.

Figure 3-44 and Figure 3-45 present visualizations of the preliminary Tensleep DFN model. The orientations of the fractures in the model and the fractures intersected by a vertical well are shown as stereonets in Figure 3-46. These simulated stereonets can be compared to the FMI data in Figure 3-37.

Rock Type	Thickness (m)	Layer Center (m)
Dolomite	2	15
Sandstone A	7	10.5
Dolomite	2	6
Sandstone B	3	3.5
Dolomite	3	0.5
Sandstone C	3	-2.5
Dolomite	2	-5
Sandstone DE	10	11

Table 3-14 Parameters for Tensleep Dolomite Layering

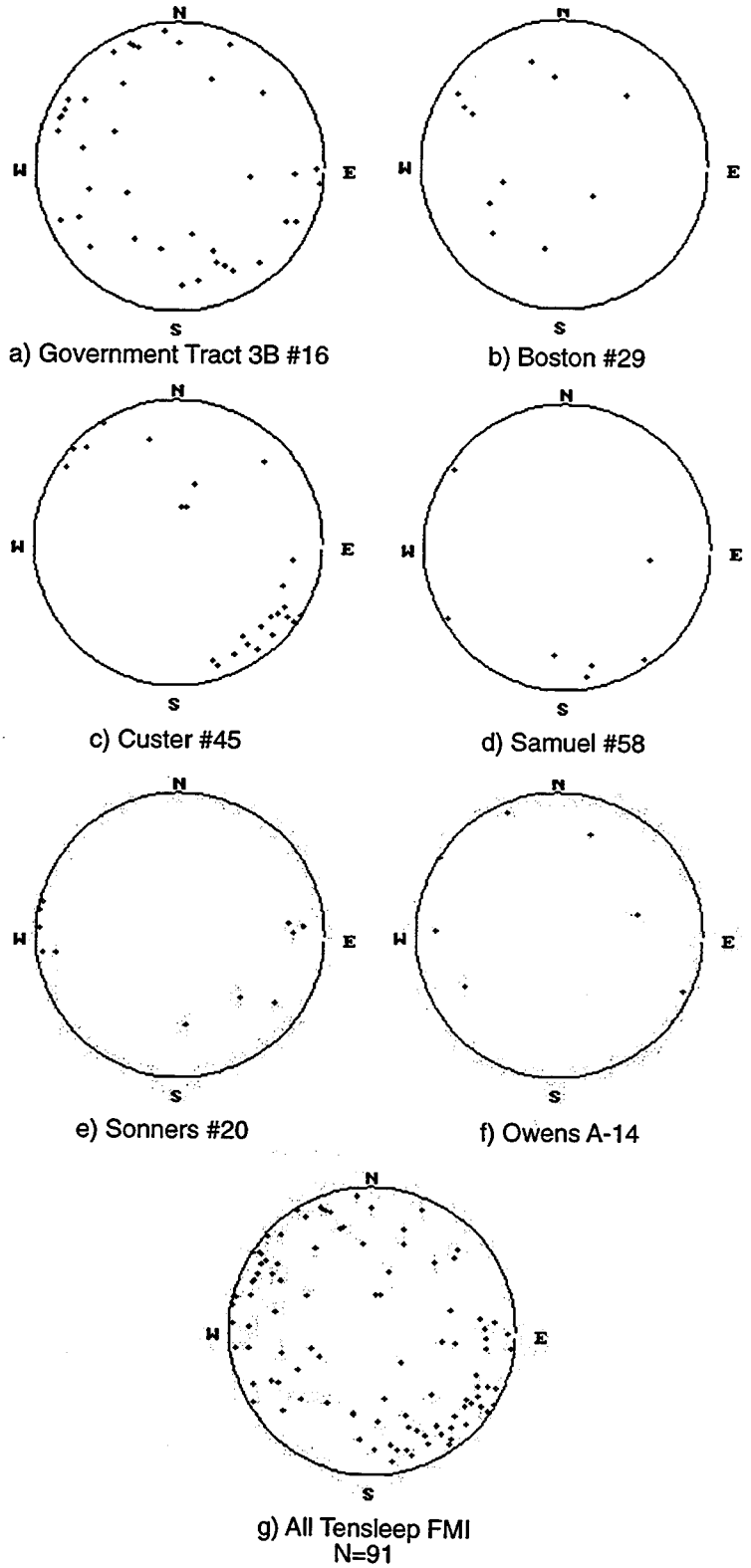

a) Government Tract 3B #16

b) Boston #29

c) Custer #45

d) Samuel #58

e) Sonners #20

f) Owens A-14

g) All Tensleep FMI
N=91

FIGURE **3-42**
FRACTURE ORIENTATIONS IN TENSLEEP FROM FMI WELLS
NPTO

PROJECT NO. 983 1258.521 DRAWING NO. 85044 DATE 8/9/99 DRAWN BY EA

Golder Associates

3.2.5.3 Task 2.4.4 DFN Model Calibration

During the reporting period, initial data was collected to support DFN model calibration. It is currently anticipated that DFN model calibration will be based on tracer test simulation.

Over twenty tracer tests have been run in the North Oregon Basin. Table 3-16 summmarizes two tracer tests the Government Tract 3B window area. Results of these tracer tests are shown in Figure 3-47 and Figure 3-48. The Bromide tracer test probably has recoveries too low to be of use for modeling; however, the Boron tracer test will be useful for DFN model calibration. Although there are no unexpected connections, there is a significant permeability enhancement in the NE-SW direction parallel to the mean fracture orientation. Currently, Golder is gathering more information on the boundary conditions of this test in preparation for simulation.

3.2.6 Task 3.2 Stoney Point Reservoir Improvement Strategy

3.2.6.1 Task 3.2.1 DFN Strategy for IOR

As described in Dershowitz (1999), production problems at Stoney Point are mostly related to lack of understanding of the gas-water-oil contacts within compartments. DFN models will be used to determine the sources and connectivity for oil and water phases, and the variation in connectivity within the reservoirs with depth.

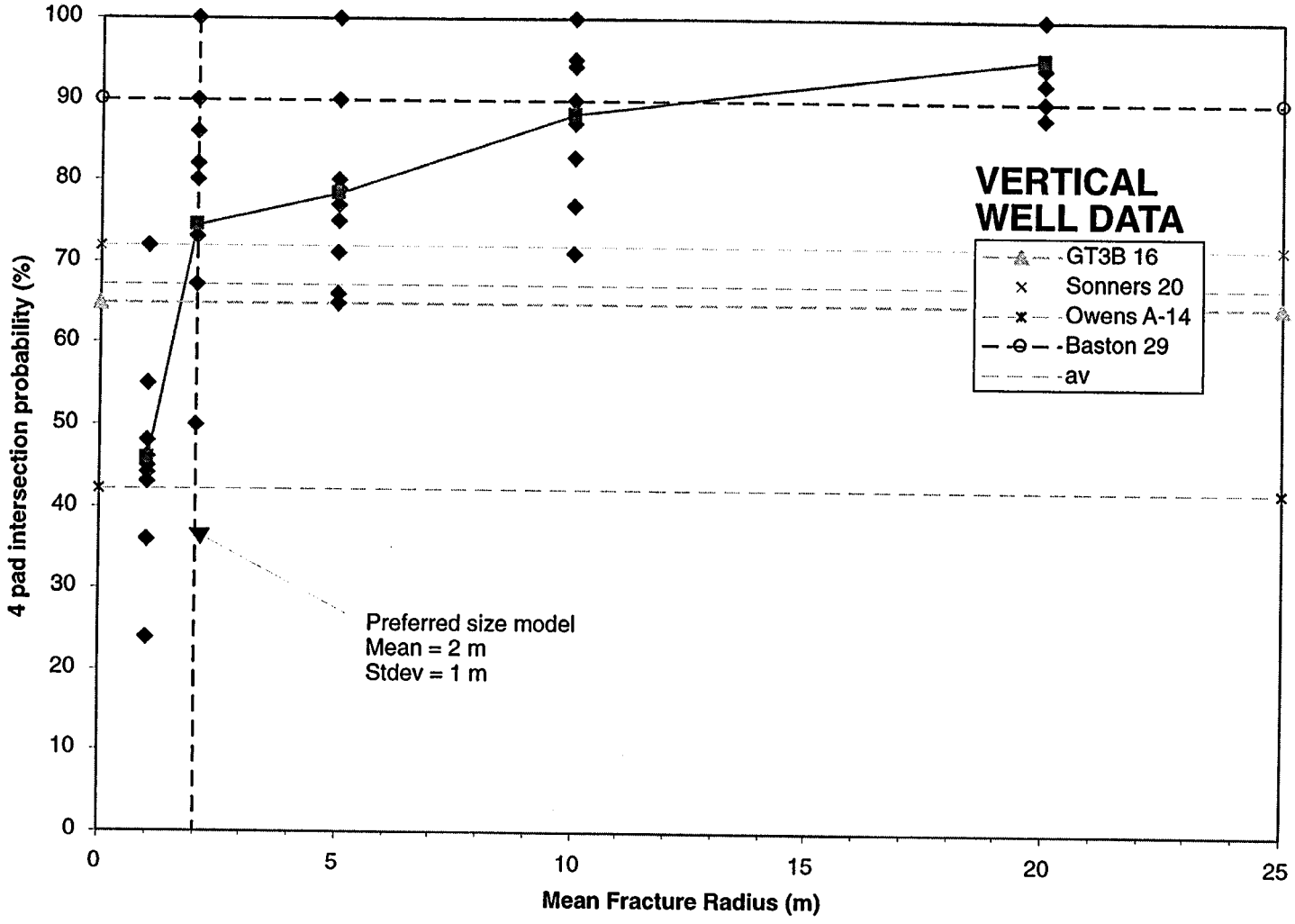

FIGURE **3-43**

FORWARD MODELING FOR FRACTRE SIZES: NOB

NPTO

PROJECT NO. 983 1258.521 DRAWING NO. 85046 DATE 7/30/99 DRAWN BY EA

Golder Associates

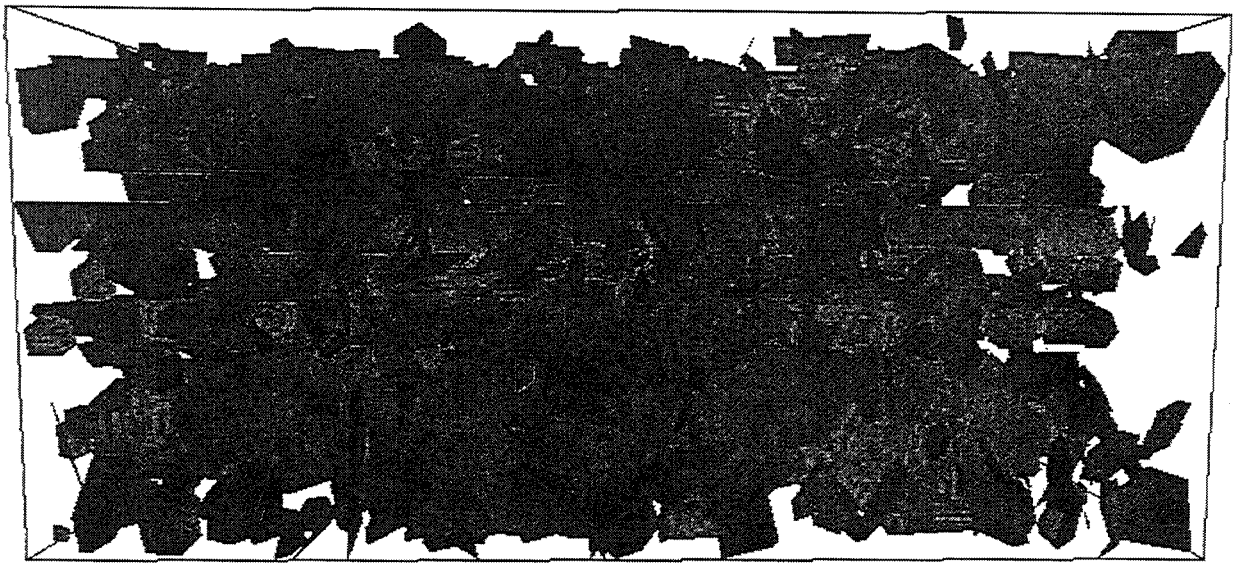

FIGURE **3-44**
3D VIEW OF DFN MODEL OF TENSLEEP AT NOB
NPTO

PROJECT NO. 983 1258.521 DRAWING NO. 85049 DATE 8/9/99 DRAWN BY TK

Golder Associates

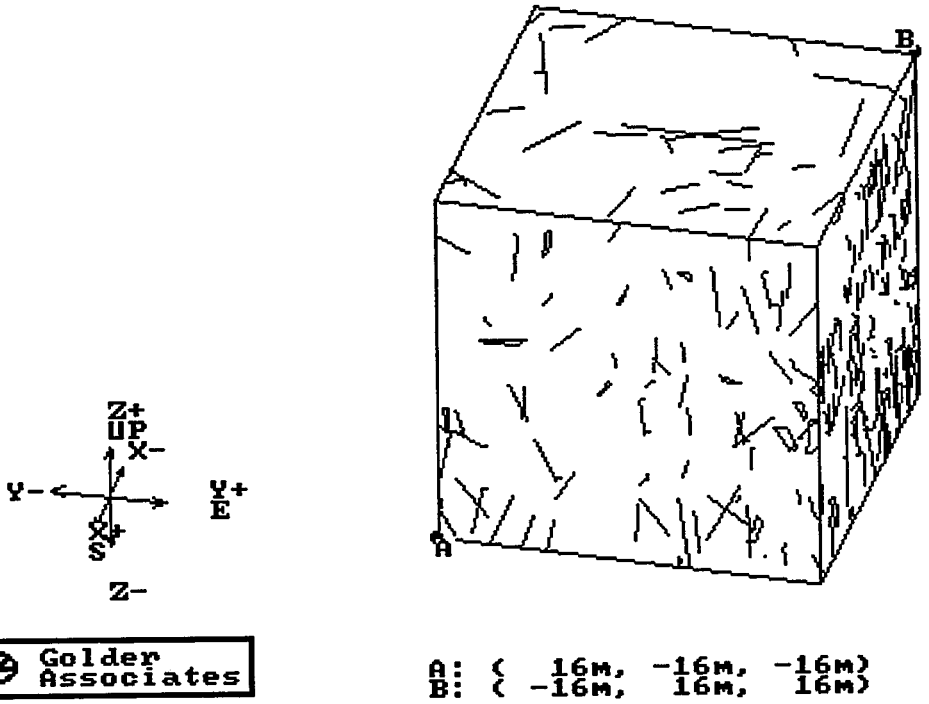

FIGURE **3-45**
BLOCK DIAGRAM OF DFN MODEL OF TENSLEEP AT NOB
NPTO

PROJECT NO. 983 1258.521 DRAWING NO. 85050 DATE 8/9/99 DRAWN BY TK

Golder Associates

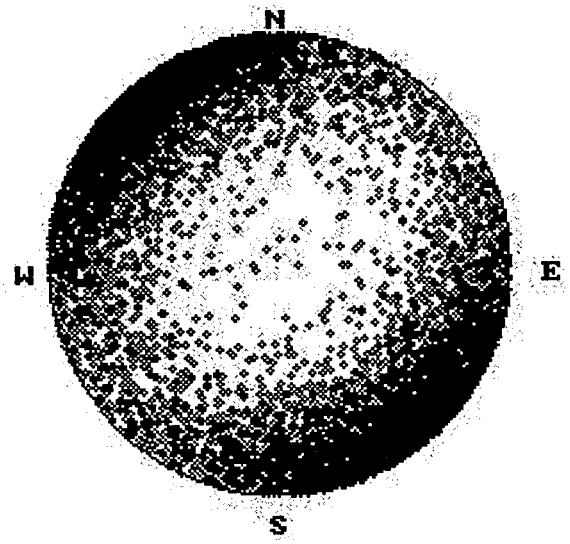

(a) All fractures in model

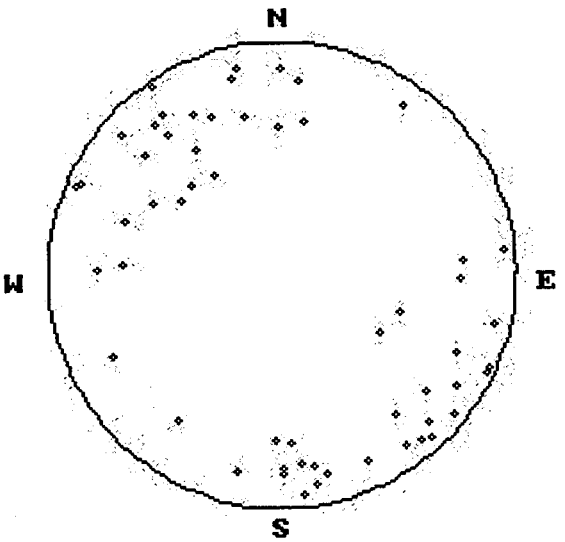

(b) Intersected by 6 simulated Vertical Wells
(i.e. compare to Figure 3-41g)

FIGURE **3-46**
FRACTURE ORIENTATIONS IN TENSLEEP DFN MODEL
NPTO

PROJECT NO. 983 1258.521 DRAWING NO. 85051 DATE 8/9/99 DRAWN BY TK

Golder Associates

Parameter	Assumption	Basis
Generation Regions	32x32x32 m box with 8 layers (Table 3-14)	100′ thickness of "A"-"B"-"C" sandstones and dolomitic sequences.
Spatial Model	Enhanced Baecher	Fracture spacing from FMI logs
Fracture Orientation	Fisher Distribution Mean pole (trend,plunge) = (127°, 0.8°) Dispersion $\kappa = 3.3$	FMI logs
Fracture Size	Lognormal Geometric mean = 2 m StDev = 1 m	Forward modeling from 4 pad intersection probability
Fracture Intensity (sandstones)	Geologic Intensity $P_{32} = 0.8\ m^{-1}$ Sensitivity Analysis $P_{32} = 0.6, 0.4, 0.2\ m^{-1}$	40 fractures in 200′ P10 = $0.66\ m^{-1}$
Fracture Intensity (dolomites)	Geologic Intensity $P_{32} = 0.4\ m^{-1}$ Sensitivity Analysis $P_{32} = 0.3, 0.2, 0.1\ m^{-1}$	Conductive fracture intensity in dolomites assumed to be 50% of sandstone
Truncation	On region boundaries	Assumption to reduce connectivity across layers
Fracture Aperture	Normal Distrib., Mean =0.2 mm = $2x10^{-4}$ m, stdev=0.05 mm = $5x10^{-5}$ m	0.1 to 0.3 mm estimate from Hurley
Fracture Transmissivity	$1x10^{-6}\ m^2/s$	Assumption

Table 3-15 Preliminary Tensleep DFN Model Parameters

Test	9/8/93	10/11/89
Injector	Govt. Tract 3B 5-T	Govt. Tract 3B 14T
Tracer(s)	Bromide	Boron
Duration (days)	42 +	125 +
# Monitoring Wells	8	8
Recovery Wells (Top 5)	7-ET 2% 4-ET 1.5% 8-T 0.5% 10-T 0.5%? Cactus 10 0.5%?	GT3B 8 9% Cactus A5 5% Sidney 14 5% GT3B 10 5%

Table 3-16 Relevant Tracer Tests, North Oregon Basin

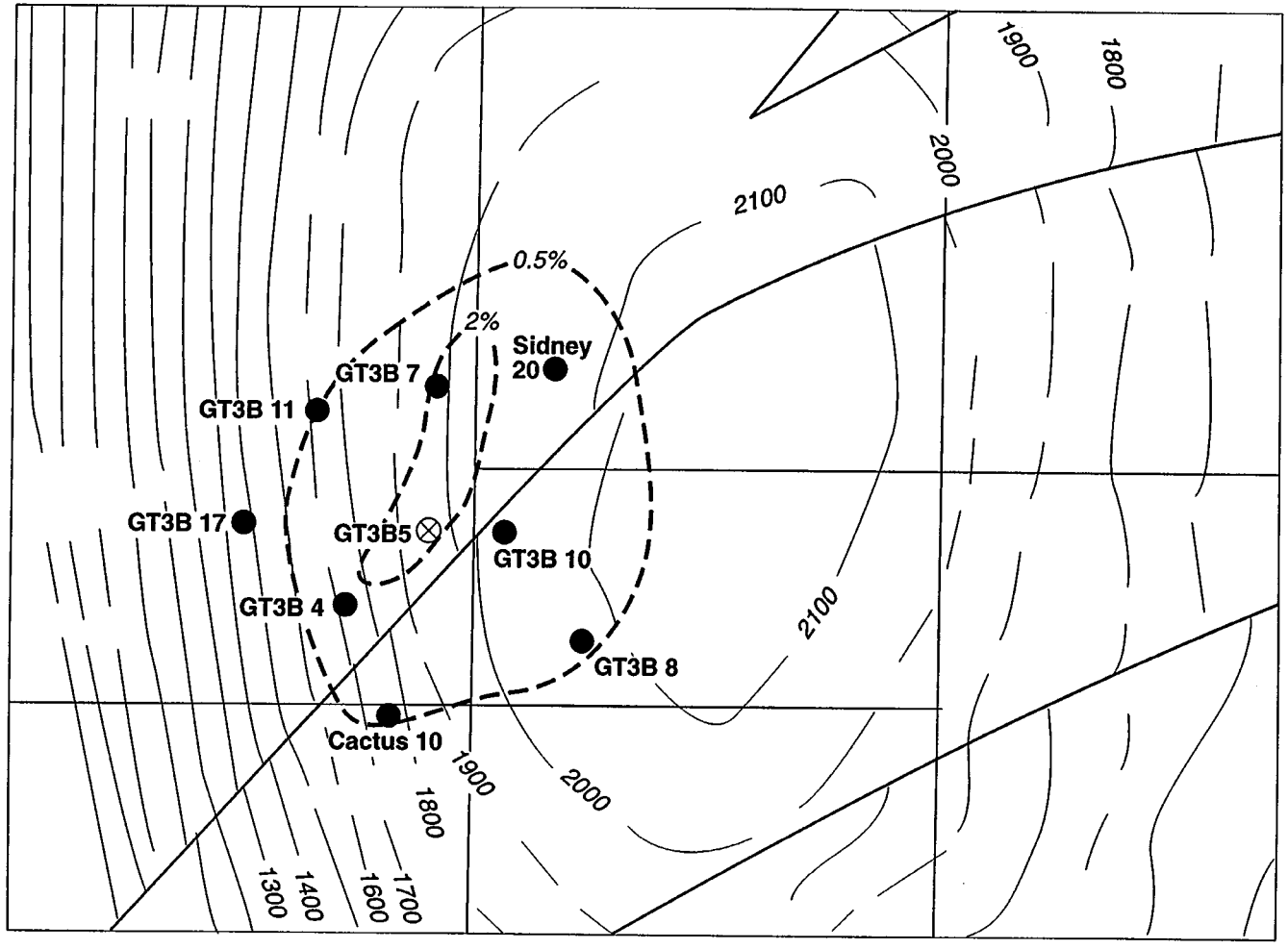

LEGEND

—2100— Contours on top of Tensleep

– –2% — · Contours of cumulative recovery of Bromide

⊗ Injection well

● Pumping well

FIGURE **3-47**

NORTH DOME TRACER TEST BROMIDE

NPTO

PROJECT NO. 983 1258.521 DRAWING NO. 85047 DATE 8/9/99 DRAWN BY EA

Golder Associates

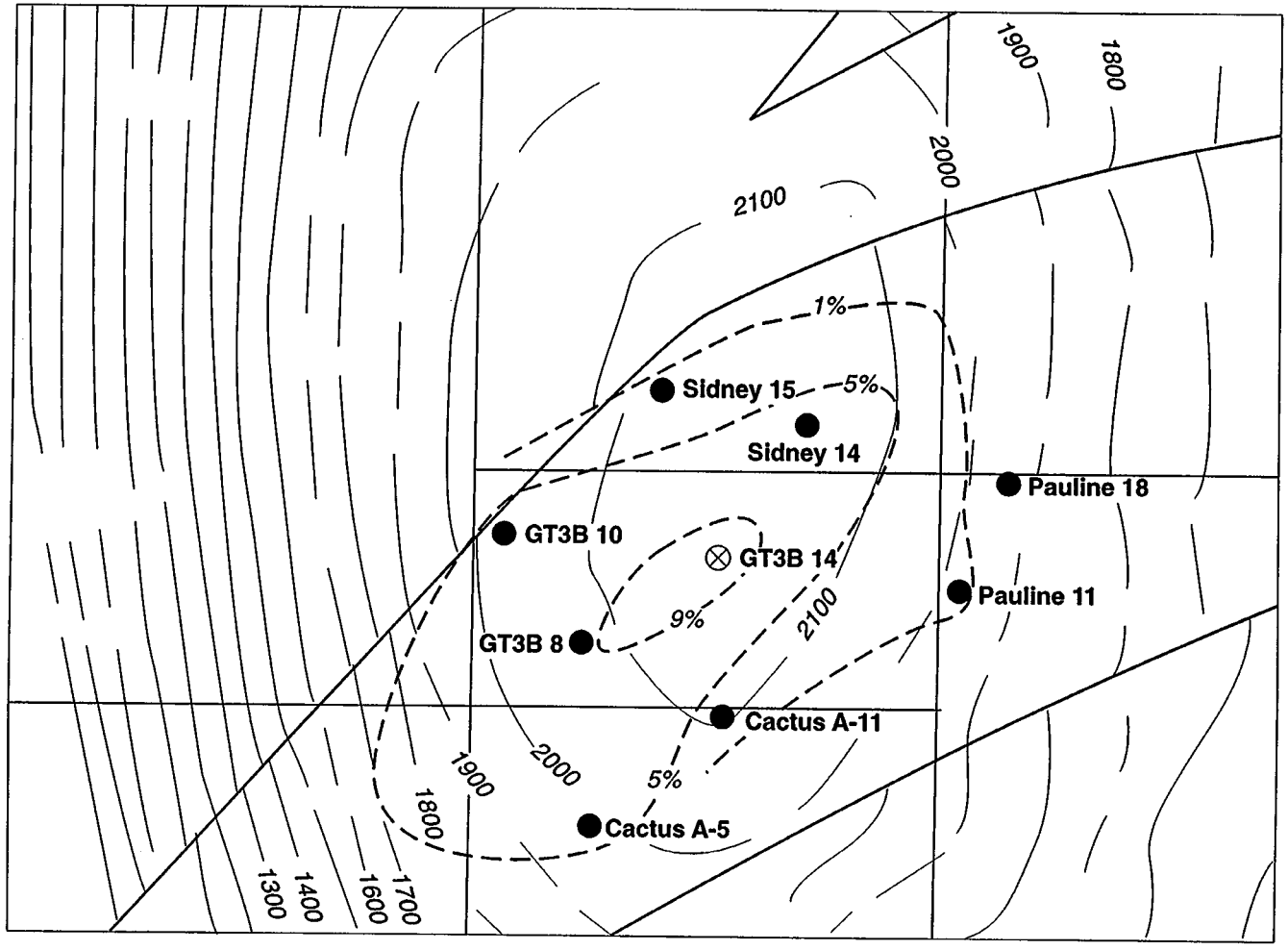

LEGEND

—2100— Contours on top of Tensleep

— -2%- — Contours of cumulative recovery of Boron

⊗ Injection well

● Pumping well

FIGURE **3-48**

NORTH DOME TRACER TEST BORON

NPTO

PROJECT NO. 983 1258.521 DRAWING NO. 85048 DATE 8/9/99 DRAWN BY EA

Golder Associates

3.2.6.2 Task 3.2.2 DFN Analysis of Stoney Point

During the reporting period, work was initiated on implementation of Discrete Fracture Network modeling to support IOR strategies for Stoney Point. As part of this effort, compartment volumes and tributary volumes were calculated for the models. This was done using the program FraCluster, which was developed under previous DOE funding (Dershowitz et al., 1998).

A compartment is a region connected by a network of fractures. Relevant information that can be calculated about a compartment are its volume, surface area, and area projected on to a horizontal plane. Tributary volume analysis is a geometric calculation of the volume accessed by a well or set of wells in a fractured reservoir (Figure 3-49). Two different methods provide a maximum and minimum estimate of the volume.

- Hull volume is the volume contained in a convex hull surrounding a fracture network connected to the well. This is a maximum volume because it can include large blocks of matrix between fractures.
- Fracture thickness volume is the volume of a one-meter slab around each fracture connected to the well.

The results of the compartment size and area analysis for the Stoney Point field are shown in Figure 3-50 through Figure 3-52. As shown graphically in Figure 3-50, at high fracture intensities the fractured reservoir defined by a convex hull includes all three portions of the structural model, from the northern fault through the step-over to the southern fault. This is likely to be too well connected compared to the real reservoir characteristics of Stoney Point. The medium (Figure 3-50b) and lower (Figure 3-50c) intensity models more closely represent the reservoir structure as indicated by reservoir development and well tests. The number of compartments and their projected areas and volumes are graphed in Figures 3-51 and 3-52 and listed in Table 3-15. This analysis shows that at the lowest fracture intensity (0.001) five small compartments form, while at an intensity one order of magnitude higher, one very large compartment forms.

The well configuration shown in Figure 3-53 was assumed for the tributary volume calculations. Vertical wells are 200-m long and spaced 200 m apart (equivalent to about a 10 acre well spacing). Horizontal wells are 50 long and have the same spacing. The graph in Figure 3-54 shows the insensitivity of the modeled reservoir to well orientation; in only one case did the SE horizontal well intersect fewer compartments than the vertical well. Much more important than well orientation is fracture intensity. Figure 3-55 also clearly demonstrates the importance of fracture intensity for well success. In the top frame 9 out of 12 wells successfully connect into a fracture network. In the bottom frame only four out of 12 simulated wells were successful.

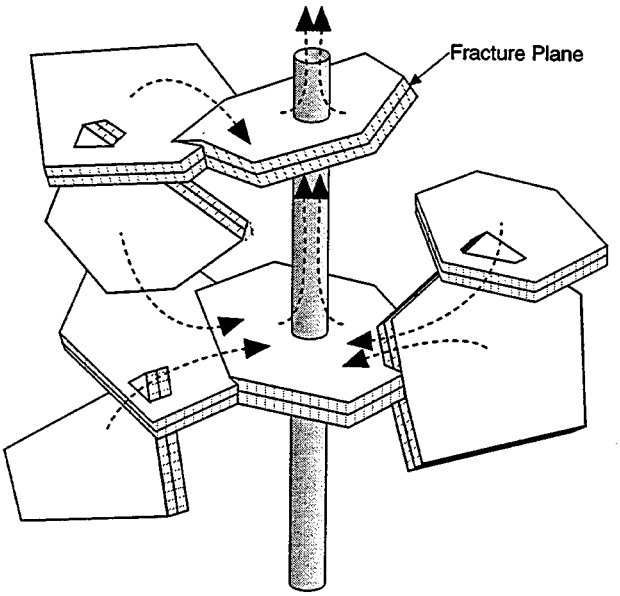

a) Slab Algorithm

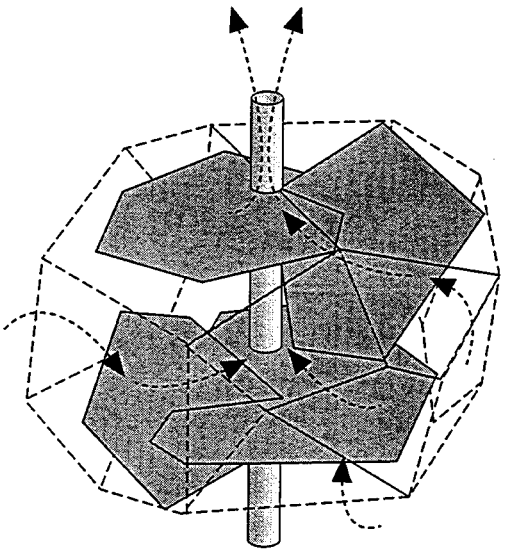

b) Convex Hull Algorithm

FIGURE **3-49**
TRIBUTARY DRAINAGE VOLUME ALGORITHMS
NPTO

PROJECT NO. 983 1258.521 DRAWING NO. 85052 DATE 7/30/99 DRAWN BY TK

Golder Associates

Projected Compartment Areas (m^2)					
P_{32}	# Compts.	Average	Std. Dev.	Minimum	Maximum
0.01	1	9.12e+5	0	9.12e+5	9.12e+5
0.005	2	4.68e+5	3.35e+5	1.3e+5	8.1e+5
0.0025	4	1.95e+5	2.21e+5	5.6e+4	5.8e+5
0.001	5	8.76e+5	3.19e+4	4.1e+4	1.4e+5
Compartment Volumes (m^3)					
P_{32}	# Compts.	Average	Std. Dev.	Minimum	Maximum
0.01	1	1.39e+8	0	1.39e+8	1.39e+8
0.005	2	6.81e+7	5.18e+7	1.6e+7	1.2e+8
0.0025	4	2.95e+7	3.62e+7	6.9e+7	9.3e+7
0.001	5	1.07e+7	4.33e+6	3.8e+6	1.7e+7

Table 3-17 Compartment Area and Volume Analysis, Stoney Point

Vertical Well Tributary Volumes (m^3)					
P_{32}	# Compts.	Average	Std. Dev.	Minimum	Maximum
0.01	1	1.39e+8	0	1.39e+8	1.39e+8
0.005	2	6.81e+7	5.18e+7	1.67e+7	1.2e+8
0.0025	1	9.21e+7	0	9.21e+7	9.21e+7
0.001	2	1.01e+7	9.9e+5	9.03e+6	1.12e+7
NE Horizontal Wells Tributary Volumes (m^3)					
P_{32}	# Compts.	Average	Std. Dev.	Minimum	Maximum
0.01	1	1.39e+8	0	1.39e+8	1.39e+8
0.005	2	6.81e+7	5.18e+7	1.67e+7	1.2e+8
0.0025	1	9.21e+7	0	9.21e+7	9.21e+7
0.001	2	1.01e+7	9.9e+5	9.03e+6	1.12e+7
SE Horizontal Wells Tributary Volumes (m^3)					
P_{32}	# Compts.	Average	Std. Dev.	Minimum	Maximum
0.01	1	1.39e+8	0	1.39e+8	1.39e+8
0.005	1	1.2e+8	0	1.2e+8	1.2e+8
0.0025	1	9.21e+7	0	9.21e+7	9.21e+7
0.001	2	1.01e+7	9.9e+5	9.03e+6	1.12e+7

Table 3-18 Tributary Volume Analysis, Stoney Point

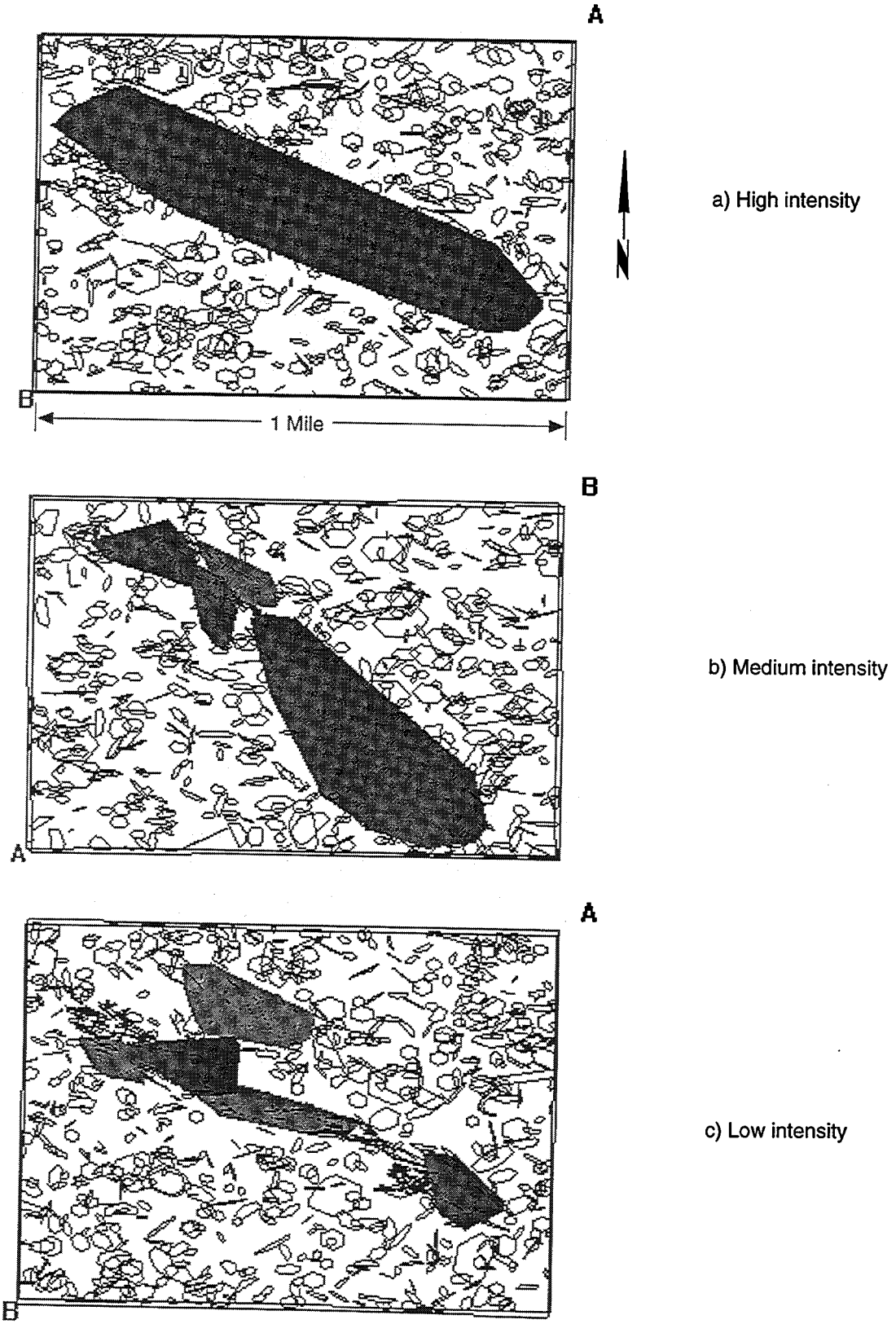

FIGURE **3-50**
COMPARTMENTS IN STONEY POINT DFN
NPTO

PROJECT NO. 983 1258.521 DRAWING NO. 85053 DATE 7/30/99 DRAWN BY EA

Golder Associates

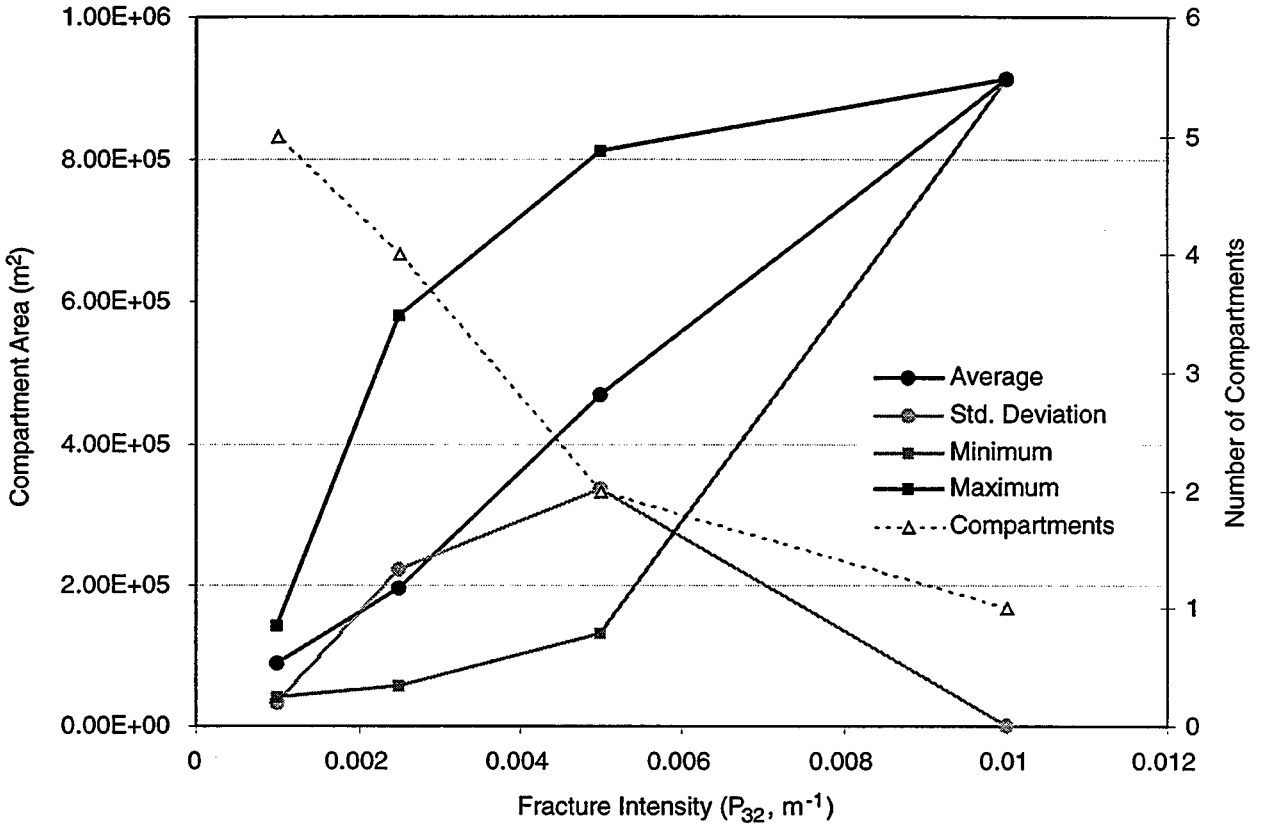

FIGURE **3-51**
PROJECTED AREAS OF COMPARTMENTS IN STONEY POINT MODEL
NPTO

PROJECT NO. 983 1258.521 DRAWING NO. 85054 DATE 7/30/99 DRAWN BY EA

Golder Associates

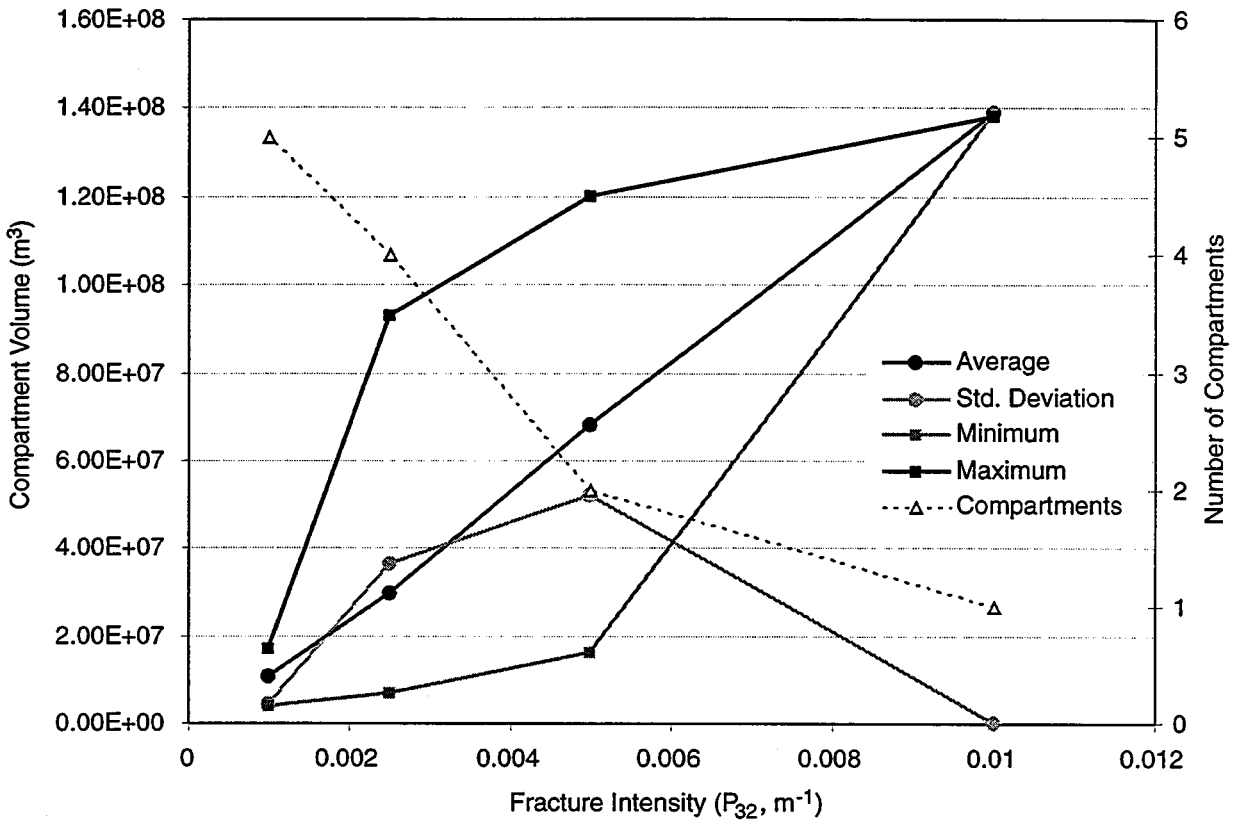

FIGURE **3-52**
VOLUMES OF COMPARTMENTS IN STONEY POINT MODEL
NPTO

PROJECT NO. 983 1258.521 DRAWING NO. 85055 DATE 7/30/99 DRAWN BY EA

Golder Associates

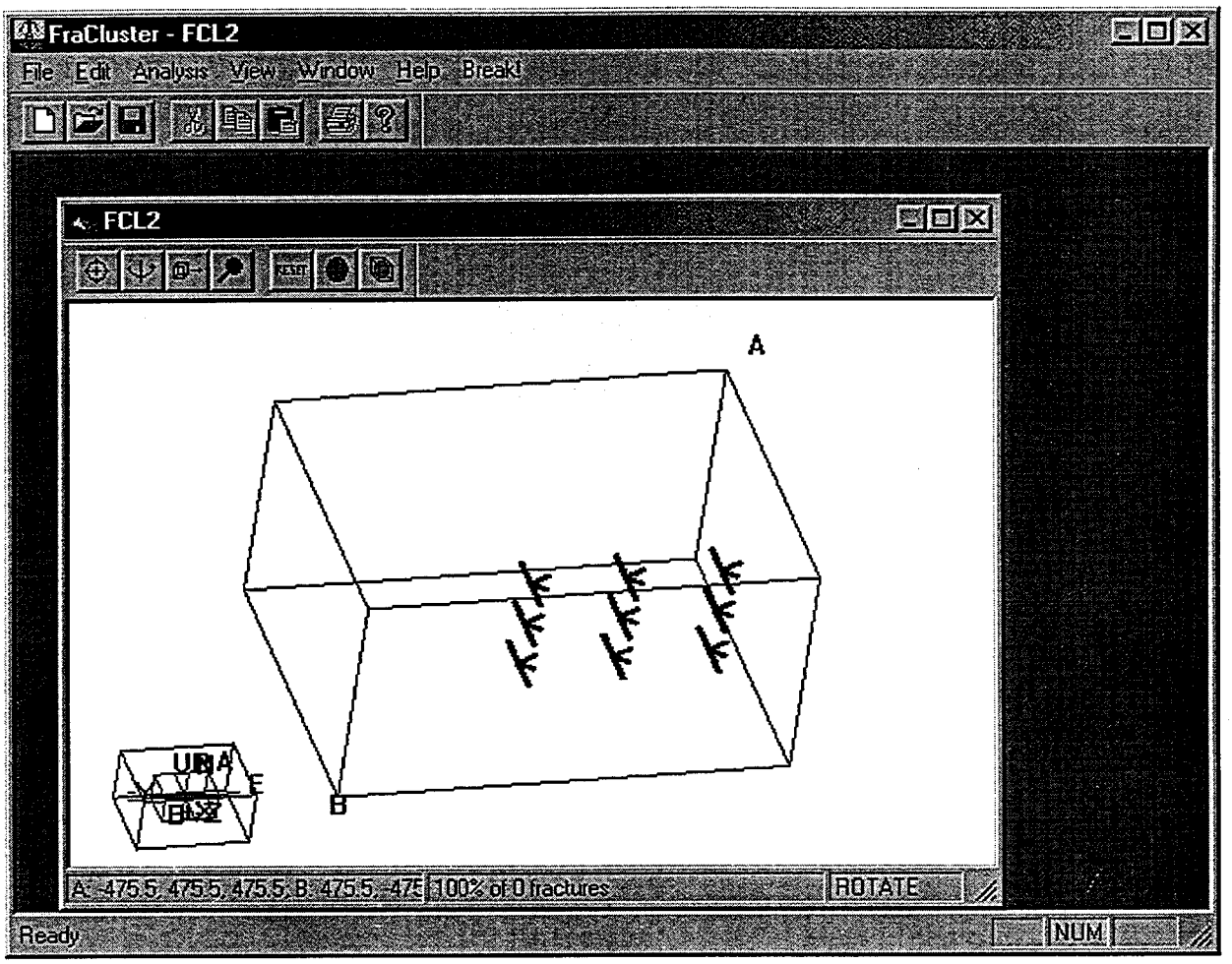

FIGURE **3-53**

WELL CONFIGURATION FOR TRIBUTARY VOLUME ANALYSIS OF STONEY POINT MODEL

NPTO

PROJECT NO. 983 1258.521 DRAWING NO. 85056 DATE 7/30/99 DRAWN BY EA

Golder Associates

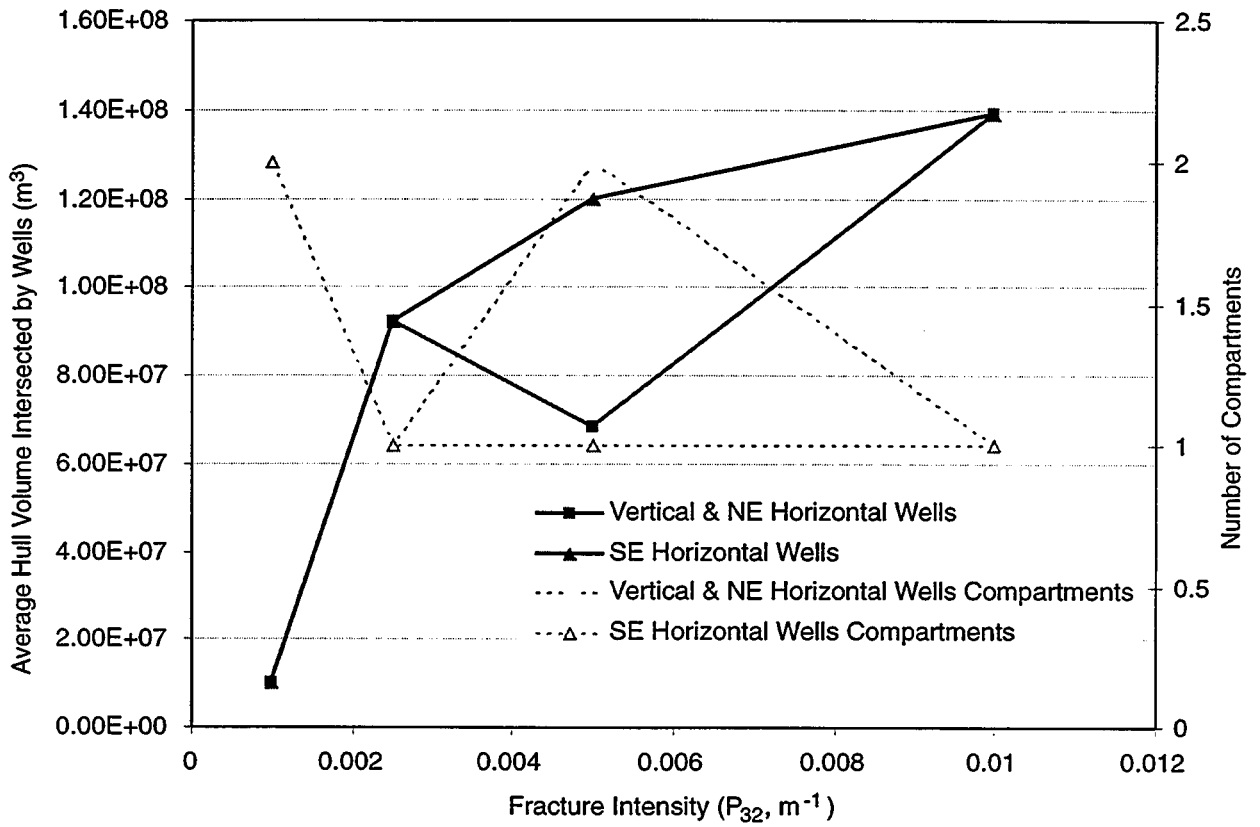

FIGURE **3-54**
TRIBUTARY VOLUMES OF STONEY POINT MODEL
NPTO

PROJECT NO. 983 1258.521 DRAWING NO. 85057 DATE 8/12/99 DRAWN BY EA

Golder Associates

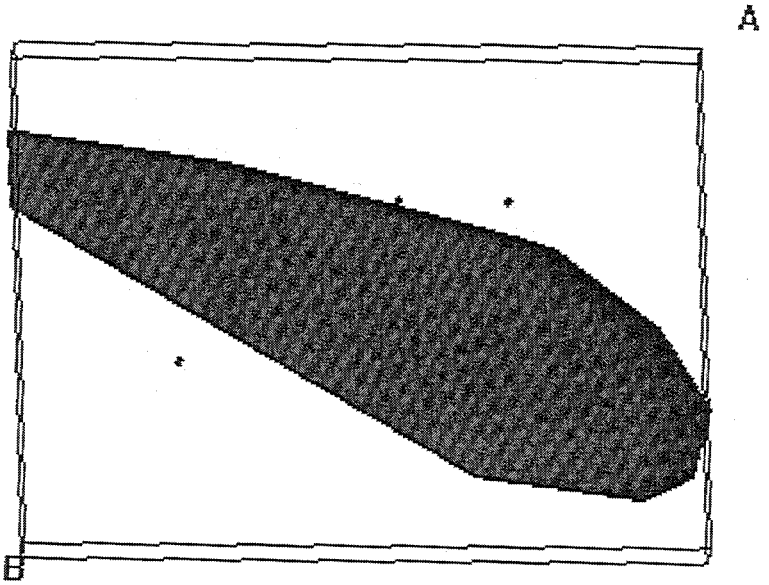

a) Medium intensity

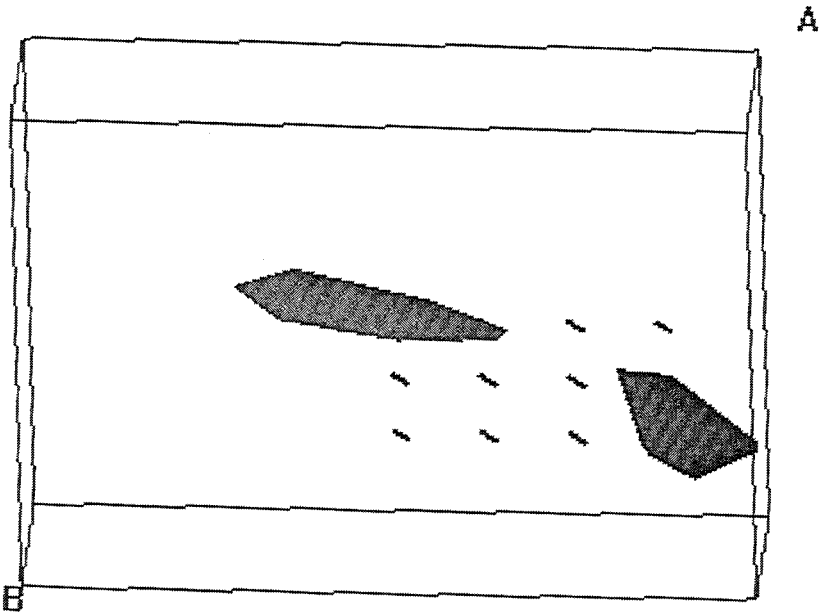

b) Low intensity

FIGURE **3-55**

WELL PATTERN AND TRIBUTARY VOLUMES INTERSECTED IN STONEY POINT MODEL

NPTO

PROJECT NO. 983 1258.521 DRAWING NO. 85058 DATE 7/31/99 DRAWN BY EA

Golder Associates

3.2.7 Task 3.3 South Oregon Basin Reservoir Improvement Strategy

3.2.7.1 Task 3.3.1 DFN Strategy for IOR

The IOR issue at South Oregon Basin relates to bypassed oil in the uppermost Phosphoria. Oil saturation in the upper Phosphoria is 80% whereas in the lower part of the formation saturation is as low as 30-40%. The perceived connectivity problem in the upper Phosphoria (B. Curran, pers. comm.) is that the pores are unconnected except by fractures. The engineering solution to this problem is more strategic well placements.

In the first progress report (Dershowitz, 1999) Golder identified that the primary tasks for South Oregon Basin would be "carrying out compartment and tributary volume calculations including a range of oriented well locations." Table 3-19 lists these engineering questions and the respective DFN solutions as well as other possible questions and solutions that we anticipate will be addressed in the future.

Engineering operation or question	Potential DFN tool to answer	Timing
Well orientation and placement to maximum horizontal connection	Compartment and tributary volume calculations in FracCluster	Preliminary analysis this quarter
Surface area to volume for gel (WALRUS) treatment		
What is the flow dimension of the fracture network in the Phosphoria?	Fracdim and Flare	Next quarter or later?
Can tracer tests which show NNE permeability trends be used for model calibration?	Flow solution and particle tracking in MAFIC	Next quarter or later?

Table 3-19 IOR Engineering Issues, South Oregon Basin

3.2.7.2 Task 3.2.2 DFN Analysis of South Oregon Basin

During the reporting period, work was initiated on implementation of discrete fracture network (DFN) modeling to support IOR strategies for South Oregon Basin. As part of this effort connectivity analyses were carried out using the DFN model developed for Task 2.3.3. These models focussed on the "percolation threshold", which defines the transition in connectivity with increases in fracture intensity. Results of this compartmentalization analysis are shown in Figure 3-56 and summarized in Table 3-20. At low fracture intensities ($P_{32}<0.2$ m^{-1}), the fractures do not connect into any significant compartments. At high fracture intensities ($P_{32}>0.4$ m^{-1}), the fractures connect the entire volume around the well. The transition from unconnected fractures to fully connected fractures is called the percolation threshold. For the South Oregon Basin Phosphoria model, this occurs near 0.3 m^2/m^3.

Projected Compartment Areas (m^2)					
P_{32}	# Compts.	Average	Std. Dev.	Minimum	Maximum
0.2	5	482	343	180	1000
0.3	16	471	403	120	1500
0.4	10	680	1170	110	3848
0.6	2	1984	2636	120	3848
0.8	2	1984	2636	120	3848
Projected Compartment Volumes (m^3)					
P_{32}	# Compts.	Average	Std. Dev.	Minimum	Maximum
0.2	5	13100	13000	2600	35000
0.3	16	12700	16800	1500	56000
0.4	10	32000	78400	1100	269392
0.6	2	135246	189711	1100	269392
0.8	2	135396	189499	1400	269392

Table 3-20 Compartment Area and Volume Analysis, South Oregon Basin

In order to assess the importance of well orientation on fracture volumes intersected, three wells were simulated: a SE-trending horizontal well, a NE-trending horizontal well, and a vertical well. The results of the tributary volume analysis are shown graphically in Figure 3-57 and Figure 3-58, and are summarized in Figure 3-59. At low fracture intensity (P_{32}=0.2 m^{-1}) there are five compartments formed in the region surrounding the wells; however, none are intersected by the three perpendicular wells. In one instance in Figure 3-56, the well intersects the convex hull of a fracture network, but no fracture in that network intersects the well. If this geometry were the case in a real well, induced fracturing would prove very successful by making the connection to the fracture cluster. At a slightly higher fracture intensity (P_{32}=0.3 m^{-1}), large, vertical NE-SW trending compartments are formed. Because of their orientation, the SE-NW horizontal well, intersects the greatest fracture volume (Figure 3-59). The lower half of Figure 3-59 shows the difference between the hull volume and slab volume methods of calculating tributary drainage. The hull volume could be used to calculate the total oil accessible to a well. The flow from the matrix blocks into the fractures would depend upon the matrix permeability (due either to connected pores or microfracturing). The fracture slab volume is roughly 10% of the hull volume (Figure 3-59). This volume would correspond to the volume of injected fluids necessary for tracer tests and gel treatments. Table 3-22 summarizes the preliminary conclusions, which can be drawn from the cluster analysis of the Phosphoria formation at South Oregon Basin.

Vertical well Tributary Volumes		Hull volumes				Volumes from fracture thickness			
P_{32}	# compts.	mean	stdev	min	max	mean	stdev	min	max
0.2	0								
0.3	1	50100	0	50100	50100	6190	0	6190	6190
0.4	2	134000	133000	1100	270000	26000	25600	40000	62000
0.6	1	397000	0	397000	397000	112000	0	112000	112000
0.8	1	420000	0	420000	420000	150000	0	150000	150000
H1 well Tributary Volumes		Hull volumes				Volumes from fracture thickness			
P_{32}	# compts.	Mean	stdev	min	max	mean	stdev	min	max
0.2	0								
0.3	3	30000	17200	7900	51000	4430	1820	1900	6300
0.4	2	134000	133000	1100	270000	26000	25600	40000	62000
0.6	1	397000	0	397000	397000	112000	0	112000	112000
0.8	1	420000	0	420000	420000	150000	0	150000	150000
H2 well Tributary Volumes		Hull volumes				Volumes from fracture thickness			
P_{32}	# compts.	mean	stdev	min	max	mean	stdev	min	max
0.2	0								
0.3	1	50100	0	50100	50100	6190	0	6190	6190
0.4	1	267000	0	267000	267000	51500	0	51500	51500
0.6	1	397000	0	397000	397000	112000	0	112000	112000
0.8	1	420000	0	420000	420000	150000	0	150000	150000

Table 3-21 Tributary Volume Analysis, South Oregon Basin

Question	**Answer**	**Uncertainties or assumptions**
Does the Phosphoria break into compartments at the well scale?	Yes, if conductive fracture intensity is less than 25% of the geologic intensity ($P_{32}<0.4\ m^{-1}$)	Fracture size
Minimum volume of surfactant to inject?	~1,000,000 gallons 264* m^3	$P_{32}=0.3\ m^{-1}$ and assuming 1 m penetration around each fracture

Table 3-22 Implications of Tributary Volume Analysis, South Oregon Basin

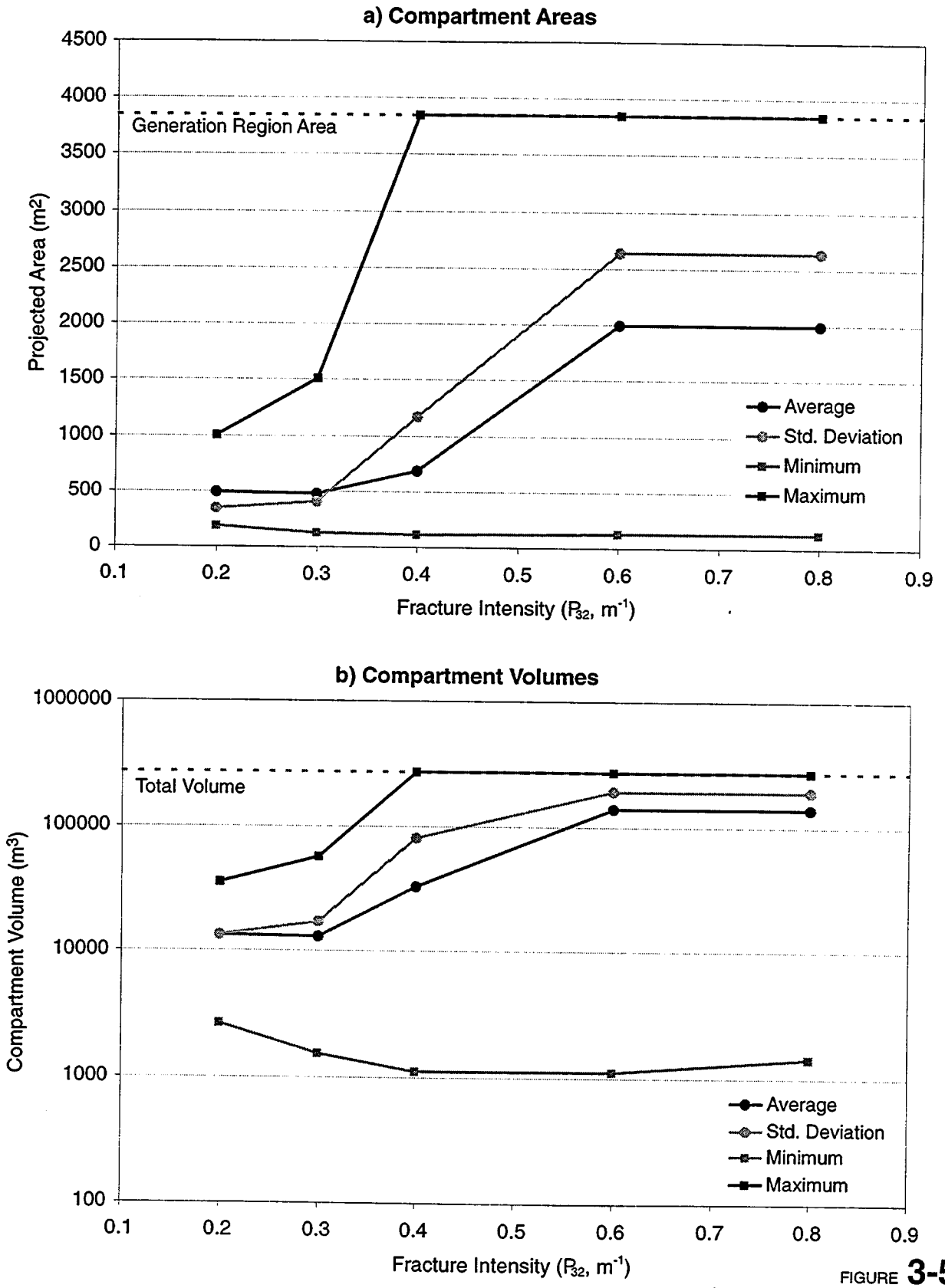

FIGURE **3-56**

SOUTH OREGON BASIN COMPARTMENTALIZATION ANALYSIS

NPTO

PROJECT NO. 983 1258.521 DRAWING NO. 85061 DATE 8/12/99 DRAWN BY EA

Golder Associates

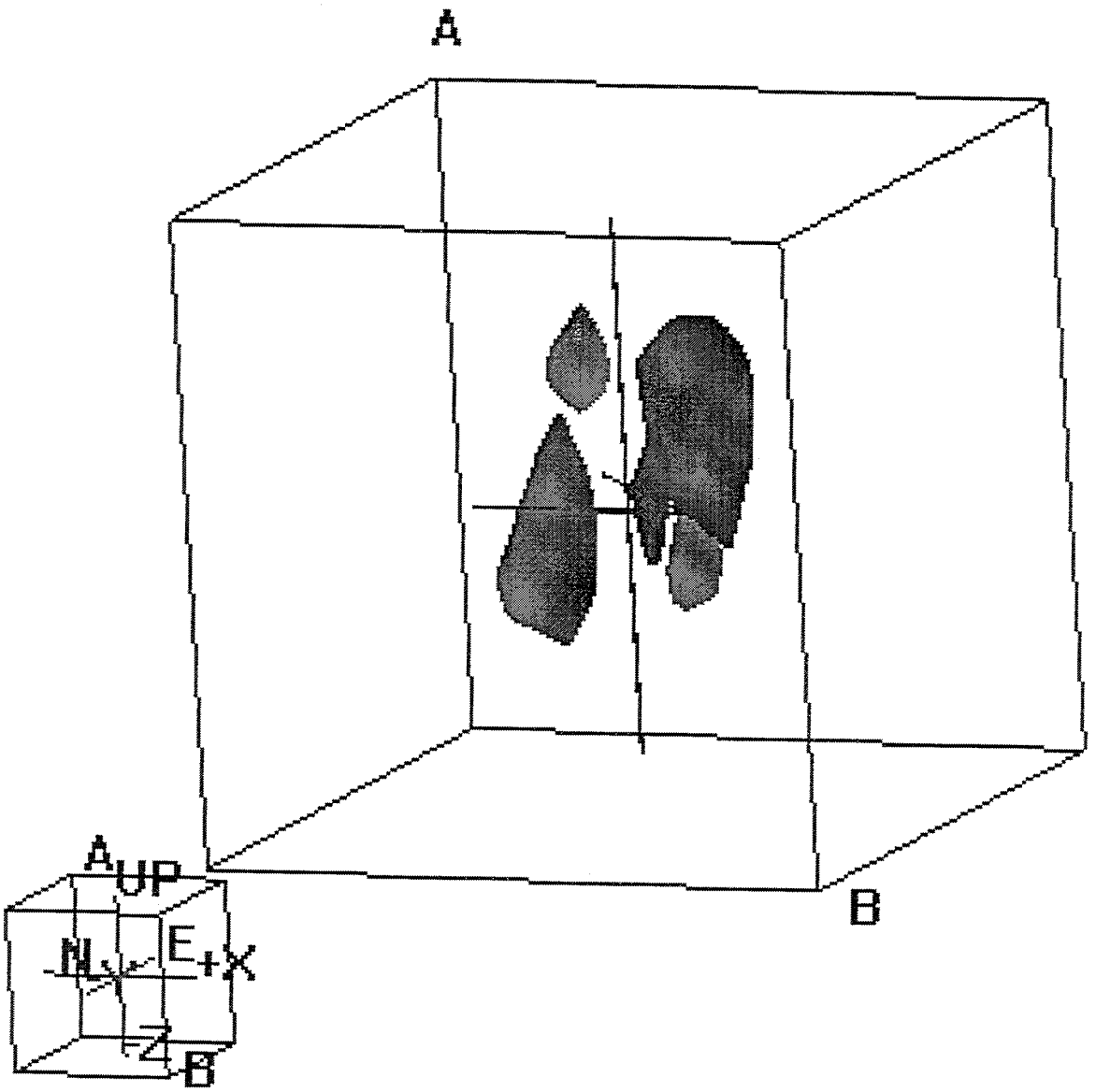

FIGURE **3-57**
TRIBUTARY VOLUMES IN SOUTH OREGON BASIN MODEL FOR P_{32} = 0.2 MODEL
NPTO

PROJECT NO. 983 1258.223 DRAWING NO. 85059 DATE 8/12/99 DRAWN BY TK

Golder Associates

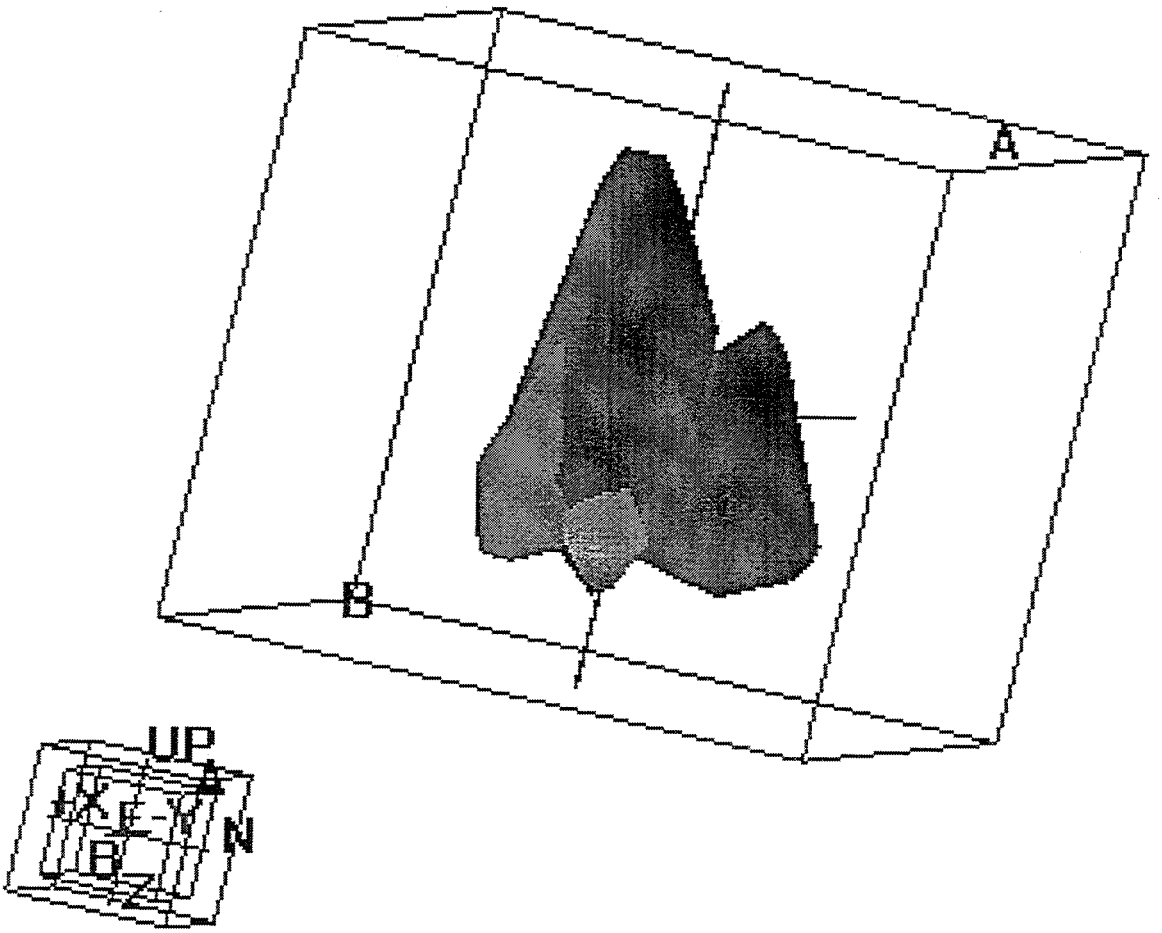

FIGURE **3-58**
TRIBUTARY VOLUMES IN SOUTH OREGON BASIN MODEL FOR P_{32} = 0.3 MODEL
NPTO

PROJECT NO. 983 1258.521 DRAWING NO. 85060 DATE 8/12/99 DRAWN BY TK

Golder Associates

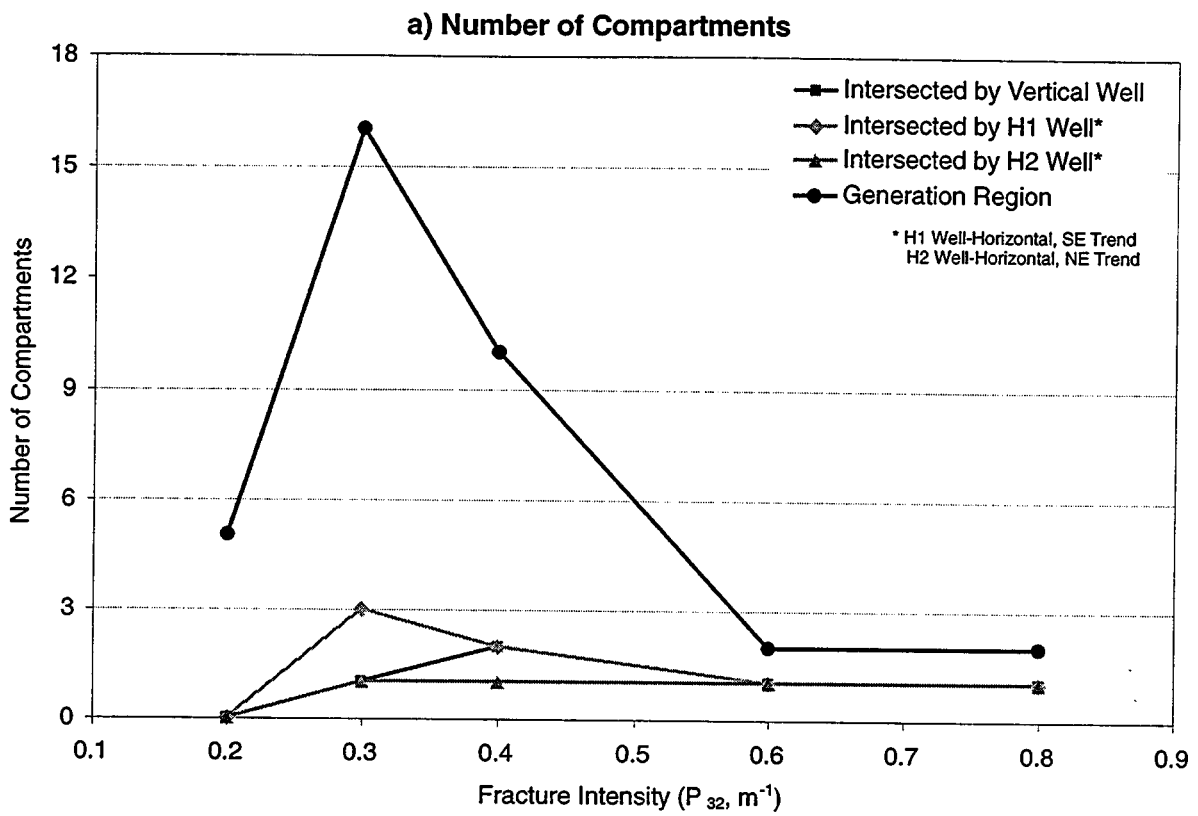

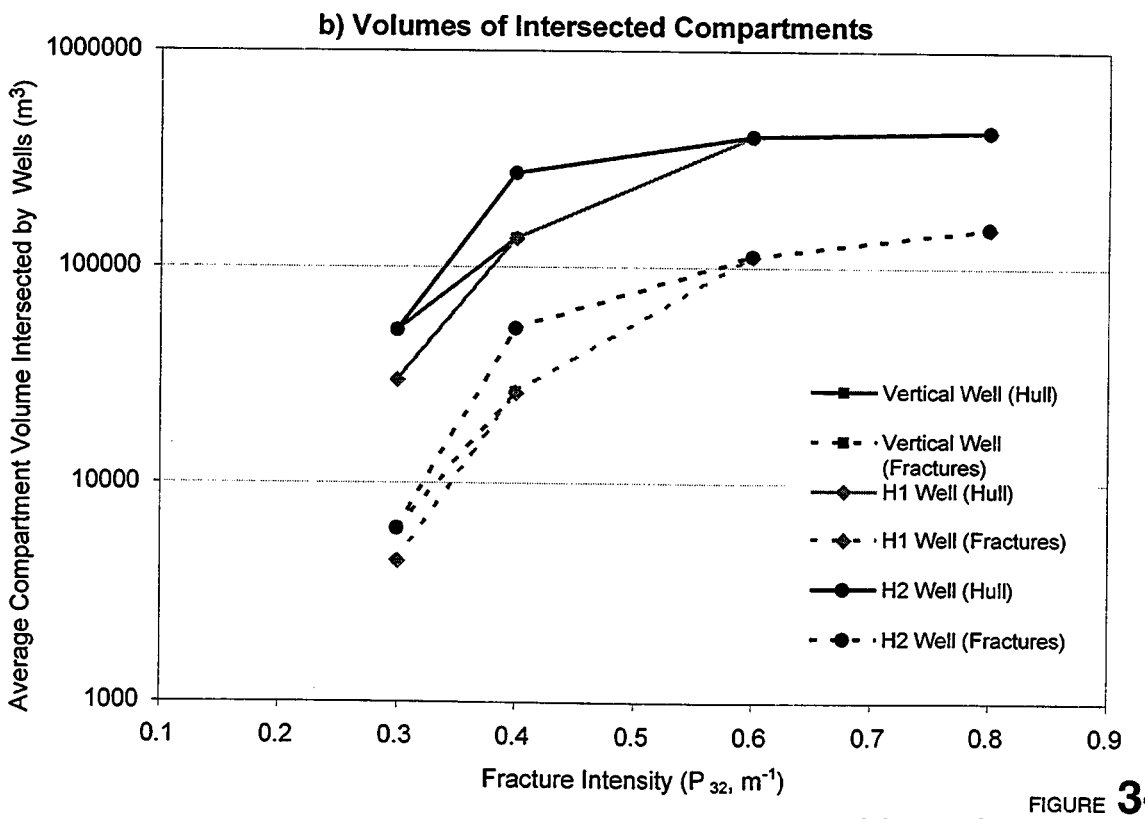

FIGURE **3-59**
SOUTH OREGON BASIN
TRIBUTARY VOLUME ANALYSIS
NPTO

PROJECT NO. 983 1258.521 DRAWING NO. 85062 DATE 7/30/99 DRAWN BY EA

Golder Associates

3.2.8 Task 3.4 North Oregon Basin Reservoir Improvement Strategy

3.2.8.1 Task 3.4.1 DFN Strategy for IOR

The IOR issues at South Oregon Basin relate to bypassed oil in the "ABC" sandstones of the upper Tensleep. Dolomite intrabeds, water-filled fractures, deformation bands, and dune cross-bedding all create horizontal compartments in the upper Tensleep reservoir (Table 3-14). Breaches of the horizontal compartments occur where fracturing in the dolomite intrabed between the C and D sandstone allows communications across the dolomites. These vertical connections allow coning from the lower Tensleep, which has a much higher, water-cut than the upper Tensleep. Engineering solutions to these problems are (Dershowitz et al. 1999);

- Targeting of water injection for waterfloods,
- Horizontal drilling to connect low recovery portions of the reservoir, and
- Gel placement to reduce water cycling.

Table 3-23 summarizes DFN strategies developed for IOR in the North Oregon Basin.

IOR Problem	DFN Solution
Fractures in dolomites connect upper and lower Tensleep	Calculate pore volume and connectivity of lower and upper Tensleep for gel treatment design
Baffles due to crossbedding and deformation bands create compartments in ABC Tensleep sands	Determine optimal drilling directions to connect compartments
Water-filled fractures create compartments	

Table 3-23 IOR Engineering Issues at North Basin

3.2.8.2 Task 3.4.2 DFN Analysis of North Oregon Basin

During the reporting period work was initiated on implementation of Discrete Fracture Network modeling to support IOR strategies for North Oregon Basin. Like the South Oregon Basin DFN model of the Phosphoria formation the preliminary DFN model of the Tensleep formation at North Oregon basin was used to evaluate compartment size and locations distributions, and to calculate tributary volumes for specific well patterns. These results can be used to estimate the at-well connectivity of the reservoir and the volumes of water or gel injection necessary to achieve IOR objectives.

The results of the compartment area and volume analyses are illustrated in Figure 3-60 and summarized in Figure 3-61 and Table 3-24. Like the South Oregon Basin Phosphoria model, the percolation limit of the North Oregon Basin Tensleep model occurs near 0.3 m^2/m^3. Unlike the Phosphoria model, compartments in the Tensleep are horizontal due to the dolomite layering, rather than vertical.

Figure 3-62 and Figure 3-63 illustrate tributary drainage volumes for different well configurations. Figure 3-62 shows tributary volumes for a NE trending horizontal well, and Figure 3-36 shows tributary drainage volumes for a system of vertical and horizontal wells. Figure 3-64 and Table 3-25 summarize the results of this analysis. The shape and size of these wells can be used to assist in the design of strategic completions and well locations.

Projected Compartment Areas (m^2)					
P_{32}	# Compts.	Average	Std. Dev.	Minimum	Maximum
0.2	7	204	146	77	550
0.4	32	339	352	67	1400
0.6	6	882	1790	49	4900
0.8	1	4900	0	4900	4900
Projected Compartment Volumes (m^3)					
P_{32}	# Compts.	Average	Std. Dev.	Minimum	Maximum
0.2	7	1490	1320	520	4600
0.4	32	3240	4280	340	16000
0.6	6	26200	57400	120	156000
0.8	1	156000	0	156000	156000

Table 3-24 Compartment Area and Volume Analysis, North Oregon Basin

SE Horizontal well Tributary Volumes		hull volumes				volumes from fracture thickness			
P_{32}	number of compartments	mean	stdev	min	max	mean	stdev	min	max
0.2	0								
0.4	3	9100	4550	4400	15000	2010	1170	920	3700
0.6	1	154000	0	154000	154000	48400	0	48400	48400
0.8	1	156000	0	156000	156000	60200	0	60200	60200
NE Horizontal well Tributary Volumes		**hull volumes**				**volumes from fracture thickness**			
P_{32}	number of compartments	mean	stdev	min	max	mean	stdev	min	max
0.2	0								
0.4	3	6150	4180	530	11000	1270	743	220.	1900
0.6	1	154000	0	154000	154000	48400	0	48400	48400
0.8	1	156000	0	156000	156000	60200	0	60200	60200
Vertical well Tributary Volumes		**hull volumes**				**volumes from fracture thickness**			
P_{32}	number of compartments	mean	stdev	min	max	mean	stdev	min	max
0.2	0								
0.4	1	15300	0	15300	15300	3640	0	3640	3640
0.6	1	154000	0	154000	154000	48400	0	48400	48400
0.8	1	156000	0	156000	156000	60200	0	60200	60200

Table 3-25 Tributary Volume Analysis, North Oregon Basin

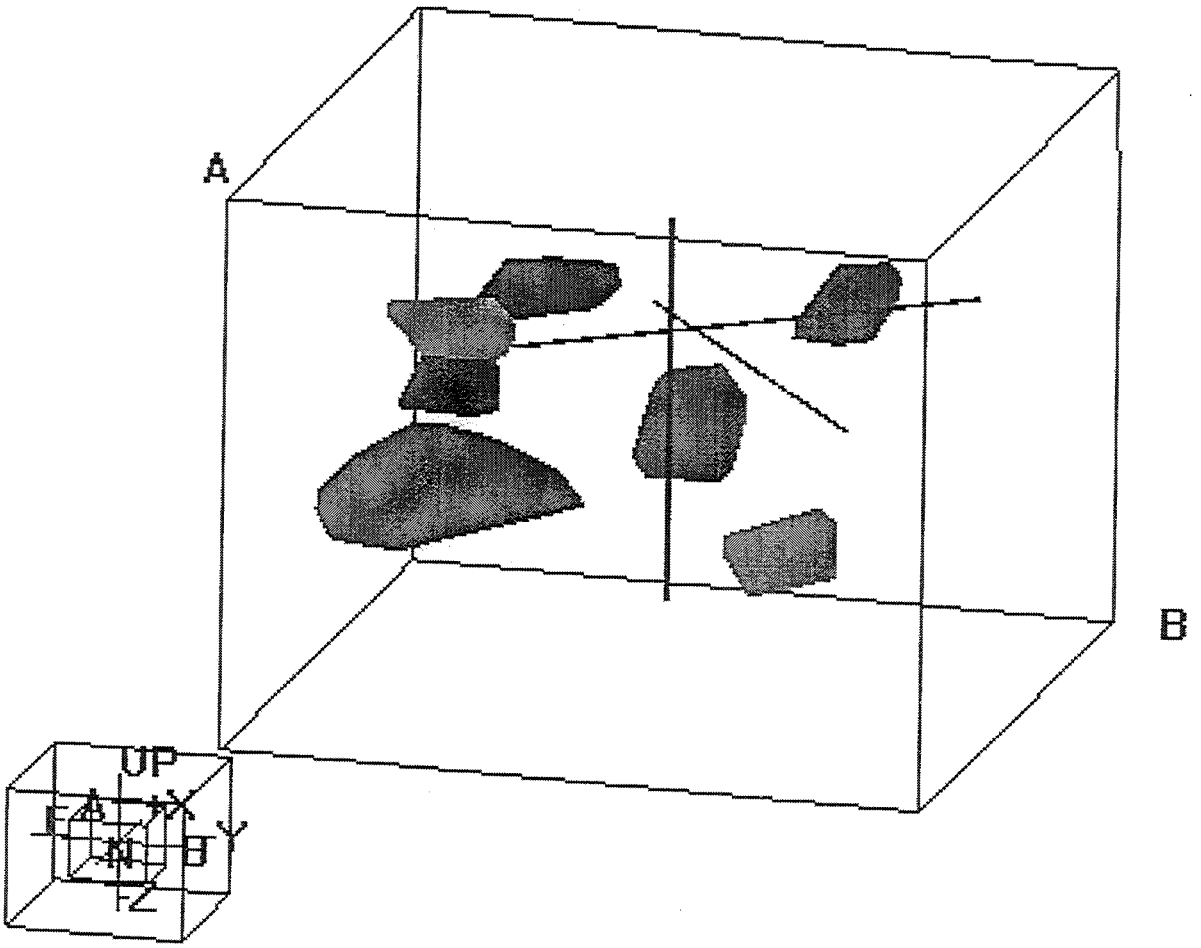

FIGURE **3-60**
COMPARTMENTS IN NORTH OREGON BASIN MODEL WITH P_{32} = 0.2
NPTO

PROJECT NO. 983 1258.521 DRAWING NO. 85063 DATE 7/30/99 DRAWN BY TK

Golder Associates

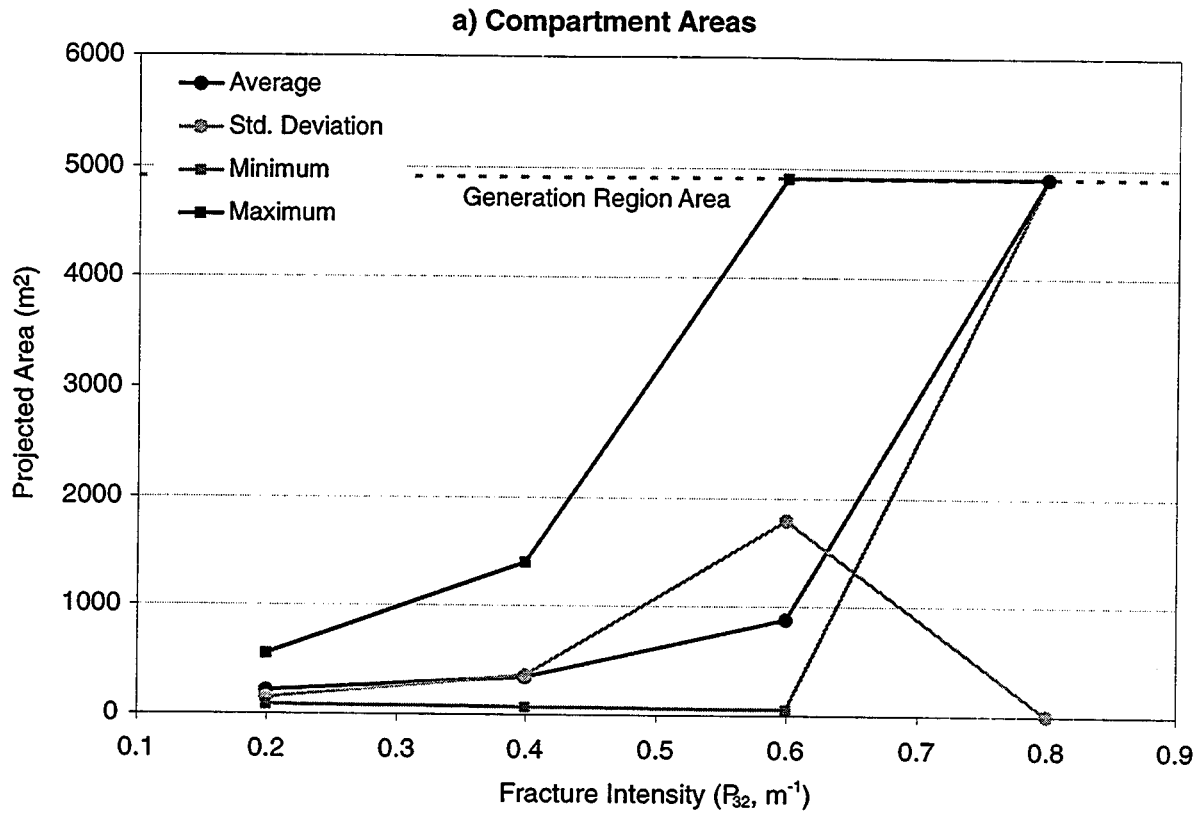

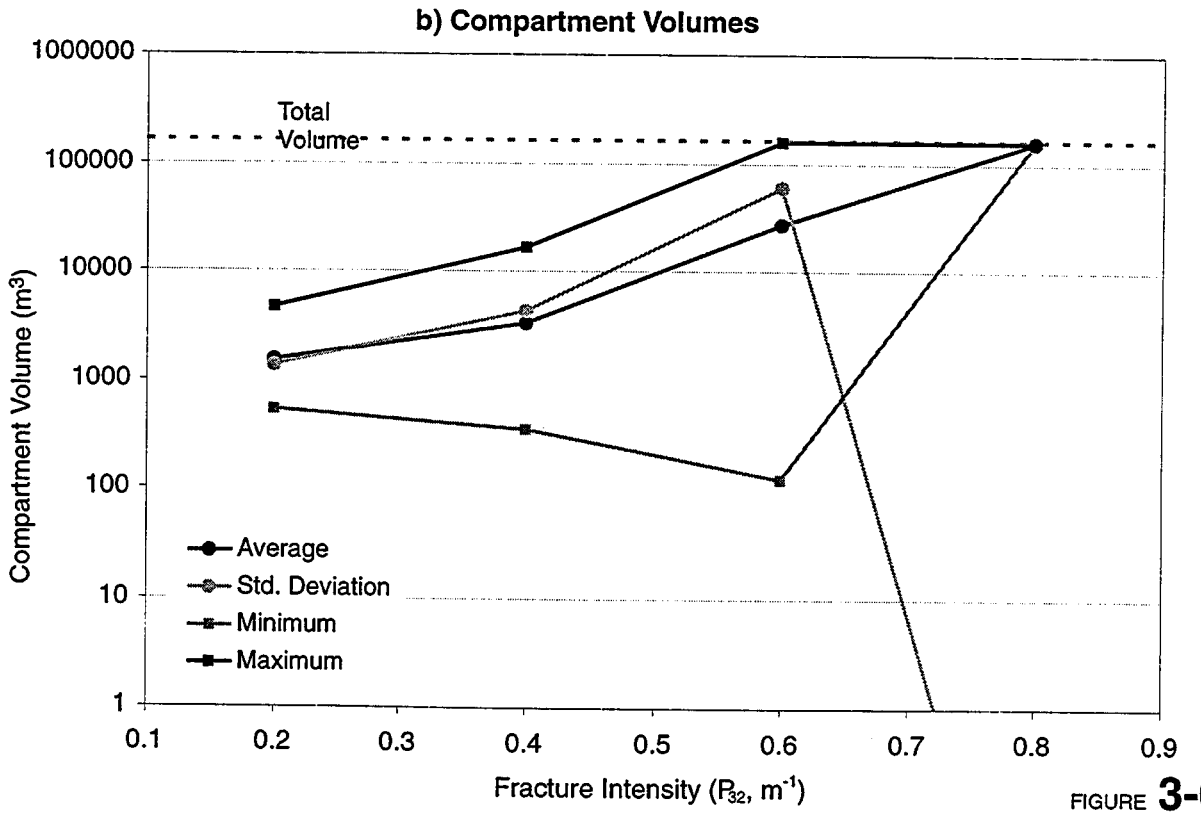

FIGURE **3-61**
NORTH OREGON BASIN COMPARTMENTALIZATION ANALYSIS
NPTO

PROJECT NO. 983 1258.521 DRAWING NO. 85066 DATE 8/12/99 DRAWN BY EA

Golder Associates

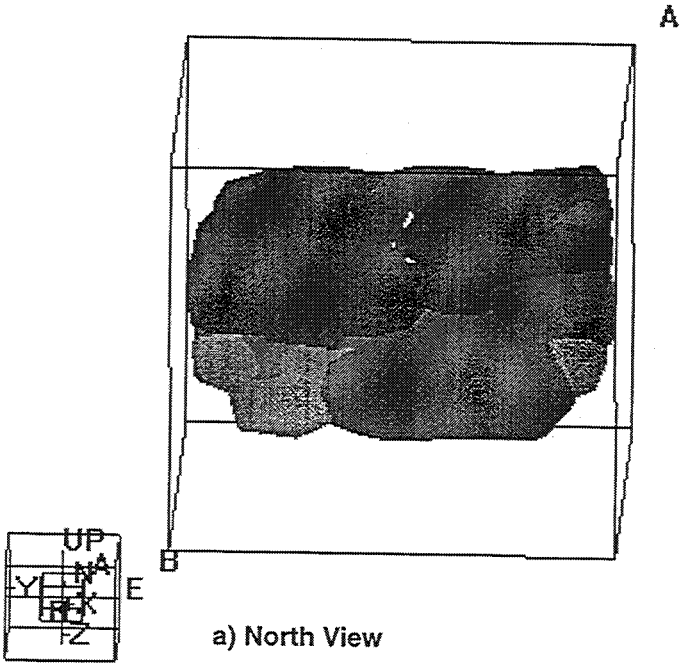

a) North View

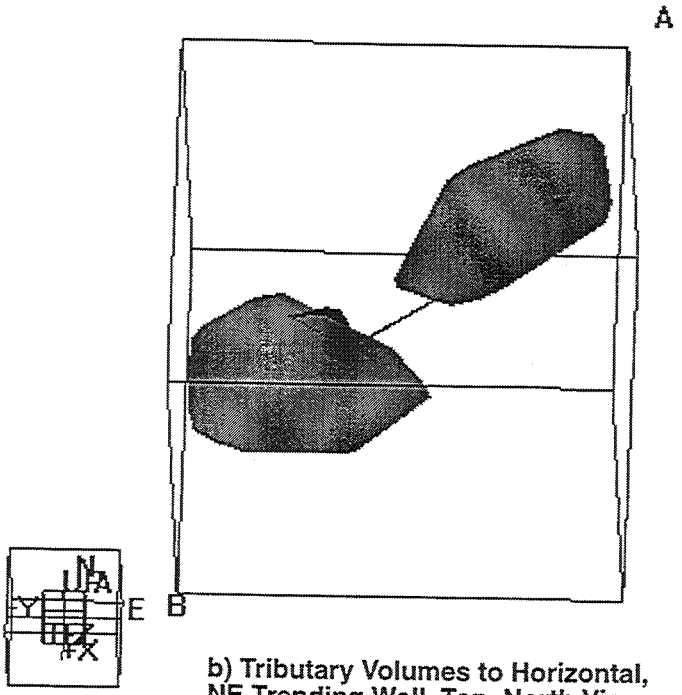

b) Tributary Volumes to Horizontal, NE Trending Well, Top, North View

FIGURE **3-62**
NORTH OREGON BASIN MODEL WITH P_{32} = 0.2
NPTO

PROJECT NO. 983 1258.521 DRAWING NO. 85064 DATE 8/12/99 DRAWN BY TK

Golder Associates

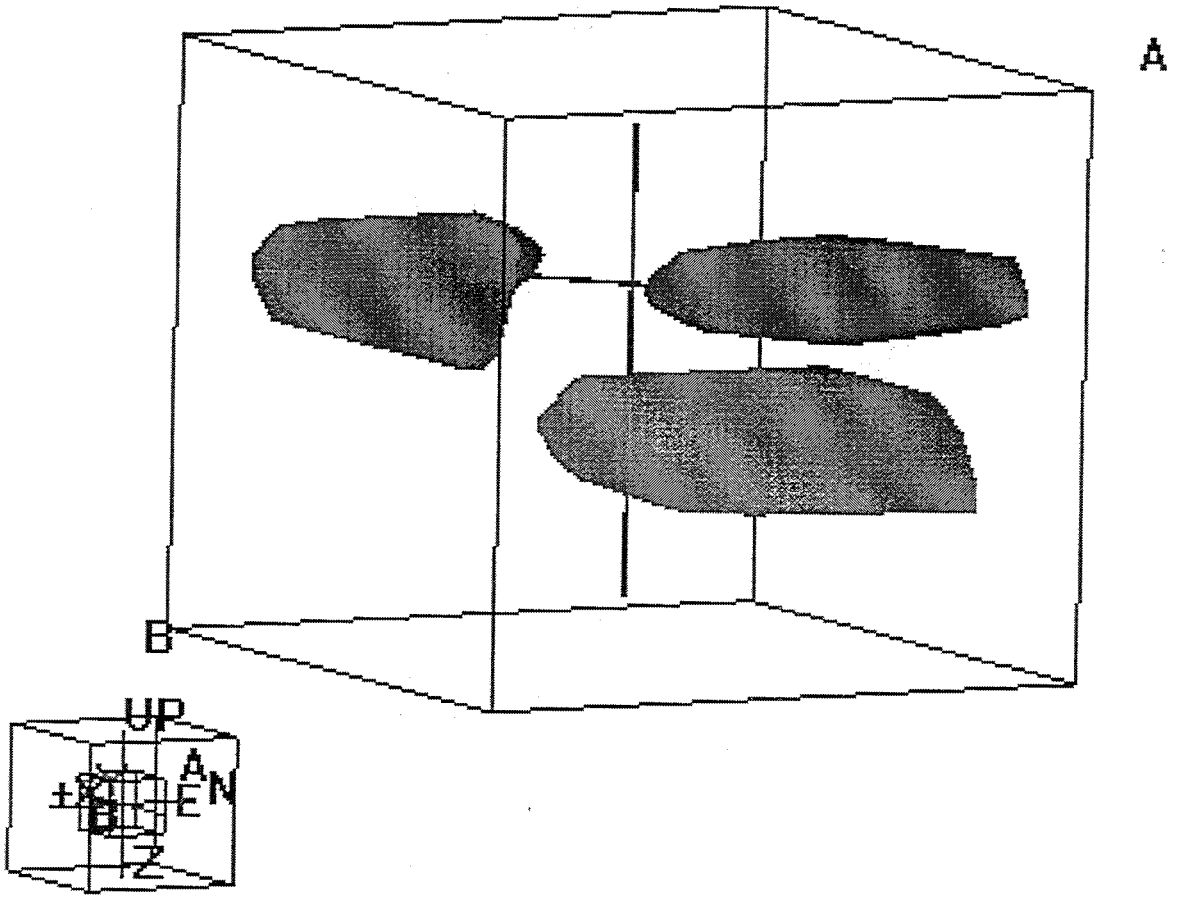

FIGURE **3-63**
SIDE VIEW OF TRIBUTARY VOLUMES OF VERTICAL AND HORIZONTAL WELLS IN NORTH OREGON BASIN MODEL WITH P_{32} = 0.2
NPTO

PROJECT NO. 983 1258.521 DRAWING NO. 85065 DATE 8/12/99 DRAWN BY TK

Golder Associates

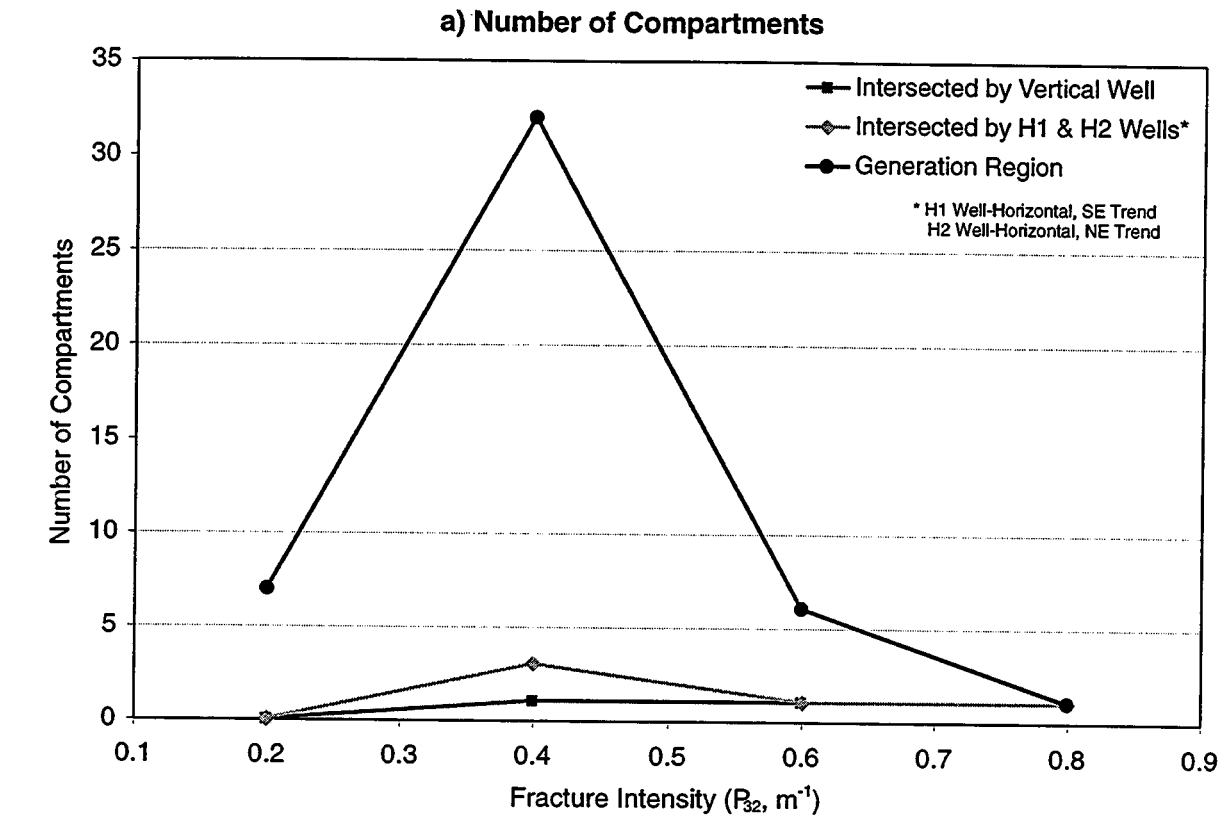

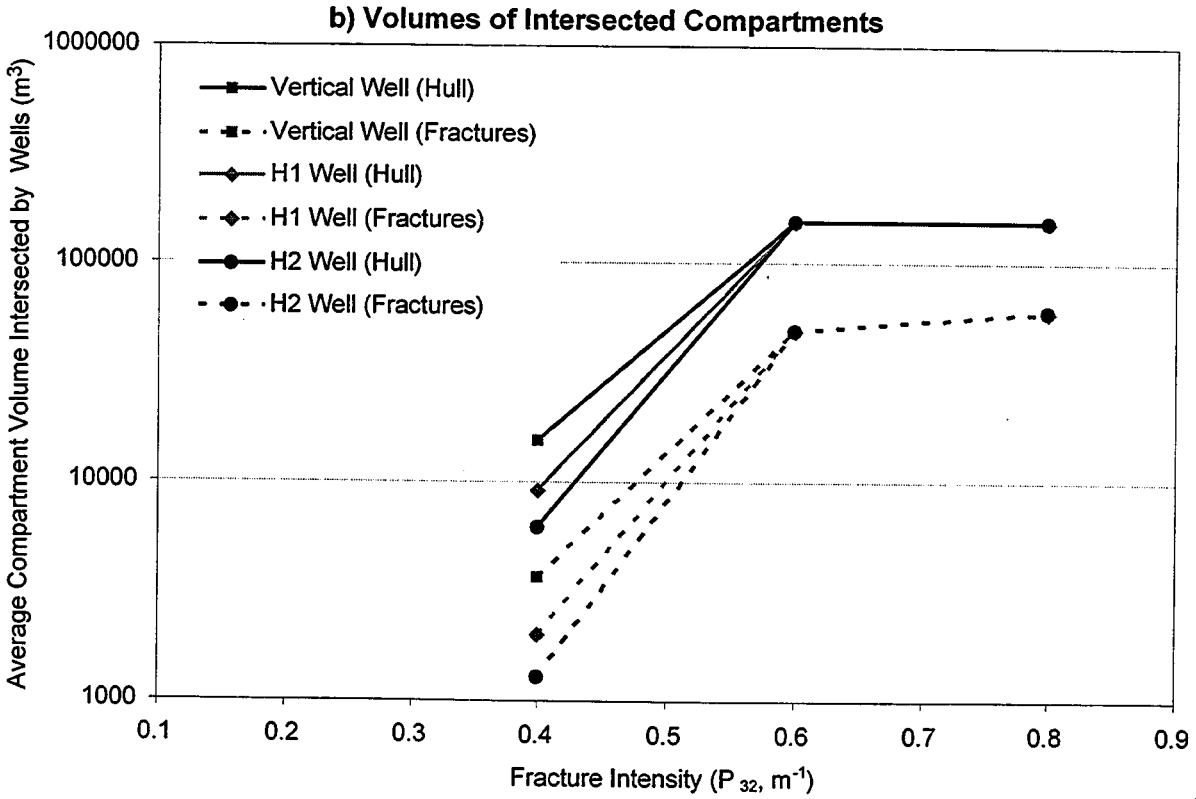

FIGURE **3-64**
NORTH OREGON BASIN
TRIBUTARY VOLUME ANALYSIS
NPTO

PROJECT NO. 983 1258.521 DRAWING NO. 85067 DATE 7/30/99 DRAWN BY EA

Golder Associates

Table 3-26 summarizes the preliminary conclusions, which can be drawn from the cluster analysis of the North Oregon Basin.

Question	Answer	Uncertainties or assumptions
Does the Tensleep break into fracture compartments at the well scale?	Yes, if conductive fracture intensity is less than 75% of the geologic intensity (P_{32}<0.6 m^{-1})	Fracture size
What is the best well orientation to minimize gel volume?	NE Horizontal	
What is the minimum volume of surfactant to inject?	~340,000 gallons 264 gallons/m^3	P_{32}=0.4 m^{-1} and assuming 1 m penetration around each fracture

Table 3-26 Implications of Tributary Volume Analysis, North Oregon Basin

3.2.9 Task 5.1.2 Web Site Updates

During the reporting period, significant updates were made to the project web site, http://HeterOil.golder.com. These included posting of site data provided by Marathon Oil Company (MOC), and descriptions of project study sites and IOR strategy planning. VRML versions of project DFN models were also posted to the project study site during the reporting period.

3.2.10 Task 5.2.1 Reports

During the reporting period, the report, "October 1, 1998-December 31, 1998 Progress Report, Discrete Feature Approach for Heterogeneous Reservoir Production Enhancement" was prepared and submitted to DOE/NPTO.

3.2.11 Task 5.2.3 Presentations

The following presentations were made during the reporting period:

La Pointe, P. R. (1999). Predicting Hydrology of Fractured Rock Masses from Geology: Techniques, Successes and Failures from Recent Case Histories. International Symposium on the Dynamics of Fluids in Fractured Rocks: Concepts and Recent Advances. 10-12 February, 1999. Berkeley, CA. (Invited Presentation).

Dershowitz, W.S. (1999) Discrete Feature Network Methods for IOR in Heterogeneous Reservoirs. 1999 DOE Oil and Gas Conference, Technology Options for Producer Survival. Dallas, June 28-30, 1999.

3.2.12 Task 6 Management

During the reporting period, significant project management activities included negotiation of the project subcontract with MIT, and tracking of labor costs and schedules.

4. CONCLUSIONS

Excellent progress was made during the reporting period on data analysis and DFN model implementation and preliminary application of project study sites at North and South Oregon Basin and Stoney Point. These sites now have DFN models comparable to the pre-existing models for the Yates project study site.

During the upcoming reporting period, the project will focus on further research on fracture data analysis and DFN modeling proceedings and IOR approaches for the study sites.

5. REFERENCES

Aviantara, A. (1996) Facies and Fracture Architecture of the Tensleep Sandstone, Bighorn Basin, Wyoming : Preliminary result of an outcrop and subsurface study, 1996 AAPG Annual meeting.

Blackstone, D.L. 1986: Foreland Compressional Tectonics: Southern Bighorn Basin and adjacent areas, Wyoming. Report of Investigations No. 34, Geological Survey of Wyoming.

Cordiner, F.S. and Livingston, A.R. 1977: Tensleep Reservoir Study, Oregon Basin Field, Wyoming – Engineering Plans for Development and Operation, South Dome, American Association of Petroleum Geologists Bulletin. Vol. 62 No. 4 (April 1978) p. 609-632.

Dershowitz, W., Foxford, T., Cladouhos, T., Eiben, T; Fox, A. 1998: FRACMAN Interactive Discrete Feature Data Analysis, Geometric Modeling and Exploration Simulation; User Documentation version 2.6.

Dershowitz, W.S., Einstein, H.H., LaPointe, P.R., Eiben, Th., Wadleigh, E., and Ivanova, V., 1998, Fractured Reservoir Discrete Feature Network Technologies, National Petroleum Technology Office, U.S. Department of Energy, Tulsa, Oklahoma.

Dershowitz, W. 1999: Discrete Feature Approach for heterogeneous reservoir production enhancement. October 1, 1998 – December 31, 1998 Progress Report, Fundamental Geoscience for Reservoir Characterization.

Dunn, T. 1997: Anisotropy and spatial variation of relative permeability and lithologic character of Tensleep Sandstone reservoirs in the Big Horn and Wind River Basins, Wyoming. Final Report, Bartlesville Project Office, U.S. Department of Energy.

Ellis, M. 1989: Geologic map of the Powder River Basin and surrounding area, Wyoming, Montana, South Dakota, North Dakota, and Nebraska.
US Geological Survey Miscellaneous Field Studies MF-2095

Hewett, D. 1926: Geology and oil and coal resources of the Oregon Basin, Meeteetse, and Grass Creek Basin quadrangles, Wyoming. US Geological Survey Professional Paper 145, 107p.

Kerr, D.R. and Tapp, J.B. 1998. Facies and Fracture Architecture of the Tensleep Sandstone, North-Central Wyoming. An Abbreviated Field Guide, University of Tulsa, Tulsa, OK.

Kohonen, T. (1988). Self-Organization and Associative Memory. Springer-Verlag, New York.

Lapointe, P., Wallmann, Peter C., Dershowitz, W. 1993: Stochastic estimation of fracture size through simulated sampling. International Journal of Rock Mechanics, Mineral Sciences and Geomechanics Abstracts, Vol. 30, No. 7, pp. 1611-1617.

Morgan, J. T., Cordiner, F. S., and Livingston, A. R. 1977: Tensleep Reservoir, Oregon Basin Field, Wyoming. American Association of Petroleum Geologists Bulletin. Vol. 62 No. 4 (April 1978) p. 609-632.

Pierce, William G. 1997: Geologic Map of the Cody 1° x 2° Quadrangle, northwestern Wyoming. USGS Miscellaneous Investigations Series Map I-2500.

Stone, D.S. 1984: Geologic Interpretation of seismic profiles, Big Horn Basin, Wyoming, Part 1: East Flank, in Rocky Mountain Association of Geologists and the Denver Geophysical Society Atlas, p165-174

Stone, D.S. 1984: Geologic Interpretation of seismic profiles, Big Horn Basin, Wyoming, Part 2: West Flank, in Rocky Mountain Association of Geologists and the Denver Geophysical Society Atlas, p175-186

Todd, T.W., 1964, Petrology of Pennsylvanian Rocks, Big Horn Basin, Wyoming, American Association of Petroleum Geologists Bulletin, 1063-1090.

Twiss, R.J. and Moores, E.M., 1992, Structural Geology. W.H. Freeman and Company, New York.

Walton, P. T. 1947: Oregon Basin oil and gas field, Park County, Wyoming in Big Horn Basin: Wyoming Geological Assoc. Guidebook, p 210-222; also American Association of Petroleum Geologists Bulletin v31, p1431-1453.